Spring 2017

Manufacturing of advanced continuous fiber reinforced composites for high temperature applications

James Robert Nicholas

Department: Mechanical and Aerospace Engineering

MANUFACTURING OF ADVANCED CONTINUOUS FIBER REINFORCED COMPOSITES FOR HIGH TEMPERATURE APPLICATIONS

by

JAMES ROBERT NICHOLAS

A DISSERTATION

Presented to the Faculty of the Graduate School of the

MISSOURI UNIVERSITY OF SCIENCE AND TECHNOLOGY

In Partial Fulfillment of the Requirements for the Degree

DOCTOR OF PHILOSOPHY

in

MECHANICAL ENGINEERING

2017

Approved by

K. Chandrashekhara, Advisor
E. Kinzel
C. Wang
C. Castano
G. Hilmas

PUBLICATION DISSERTATION OPTION

This dissertation has been prepared in the style and format utilized by the journals for publication as follows:

Paper I: Pages 17-51 are intended for submission to *Journal of Composite Materials*

Paper II: Pages 52-74 are intended for submission to *Composites Science and Technology*

Paper III: Pages 75-101 have been published in *Composites Part B*

ABSTRACT

New resin systems have enabled composites to be considered as attractive alternatives in structural applications that require material to be stronger, lighter and/or more resilient to environmental effects. The current work is on the development of processes to produce continuous fiber reinforced materials from two state of the art resin systems. Two processes were developed to produce continuous fiber reinforced ceramic materials from a preceramic polymer. The first was a vacuum forming process developed using the out-of-autoclave polymer composite manufacturing technique in conjunction with the polymer infiltration and pyrolysis process to produce ceramic composite material of zirconium diboride-silicon carbide reinforced with continuous silicon carbide fibers for use in ultra high temperature applications. A second process was developed using the dry press ceramic manufacturing technique in conjunction with the polymer infiltration and pyrolysis process to produce ceramic composite material of silicon carbide reinforced with continuous silicon carbide fibers for use in high temperature nuclear applications. The materials from these two processes were characterized using microstructure analysis techniques and standardized mechanical testing. The third process produced a polymer reinforced composite from novel thermoset polyurethane. A vacuum assisted resin transfer molding technique was used to produce a composite material from a new two-part polyurethane resin infused into plane weave E-glass fiber mats. The effects on the microstructure and the impact behavior of thermoset polyurethane composite material, exposed to an accelerated UV-aging environment, were assessed. The work performed provides valuable information with respect to the processing of continuous fiber reinforced composites using new materials and processes.

ACKNOWLEDGMENTS

I wish to express my deep sense of gratitude and sincere appreciation to my advisor, Prof. K. Chandrashekhara, who guided me with diligence and patience throughout my graduate study at Missouri University of Science and Technology. He has been an incredible mentor and friend. I am very grateful for his exceptional expertise, scientific advice and many insightful discussions and suggestions. Through the difficult time of writing this dissertation he has kept me firmly rooted on the right track. It has been a great pleasure working under his tutelage.

I would also like to thank my committee members Dr. Cheng Wang, Dr. Edward Kinzel, Dr. Carlos Castano, and Dr. Greg Hilmas for their valuable time and advice in the review of this dissertation.

I would also like to acknowledge my colleagues of KC Lab Group: Dr. V. Bheem Reddy, Dr. Z. Huo, Dr. M. Mohaned, Dr. H. Li, Mr. A. Abutunis, Mr. S Anandan, Mr. R. Hussein, Mr. G. Taylor, Mr. R. Meinders, Mr. M. Fal, Mr. G. Dhaliwal and Mr. X. Wang for useful thoughts and engaging in fruitful discussions over the duration of this work.

Finally, I would like to give thanks to my parents who molded me into the person I am. I would like to express a deep sense of gratitude to my siblings who balance me: my brother Jason and his wife Claudia who strengthened my resolve in all situations; my brother Johnthomas who reminds me to be creative; my sister Jessica and her husband Jim who have kept me intrigued in all things. A special thanks to my wife, Emily, and children, Sage, Cole and Oen, to whom I owe my life for their companionship, encouragement, and patience. Without their support, especially my wife's, I would not be able to accomplish and fulfill this achievement.

TABLE OF CONTENTS

Page

LIST OF ILLUSTRATIONS

SECTION Page

PAPER III

LIST OF TABLES

SECTION Page

1. INTRODUCTION

Composite materials are materials that are made up of two or more constituents that have bulk properties that are different than the sum of the individual parts. These materials can be tailored for specific applications to achieve preferred properties as compared to traditional materials; such as, lighter weight, stronger, tougher, more resilient to environment effects, and/or less expensive. The ability to be tailored makes composite materials a prime candidate for many of today's structural applications.

The need for improved gas turbine efficiency, advances in hypersonic vehicle design, increase of nuclear reactor operation temperatures, and other advanced applications are driving the need for material with higher mechanical property performance at extremely high temperatures. The materials that are used in these applications are referred to as ultra high temperature materials (UHTM) and are required to be able to perform in temperatures ranging from 1600 °C to 3000 °C. The increase in demand on these materials has driven an increase of research and development of new UHTM and of novel approaches to the manufacturing processes of these materials. Continuous fiber reinforced ceramic composites (CFCCs) are currently considered a prime candidate for these applications; therefore, a focus of this study is on this category of materials for ultra high temperature applications.

The aerospace industry has had the strongest push for ultra-high temperature applications. Matsuda et al. [1] from Japan's Kawasaki Heavy Industries are working to develop a ceramic matrix composite (CMC) material for propulsion system combustor liners that have been pushed to temperatures that exceed current super-alloy capability in order to improve turbine efficiencies in small turbo-shaft engines for helicopters. For

their work, a woven ceramic fiber preform was used as a reinforcment in a SiC matrix that was formed using a polymer impregnattion and pyrolysis process. Also, Watanabe et al. [2] at Ishikawajima-Harima Heavy Industries have been working on CMC materials for hollow vane structures that will be subjected to extreme conditions in the aft section of gas turbine engines with temperatures in excess of 1320 °C. Their study explores the use of a SiC fiber reinforced SiC matrix as a prospective candidate to replace a Ni-based super alloy. Other studies [3] have been on the development of hypersonic flight cruise missiles and vehicles that require control surfaces and nose cone materials to withstand sustained temperatures exceeding 2000 °C.

Studies on non-airspace applications are also contributing to the development of new ultra high temperature materials. Materials for use as control rod cladding and guide tubes within very high temperature reactor designs that are required to have high thermal stability, good fracture toughness, and high irradiation stability during service [4]. Materials that are chemically and physically stable at high temperatures while exposed to a reactive atmosphere are required for use in these, and other ultra high temperature applications.

As the demand for these materials has increased, the need for more knowledge on these materials has also increased. Found from a search on a database of abstracts and citations in the last 20 years, the number of publications on UHTM has increased by over a factor of 10. During the last 10 years, there has been a growing interest in CFCCs due to their improved damage tolerance over monolithic ceramic materials and improvements on pre-ceramic polymers and manufacturing processes [5-8].

Other structural application, though not high temperature, still require materials that are chemically and physically stable in reactive environment. The infrastructure industry requires materials that are inexpensive with high strength-to-weight ratio. These materials are needed to be resistant to moisture and ultraviolet exposure. Polymer reinforced composites are good candidates for these applications, because of new inexpensive polymers being developed. [9-10]

Experimental studies on the manufacturing processing of these new materials are an important aspect to the development of introducing new materials into the aforementioned industries. Therefore the focus of this study is the processing of new composite constituent materials for use as structural materials.

2. REVIEW OF LITERATURE

2.1. ULTRA HIGH TEMPERATURE MATERIALS

UHTMs are a category of materials that are required to be chemically inert as well as retain strength and elastic modulus at temperatures above 1600 °C and up to 3000 °C. There are three main groups of materials that have been developed for ultra high temperature applications. Some superalloys have shown promise for high temperature applications, but have limitations that have driven a need for an alternative. Certain monolithic ceramics have traditionally exhibited properties that satisfy the requirement for these applications; however, low fracture toughness and manufacturing limitations have propelled the drive for the next generation of UHTMs. Ceramic composites have shown promise of being the next generation of UHTMs with the potential for increased toughness over monolithic ceramics and more flexible fabrication techniques.

Ultra high temperature superalloys, termed as “refractory superalloys”, are designed to have retain toughness and strength at high temperatures, but are limited to use on the low end of the ultra high temperature spectrum. The temperature capability of these superalloys has improved over the last 50 years; however, excessive creep rates at high temperatures limited their use to around 1400 °C to 1600 °C [12-15]. Applications at temperatures that exceed this threshold require the use of alternative materials.

Due to temperature resistive properties, monolithic ceramics have historically been used for ultra high temperature applications that exceed 1600 °C. Shown in Table 2.1 is the limited number of materials that are able to withstand such extreme temperatures. This list largely consists of the borides, carbides, and nitrides of transition metals such as ZrB2, HfB2, ZrC, and HfN, which have melting temperatures in excess of

3000 °C [16,17]. Recent studies on ZrB2-based SiC composites for ultra high temperature applications have shown that these materials maintain mechanical properties in the extreme environments needed for ultra-high temperature applications [18,19]. These studies are on the behavior of particle and whisker type composites. The low fracture toughness leading to catastrophic failure has limited their applications and has driven the development of CFCC's [20]. There are limited studies on the continuous fiber reinforced ZrB2-based SiC composites.

Table 2.1 Materials with melting temperatures above 3000 °C

Carbon	TaB_2	Re
W	HfC	BN
HfB_2	HfN	ZrC
TaC	ZrB_2	TiC
TaN	NbC	ThO_2

2.2. CONTINUOUS FIBER REINFORCED CERAMIC COMPOSITES

CFCCs offer substantial improvements in damage tolerance over monolithic ceramic materials, as can be seen in Figure 2.1(left). The damage tolerance is a result of the complex failure mechanisms of CFCCs such as matrix cracking, fiber pull-out, and fiber breakage. Figure 2.1(right) is an illustration of the crack propagation through a ceramic composite. This image shows the ideal failure mechanism that will accrue to result in a toughened material. The top image shows the deflection of crack path as it encounters a fiber. This deflection is due to a weak interface between the fiber and the matrix allowing for debonding that prevents the crack from proceeding straight through

the fiber. The debonding prior to fiber failure, and the resultant load retention from the fiber pullout phenomena have both been shown to retard crack propagation and increase the toughness of the ceramic materials [20-22].

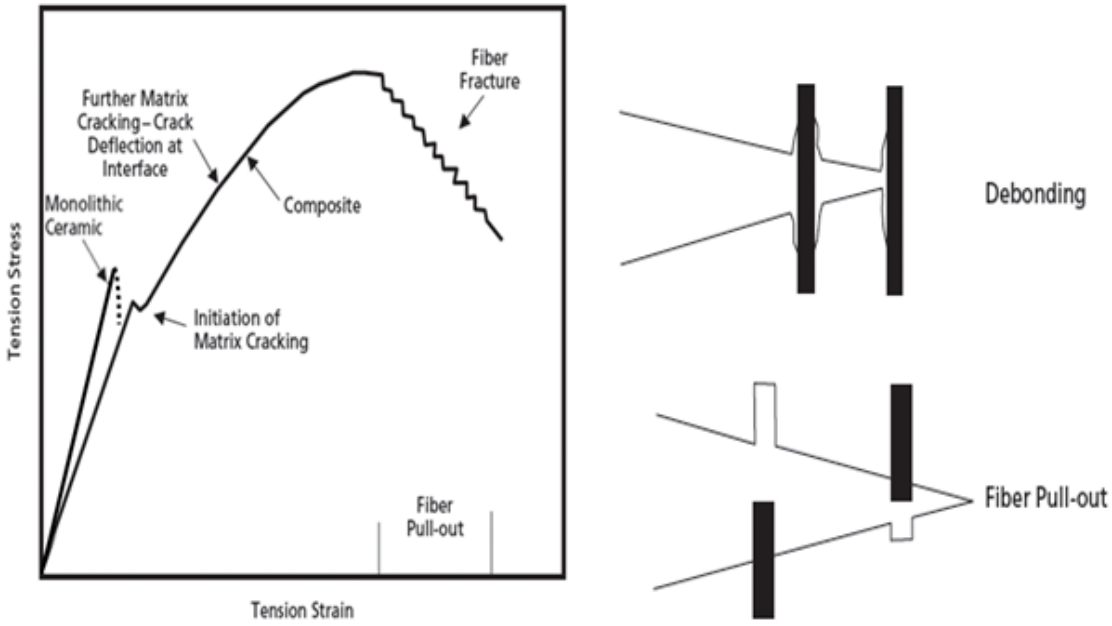

Figure 2.1 Theoretical Stress vs. Strain comparison between monolithic ceramic and CFCC materials (left) diagram of complex failure mechanism (right)

The interface of the fiber/matrix plays a significant role in determining the fracture behavior and mechanical properties of ceramic matrix composites. The predominant approach in developing a desired weak interface has been to use a thin, 0.1-5 μm, coating around the fibers to develop the desired crack deflection and the required sliding friction. These coatings traditionally have been graphitic carbon, boron nitride and oxides. The process of applying these coating greatly increase the cost of the fibers. An alternative to this is to produce matrices with residual porosity, often time exceeding

40%. These composites exhibit damage tolerance through progressive and distributed damage under off-axis loading. [23]

2.3. POLYMER PRECURSORS

Polymer precursors, or preceramic polymers, are inorganic/organometallic compounds that behave as characteristic polymers at low temperatures and transform into ceramic materials upon heating to temperatures above 450 °C. Manufacturing of ceramic compounds from the preceramic polymers requires a heat treatment to form the inorganic compounds designated for the end use. These polymers are used to produce a variety of non-oxide ceramics by molecularly altering the compound to suit the end use. A diagram of the preceramic organosilicon polymer is shown in Figure 2.2. With this unique class of polymers to produce ceramic compounds, unique challenges have risen to create a fully densified ceramic component. [23]

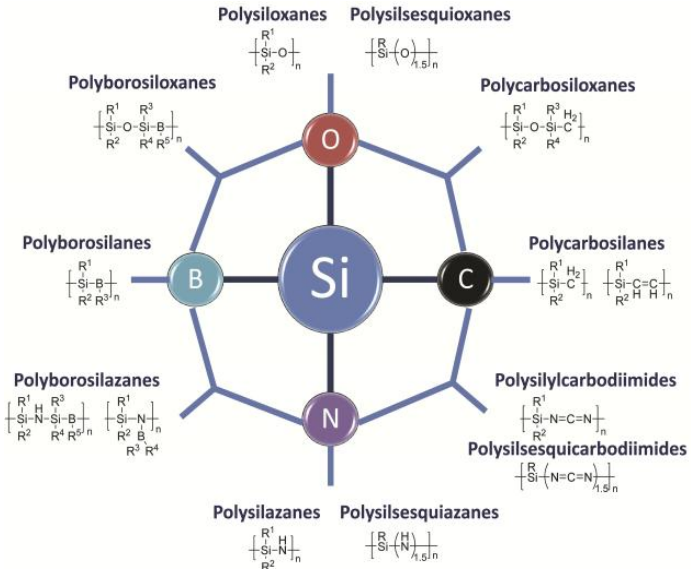

Figure 2.2 Examples of Preceramic Organosilicon Polymers [23]

Preceramic polymers are long chain molecules that are made up of a backbone of inorganic elements with organic branches. The organometallic polymer converts from polymer-to-ceramic at temperatures that range from 500 °C to 800 °C as the organic components are shed. This forms a network of inorganic elements which can be crystallized by heating to higher temperatures (1000 °C to 1600 °C). A diagram of the polymer-to-ceramic conversion process is shown in Figure 2.3 [25].

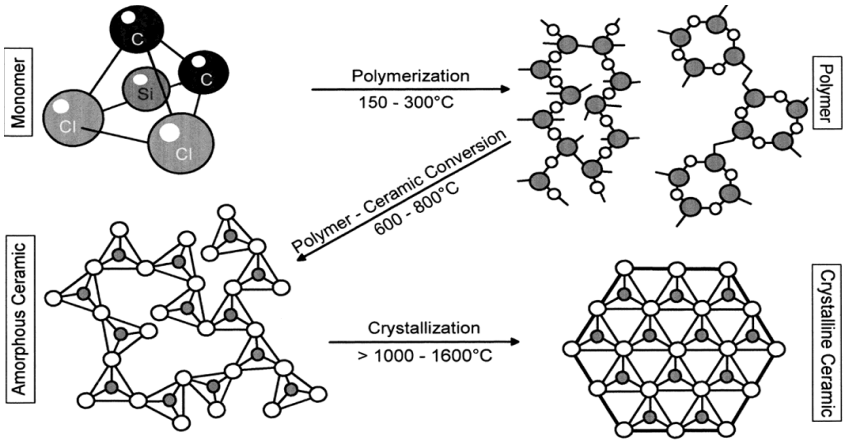

Figure 2.3 Schematic of molecular and microstructural transition of polymer-to-ceramic conversion [25]

Polymer precursors contain a silicon group, or in some cases a boron or aluminum group, in the backbone of the chain molecule and are used to obtain a variety of ceramic compounds such as SiC, SiCO, SiCN, BN, and AlN [26,27]. The organosilicon polymers are represented by the general formula:

$$\begin{array}{c} R^1 \\ | \\ -[Si - X]_n- \\ | \\ R^2 \end{array}$$

Modifying the group X on the polymer backbone and the substituent R1 and R2, the preceramic compound can be tailored at the molecular level. CFCCs produced from polymer precursors offer several advantages to designers. The chemical composition and nanostructural organization of these ceramics can be tailored to the requirements of the end-user application by controlling the curing and pyrolysis processes. Complex shapes, with sharp radii edges, that were not possible with ceramics earlier were produced using polymer precursors [24].

Even though ceramic yields as high as 85% had been reported, the main challenge in processing ceramics via a polymer precursor is the open pores and cracks that form [28]. These flaws are due to the evolution of organic volatiles, a less than 100% ceramic yield, along with the volumetric shrinkage due to the increase in density of the material as it converts from the low density polymer to the higher density ceramic. Hence, several re-infiltration cycles are required to fully densify the ceramic component.

2.4. PRECERAMIC POLYMER PROCESSING

In the early 1970s, Verbeek et al. [29] produced the first practical production of Si_3Ni_4/SiC from a polymer precursors transformation based on polysilazanes, polysiloxanes, and polycarbosilanes. Further progress was achieved by Yajima et al. [30] in synthesizing high tensile strength silicon carbide fibers using polycarbosilanes. Johnson et al. [31]at NASA Ames Research Center studied the thermal conductivity, fracture toughness, and oxidation resistance of the hafnium and zirconium based composites manufactured via a hot pressing process. Nejhad et al. [32,33] investigated the manufacturing of CFCCs using Nicalon and Nextel fibers with a preceramic polymer

derived matrix utilizing filament winding and vacuum assisted resin transfer molding processes. Lee et al. [34] fabricated composites with carbon fiber and two-component Si-B-C-N precursor using a vacuum infiltration process. Stepwise thermal cross-linking was used during the curing process and flexural properties were reported. Yao et al. [35] performed studies on impact damage evaluation of carbon fiber reinforced SiC polymer precursor composites. Zhu et al. [36] reported monotonic tension, fatigue and creep behavior of Hi-Nicalon SiC fiber reinforced SiC composites manufactured using a CVI process. The authors reported that Hi-Nicalon fibers composites had similar properties to enhanced SiC/SiC composites, with an ultimate stress of at least 209 MPa, but at higher costs. Sayir et al. [37] from NASA Glenn Research Center manufactured hafnium carbide composites using a CVI process and studied the microstructure and tensile properties. Al-Dawery and Butler [38] used Nextel 720 fibers in a combination of ZrO_2 and AKP50 alumina powder to manufacture ceramic composites using pressure less sintering process.

2.5. SILICON CARBIDE

Though there are a variety of ceramic compounds that can be produced using polymer precursor, the focus of this study is on organosilicon polymers that produce silicon carbide (SiC). SiC is one of the most prevalent ceramics used due to its high strength (500 MPa), modulus (410 GPa), creep resistance, and oxidation resistance at temperatures as high as 1600 °C [39,40]. Because of these properties and others, polymer-derived SiC is an excellent candidate for use as a component in ultra high temperature ceramic composites.

Silicon carbide is a superior candidate as a component in an ultra high temperature composite due to its thermal shock resistance and chemical stability. These characteristics have attracted attention to use of SiC as a potential component in advanced composite material systems [41]. Ultra high temperature materials will often experience a repeated heating and cooling cycle. This makes the resistance to thermal shock important. Lee et al. [42], performed a study of the effect of cyclical thermal shock on candidates as matrix materials for nuclear fuels. It was observed that no change in the hardness and even an increase in fracture toughness for SiC as compared to the other ceramics considered.

2.6. ALLYLHYDRIDOPOLYCARBOSILANE

Silicon carbide is the polymer derived ceramic that is of interest to this investigation. The first of the organosilicon polymers examined to produce SiC for this study is allylhydridopolycarbosilane (AHPCS). It is a poly(carbosilane) that yields a near 1:1 atomic ratio of silicon to carbon upon complete pyrolysis with a low oxygen content [43]. Its high ceramic yield (72-78%), which leads to low shrinkage, and ability to be handled in ambient conditions has attracted wide attention as a precursor to SiC fibers, and as a matrix material [41,43,44].

In 1958, the first reported formation of poly(carbosilane) from a polysilane was performed by Kumada et al. [46]. Whitmarsh et al. [47] first reported the synthesis of AHPCS from (chloromethyl)trichlorosilane in 1991. AHPCS is commercially available through Starfire Systems and is being widely researched as a binder for ceramic powders, and as a matrix source for polymer derived ceramic matrix composites [26,48].

2.7. MANUFACTURING PROCESSES

There has been a multitude of approaches for manufacturing CFCCs, but only a few are considered viable approaches to making quality materials. Many traditional monolithic ceramic manufacturing techniques have proven to be ineffective at producing CFCCs; however, there are currently several different processes that are considered effective techniques for the manufacturing of CFCCs: Chemical Vapor Infiltration (CVI), Melt Infiltration (MI) also called Liquid Silicon Infiltration (LSI), and Polymer Infiltration and Pyrolysis (PIP) also called Liquid Polymer Infiltration (LPI) [49].

Traditional ceramic manufacturing techniques are limited in their use to produce CFCCs because of damage incurred by the fibers during manufacturing. It has been shown that the high-pressure heat treatment required in densifying ceramic powder compacts causes decomposition in fibers that have an oxygen containing phase such as Si-O-C [50-52]. It has also been shown that even in fibers with low crystallinity, the high-pressure heat treatment causes creep deformation in the fibers that leads to strength degradation [53]. These downfalls of traditional manufacturing methods have pushed for the development of new manufacturing techniques.

In the last few decades, there has been an increase in research interest in the development of alternative, low-pressure and low-temperature methods for the preparation of ceramics [54]. Ceramics manufactured using CVI processes produce materials that have low porosity, offering high mechanical strength and high strain capability, at least 250 MPa and 0.5%, respectively [26]. This process involves the deposition of a solid material on to an activated or heated surface by reaction with a gaseous phase of an inorganic precursor in forms of halides and metal carbonyls as a

source of vapor [55,56]. CVI has been successfully used to produce monolithic parts and ceramic composites and is considered an effective technique for forming fiber reinforced ceramic [57,58]. For full densification of the ceramic materials, multiple infiltration cycles are required. Chemical vapor infiltration is widely used for fabrication of ceramic matrix composites; however, this process requires highly specialized equipment.

The polymer infiltration and pyrolysis process is showing potential promise to be a considerably more simple process of developing CFCCs than the CVI technique and producing materials with similar microstructure. This method involves condensing of organometallic compounds, referred to as polymer precursors, into inorganic materials via heat treatment under controlled atmosphere. Fabrication of CFCCs by this method can be processed and shaped using conventional fiber reinforced polymer composite processing such as resin transfer molding, vacuum assisted resin transfer molding, and out-of–autoclave bagging techniques at relatively low processing temperatures, temperatures under 250 °C and at atmospheric pressure [59,60]. The lower processing temperatures reduce the occurrence of fiber damage in reinforced ceramic matrix composites; therefore the PIP process has been deemed an attractive option for fabrication of continuous fiber reinforced ceramic composites [61].

2.8. POLYURETHANE

Polyurethane (PU) is increasingly being used as a resin in composite materials and is showing superior performance compared to polyester and vinyl ester and is more cost effective than epoxy, but few studies have investigated the behavior of PU composites [62]. Mohamed et al. [62] evaluated the performance of a new generation of

two part thermoset resin showing that both systems exhibited excellent properties and would be suitable for use in structural applications. Many of these structural applications will require exposure to environmental elements such as moisture and ultraviolet radiation. There have been many investigations into the effect of the environmental effects on pure polyurethane [63-68], but there is a need for knowledge of the environmental effects on polyurethane when used as a constituent in a composite material.

3. SCOPE AND OBJECTIVES

This dissertation comprises of three papers corresponding to the following problems:

The first paper is titled “Out-of-Autoclave PIP Fabrication Process of ZrB2-SiC/SiCf Composites for Ultra High Temperature Applications.” The objective in this paper was to produce a cost effective, toughened ceramic composite material for use in ultra high temperature applications. An allylhydridopolycarbosilane preceramic polymer was used to manufacture a SiC-ZrB2 continuous SiC fiber reinforced ceramic material. A low cost vacuum bagging process was adapted to manufacture the material. The temperature profile used to cure the polymer was developed and optimized from a combination of thermogravimetric analysis and differential scanning calorimetry investigations. A cost effective toughening method of producing a matrix of incomplete densification reinforced with continuous fiber mats was employed. To achieve ultra high temperature capable material, the matrix was loaded with powdered ZrB2. The microstructure is investigated using scanning electron microscopy and density analysis to determine the effectiveness of the re-infiltration during the polymer infiltration and pyrolysis cycles and to describe the material produced. The mechanical performance of the manufactured samples was evaluated using 3-point flexure tests.

The second paper is titled “Dry Press PIP Fabrication Process of SiC/SiCf Composites for Nuclear Applications.” In this paper, a process was developed to produce β-SiC continuous fiber reinforced β-SiC composites for nuclear applications. The process was developed by combining a greenbody forming technique, dry pressing, with the polymer infiltration a pyrolysis process. A woven β-SiC fiber mat was infiltrated with a

slurry of preceramic polymer and β-SiC micro particles, dry pressed and cured to a greenbody state. The material was then subjected to a repeated cycle of pyrolyzation and re-infiltration. The pyrolyzation temperature profile was optimized using thermogravimetric analysis. A final heat treatment was used to achieve a beta crystalline matrix material. SEM and XRD analysis was employed to analyze the microstructure produced. The thermo-mechanical properties were investigated from room to high temperature using a 4-point flexure test equipped with an advanced high temperature environmental chamber.

The third paper is titled "Effects of Accelerated Environmental Aging on Glass Fiber Reinforced Thermoset Polyurethane Composites." In this paper, glass fiber reinforced polyurethane composites were manufactured from a novel two-part resin system using a low cost vacuum assisted resin transfer method. A hygrothermal and ultraviolet chamber was used in an accelerated aging procedure to simulate temperate climate conditions. Effect of UV exposure on color change of composite specimens was evaluated using image processing and colorimetry. The effects of the aging on the microstructure were assessed using optical microscopy. The accelerated aging effect on the impact resistant behavior was examined using low velocity impact.

PAPER

I. OUT-OF-AUTOCLAVE PIP FABRICATION PROCESS OF ZRB_2-SIC/SIC_F COMPOSITES FOR ULTRA HIGH TEMPERATURE APPLICATIONS

J. Nicholas[a], G. Hilmas[b], and K. Chandrashekhara[a]

[a]*Department of Mechanical and Aerospace Engineering*

[b]*Department of Materials Science and Engineering*

Missouri University of Science and Technology, Rolla, MO 65409

ABSTRACT

Monolithic ceramic materials are currently being researched for potential use in ultra high temperature applications such as hypersonic vehicles, missiles and rockets where the materials would be expected to experience extremely high temperatures (often > 2000 °C). Ceramic materials offer superior chemical and physical stability at higher temperatures compared to metals and polymers. One of the major challenges with the monolithic ceramics is their tendency to fail catastrophically. One way of significantly improving the toughness of these materials is by introducing continuous fibers to create a ceramic matrix composite material. Plain weave SiC mats have been used as the reinforcement for this study. The matrix material was an ultra high temperature material, ZrB_2 powder, bonded together using a SiC perceramic polymer. For this study, polymer infiltration and pyrolysis process was modified to produce continuous fiber reinforced ceramic composite samples from a low cost vacuum bag process. The focus points in the fabrication of ZrB_2-SiC/SiC_f continuous fiber reinforced composites were the

development of preceramic polymer slurry of SMP-10 loaded with ZrB_2 and prepreg plain weave SiC mats, along with producing reliable bagging and sealing techniques to produce low void content with desired fiber volume fractions of 40%. The issues related to the processing have been investigated. Differential scanning calorimetry and thermogravimetric analysis tests were performed to optimize the polymer cure temperature profile. An increase in mass of up to 16% was observed due to the re-infiltration process. From analysis of the microstructure using scanning electron microscopy void density was shown to be reduced from greater than 40% to less than 10%. 3-point flexure tests show that the material exhibits a toughening effect due to the fiber reinforcement.

1. INTRODUCTION

Applications such as hypersonic missiles and re-entry vehicles demand high speeds that results in extremely high temperatures (often >2000 ℃) at the leading and trailing edges of control surfaces and propulsion systems. Materials that are chemically and physically stable at high temperatures and in reactive atmospheres are typically used for these ultra high temperature applications. Chemical inertness, high strength and moduli, high temperature capability and low thermal conductivity make monolithic ceramics attractive options for ultra high temperature applications. These materials largely consist of the borides, carbides, and nitrides of transition metals such as ZrB_2, HfB_2, TaB_2, ZrC, HfC, TaC, ZrN, and HfN, which have melting temperatures in excess of 3000°C. However, the low fracture toughness and catastrophic failure behavior of monolithic ceramic materials limit their use in these applications. Continuous fiber reinforced ceramic composites (CFCCs) offer substantial improvements in damage

tolerance over monolithic ceramic materials. Complex failure behavior of CFCCs such as matrix cracking, delamination, fiber pull-out and fiber breakage increase the toughness of the ceramic materials. Significant weight savings can be achieved by replacing the metal super alloys with tough and lightweight CFCCs. However, CFCCs are newer materials and there is a need to add to the database of knowledge in the areas of processing, modeling, testing, and manufacturing.

Four different processes are currently used for the manufacturing of CFCCs: Chemical Vapor Infiltration (CVI), Polymer Infiltration and Pyrolysis (PIP) also called Liquid Polymer Infiltration (LPI), Hot Pressing, and Melt Infiltration (MI) also called Liquid Silicon Infiltration (LSI) [1]. Ceramics manufactured using CVI and PIP processes are less porous, offering high mechanical strength and high strain capability. But CVI and PIP are time consuming due to low growth rates of SiC during CVI process, and multiple densification cycles required for PIP process. The thermo-mechanical performance of the resulting composites makes the two processes attractive for space, and aerospace industries. The manufacturing costs involved with the CVI and PIP processes are major drawback to the application of the CFCCs. A possible area of cost reduction is in manufacturing. Processes utilizing tooling and ovens that do not require pressure or temperature in excess of 250 °C would be ideal for cost reductions. The advent of new polymer precursors makes the application of lower cost manufacturing processes possible.

Polymer precursors are inorganic/organometallic compounds that behave like polymers at temperatures below 250 °C and transform into ceramic materials upon

heating to temperatures above 600 °C. The organosilicon polymers are represented by the general formula:

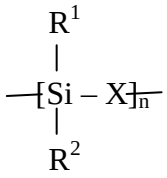

By modifying the group X on the polymer backbone and the substituents R^1 and R^2, the preceramic compound can be tailored, at the molecular level to produce the ceramic required from pyrolysis. The chemical composition and nanostructural organization of these ceramics can be further tailored to the requirements of the end-user application by controlling the curing and thermolysis processes. The advent of perceramic polymer allowed for more complex shapes that were not possible with ceramics earlier to be produced [2]. Traditionally, ceramics were manufactured via powder techniques; however, the requirements of sintering additives limited the applications of these ceramics. Polymer precursors allows application of the well established polymer processing techniques to produce fiber reinforced ceramics. In particular, vacuum assisted resin transfer molding (VARTM), filament winding, and out-of-autoclave (OOA) vacuum-bag-only-prepreg processes are low cost composite manufacturing techniques which can be applied to fabricating CFCCs.

Initially, perceramic polymers were used in the production of ceramic fibers. Fibers produced by polymer precursors based on polysilazanes, polysiloxanes, and polycarbosilanes are reported by Verbeek et al. in the 1970s [3]. Further progress was achieved by Yajima et al. in synthesizing continuous β-SiC fiber using polycarbosilanes

[4]. Johnson et al. at NASA Ames Research Center has studied the thermal conductivity, fracture toughness, and oxidation resistance of the hafnium and zirconium based composites manufactured via a hot pressing process for a found that composites based on these materials are excellent candidates for ultra high temperature applications [5]. Nejhad et al. investigated the manufacturing of CFCCs using Nicalon and Nextel fibers with Blackglas matrix utilizing filament winding and VARTM process and the properties were reported to have strength and modulus greater than 35.3 MPa and 84.6 GPa, respectively [6,7]. There have been many investigations into the processing of CFCCs but there are limited studies on the PIP processing route [8-12].

The manufacturing of CFCCs via a vacuum bag process presents several challenges that need to be addressed. During the transition process of organic precursors to inorganic ceramics at high temperatures, the matrix loses significant weight (up to 40% depending on the polymer) due to the evaporation of oligomers, making the resulting composite porous. The high porosity of the resulting composites adversely affects the mechanical performance. One solution to address this problem is to repeat the infusion process and pyrolysis until the required quality is achieved. Fillers have also been used in the literature for this purpose. Fillers can enhance properties such as electrical conductivity, thermal conductivity and thermal expansion. However, the fillers need to be uniformly dispersed in the resin system without increasing the viscosity of the precursor. Volumetric shrinkage and microcracking of the matrix during the fabrication process are other challenges to be addressed. These defects will reduce the thermal and mechanical performance of the resulting composites. In the present work, vacuum bag processes are used to manufacture SiC fiber reinforced ceramic composites via the PIP process.

2. MATERIAL

The material for this project has been selected for the intention of producing high quality CFCCs for ultra-high temperature applications. SMP-10, an allylhydridopolycarbosilane acquired from Starfire Systems, Inc. Schenectady, NY, was selected as the polymer precursor for its high ceramic yield with relatively low volumetric shrinkage, and relative ease of use. Zirconium diboride (ZrB_2), acquired from H.C. Starck Inc., Euclid, OH, was selected as the ultra-high temperature additive and a filler to limit the effect of the volumetric shrinkage of the matrix. Hi-Nicalon ceramic grade SiC fibers, acquired from COI Ceramics, Inc. manufactured by Nippon Carbon Co., Ltd of Japan were selected as reinforcement.

2.1. Polymer Precursor

The allylhydridopolycarbosilane designated SMP-10 is a polymer precursor that is an ultra high purity precursor that yields a near stoichiometric Si:C ratio upon pyrolysis completion in argon. At room temperature the resin is a clear or amber-colored, viscous liquid and has properties as listed in Table 1. Starfire Systems data sheet for SMP-10 indicates the polymer undergoes a low temperature green cure between 180 °C and 400 °C. Amorphous SiC is formed, in argon, at 850-1200 °C with a high ceramic yield of 72-78% and relatively low volumetric shrinkage of ~35%. Nano-crystalline β-SiC is then formed at 1250-1700 °C. The SiC formed is stable up to 1800 °C in air and has a 1:1 silicon to carbon atomic ratio.

2.2. Ultra High Temperature Additive

ZrB_2 is an ultra high temperature refractory ceramic material with a hexagonal crystal structure. This material has been chosen to be the additive for this investigation due to the high melting point, above 3200 °C, relatively low density of 6.09 g/cm3, and good high temperature mechanical properties. In this work the ZrB_2 is acquired from H.C. Starck with the properties presented in Table 2. Parts manufactured from this material are typically fabricated using high cost sintering techniques with SiC additive to improve oxidation resistance. This makes this material a good candidate in the low cost PIP fabrication technique as an additive to the SiC matrix in the ultra high temperature CFCCs.

2.3. Fiber Reinforcement

The Hi-Nicalon fiber is a multi-filament silicon carbide-type fiber with the properties from the manufacture's data sheet as listed in Table 3. The fiber is near oxygen free and is homogeneously composed of β-SiC crystallites and carbon. The low oxygen content, 0.5% by weight, of these fibers contributes to the high resistance to oxidation and thermal stability. These fibers are produced for the primary use in high temperature ceramic composites as a reinforcement. Hi-Nicalon ceramic fibers are available as multi-filament tows, woven cloth and as chopped fibers. For this investigation a plain weave woven cloth was used.

3. MANUFACTURING

For this study a prepreg based OOA process was utilized to manufacture the initial laminate followed by the PIP process. The initial fiber cloth mat was infiltrated

with a SMP-10/ZrB_2, cut to dimension, and laid-up in an OOA vacuum bag configuration and green cured. The samples were then removed from the bag and heated to amorphous ceramic cure temperatures. Next, the samples were re-infiltrated with a slurry bath of SMP-10 and ZrB_2. The amorphous green cure, amorphous pyrolyzation and re-infiltration processes were repeated two times; then the samples were pyrolyzed at high temperature to produce nano-crystalline β-SiC.

3.1. Slurry

The first step for production of the slurry was to ball mill the powdered ceramic additives for one hour with SiC media to eliminate any agglomerants. The powder was then subjected to a 24 hour period in a vacuum assisted drying oven at -28.9 ± 0.3 in. Hg and a temperature of 60 °C to ensure minimal moister in the mixture. As the powder completed the drying period, the resin was simultaneously degassed in a vacuum chamber for one hour at -28.9 ± 0.3 in. Hg. The two components were then mixed using a manual, high shear, vacuum assisted mixing chamber for 30 minutes at approximately 30 revolutions per min, until the mixture was fully homogenous. The slurry was then degassed for 12 hrs or until no visible bubbles were formed on the surface. It was found that introducing a vibration during the degassing of the high solids loaded slurries the required time was dramatically reduced. The slurry for the initial impregnation of the fiber mat was SMP-10 loaded with ZrB_2 at 50% by volume.

3.2. Prepreg Fabrication

The prepreg was fabrication by combining the slurry with the SiC fiber mats. The weight of the fiber mat to be infiltrated was measured and the theoretical volume was

determined from the reported density of the fibers. The slurry was measured out to produce a 40% fiber volume fraction once combined with the fiber mat. The degassed slurry was thinned by addition of methyl ethyl ketone (MEK), at 10% by volume to aid infiltration into the woven fiber mats. The viscosity of the slurry was then lowered by adding a solvent, methyl ethyl ketone, at 10% by volume. This was done to aid in infiltration and to achieve a fiber volume fraction of 40%. The fiber mats were placed on a release film and 50% of the pre-measured slurry was applied, using a spreader blade, in both directions of the weave. This process was then repeated to the reverse side of the fiber mat. After uniform impregnation, the solvent was evaporated from the fiber mat at ambient conditions for 30 min. The prepregs sheets where then sealed in dry bags and stored at -10 °C.

3.3. Laminate

The laminate was manufacture on a 40 cm x 40 cm x 0.64 cm flat Al 2024 plate. The mold was covered with fluorinated ethylene propylene (FEP) release film to prevent the resin adhering to the mold surface. The prepregs were removed from cold storage and allowed to reach room temperature prior to removing from sealed bags to prevent moisture contamination in the form of condensation. The prepregs were then subjected to a 1 hour period of vacuum assisted drying at 60 °C and -28.9 ± 0.3 in. Hg to ensure all solvents and moisture were removed. The prepreg mats were then stacked in an 8-layer $[0^o/90^o/0^o/90^o]_2$ symmetric laminate. A second FEP film was placed over the fiber layup to ensure a quality surface finish and to prevent the following layers from interacting directly with the surface of the laminate. This layer was followed by a layer of polyester fiber breather that gave passage to a vacuum hose outlet installed for trapped gases to be

evacuated. This set up was then sealed around the edges of the mold with a sealant tape that adhered to the mold and to a nylon bagging film that covered the entire mold. A diagram of this bag configuration can be seen in Figure 1. An image of the OOA set up on the flat plate mold can be seen in Figure 2. The OOA bag setup was then subjected to a 1 hr, -28.9 ± 0.3 in. Hg vacuum, to remove excess gases from between the lamina prior to the greenbody curing cycle.

3.4. Green Body Cure

During the green body cure cycle the liquid SMP-10 resin system polymerizes to a rigid, cross-linked polymer. The cure temperature profile was developed using data obtained via differential scanning calorimetry (DSC) and thermogravimetric analysis (TGA). The DSC (Q2000; TA Instruments, New Castle, DE) was performed using a ramp rate of 5 °C per minute from 25 °C to 350 °C using nitrogen as the purge gas. Three samples were tested: a virgin sample, a sample subjected to a 6 hr cure cycle at 160 ºC and a sample post cured at 200 ºC after the 160 ºC cycle. All three thermograms are shown overlaid in Figure 3. The thermogram shown in Figure 4, the virgin sample with mass of 11.539 mg, had a total heat of reaction of 360.3 J/g, an onset temperature of 183.35 ºC and a peak cure temperature of 220.67 ºC.

The TGA (Q50; TA Instruments, New Castle, DE) was performed on a virgin resin sample with a mass of 5.829 mg was heated at 10 ºC per minute from 40 ºC to 350 ºC, thermogram shown in Figure 5. It can be seen that the rate of weight loss increased as a function of temperature up to peak cure temperature. This weight loss is due to formation of volatile gases as the resin cures. This gas, if trapped in the material as it cures, will cause residual porosity and be detrimental to the final material's properties.

Using the extrapolated data from the thermograms of the virgin resin, an initial cure temperature of 160 ºC was selected with a heating rate of 0.3 ºC per minute. This was intended to restrain the rate of volatiles produced during the initial greenbody cure. This lower temperature also allowed for the use of conventional low cost bagging materials previously described.

Resin was heated to 160 ºC at 0.3 ºC per minute, while being monitored, to determine when it had cured to the point it was solid and no longer had tack. This was timed at 6 hrs. After this initial cure, a second sample, mass 8.853 mg, was subjected to DSC analysis using the same parameters as the previously described scan. It was found that it had an 80% cure. The material was then posted cured at 200 ºC for 1 hr. A third differential scanning calorimetry analysis was performed as before, with a sample mass of 5.262 mg. The material was found to be greater than 95% cured.

From this analysis the greenbody cure cycle was developed. The greenbody was initially cured at a lower temperature, 160 °C. This temperature was held, under vacuum of -28.9 ± 0.3 in. Hg, for 6 hrs. The samples were then removed from the bag setup, and an out of bag post cure cycle, ramp rate of 2.5 °C/min from 160 °C to 200 °C for 1 hr, was performed to ensure a high percent of cure of the resin system prior to pyrolyzation. The full greenbody cure cycle for SMP-10 required ~18.5 hours, shown in Figure 6. After the initial green cure, the panel was machined to a preliminary sample size of 75 mm x 105 mm with a thickness of 2.65 mm.

3.5. Low Temperature Pyrolysis

During low temperature pyrolysis the polymer's organic oligomers were thermo chemically decomposed leaving silicon carbide. The samples were heated to 800 ºC, at 1

ºC per minute, in a furnace under an argon atmosphere in accordance to the resin manufacturer's datasheet. Argon is used to prevent the reaction of the polymer chain with atmospheric gas and ensure that a near stoichiometric ratio of Si:C is produced. As the oligomers evaporate, the polymer under goes a volumetric shrinkage of 72% leaving voids in the amorphous ceramic matrix. To decrease the voids created in the samples the material was re-infiltrated.

3.6. Re-Infiltration

Re-infiltration was performed in a SMP-10 bath at 60 °C, below cure temperature, to decrease the viscosity of the resin. The samples were submerged in a resin bath to re-infiltrate the voids that formed from the prior pyrolysis processes. The samples were held in a vacuum of -28.9 ± 0.3 in. Hg until evolution of air bubbles from the composite sample stopped. The bath containing the sample was then returned to atmospheric pressure. Samples were stored at atmospheric pressure, under an argon atmosphere, the same amount of time vacuum was held to allow the resin to draw back into the samples. The process was repeated until no bubbles formed under vacuum to ensure full re-infiltration. The samples were then green cured at atmospheric conditions, and subjected to low temperature pyrolysis as previously described. The polymer infiltration and pyrolysis processes were repeated six times to attempt to decrease any residual void content in the samples. On the final cycle the samples were pyrolyzed and heat treated at high temperature.

3.7. High Temperature Pyrolysis

Once the re-infiltration cycles were complete the samples were pyrolzyed at high temperature to form crystalline ceramic from the amorphous SiC. The samples were heated at 5 °C per minute to 1600 °C under an argon atmosphere and held for 2 hours. A flow chart of this process can be seen in Figure 7. The samples were then cooled and machined to test size specifications using a precision diamond cutter (Isomet 2000; Buehler, Lake Bluff, IL).

4. POLYMER INFILTRATION AND PYROLYSIS EVALUATION

As mentioned in previous sections, voids are a main concern when producing CFCC from polymer precursors. Re-infiltration of the CFCCs is pivotal to achieve optimal material properties. This process was evaluated by tracking the increase in mass per PIP cycle to determine the percent mass increase as correlated to the number of PIP cycles.

4.1. Microstructure

The properties of CFCCs are greatly influenced by defects in the form of voids. Processing of polymer precursors inherently creates these defects; therefore the quality of CFFCs produced using the PIP process is dependent on effective re-infiltration of the material following the initial amorphous pyrolyzation. Voids in the green body are formed by several sources. Initial voids are formed in the fiber tows due to an inability for the slurry to penetrate into the center of the tows. During the lay-up process, voids are produced by air entrapment between the lamina, while other voids in the green body are formed as volatiles are formed and trapped during the cure cycle. To analyze the

effectiveness of the re-infiltrations, scanning electron microscopy analysis was performed. Samples were cut from center of un-tested flexure specimens using the precision diamond saw. These samples were then mounted using a two part epoxy resin system. The specimens were placed in a mold and a mixture of 3 parts epoxy resin and 1 part hardener was poured into the mold. The epoxy was then cured for 24 hours at room temperature. The mounted specimens were polished to a finish of 1 μm. The samples were then viewed using scanning electron microscope (SEM; S-4700, Hitachi, Schaumburg, IL) at 50X, 250X, 400X, and 2000X. The images were then post processed using ImageJ (National Institute of Health, Bethesda, MD) to analyze the void content and to determine the effectiveness of the sequential re-infiltrations.

4.2. Flexure Test

The specifics of the 3-point flexure tests performed for this investigation are based on ASTM standard C1341-06, "Standard Test Method for Flexural Properties of Continuous Fiber-Reinforced Advanced Ceramic Composites." The flexure tests were performed to provide information on the strength and to analyze the stress-strain behavior of the CFCCs. The test specimens for these tests had a span-to-depth ratio of 16:1. The support span for a sample with thickness 3 mm was set at 48 mm. The width of the sample was 9 mm to ensure that the width was greater than twice the width of the repeating unit of the weave of the fiber reinforcement. The length of the specimens was set to allow for at least 5% overhang past the outer supports to minimize shear failures and prevent the specimen from slipping through the supports. The final test specimen dimensions were set as 3 mm x 9 mm x 60 mm. Crosshead speed was maintained at 0.13 mm/sec.

5. RESULTS

5.1. Polymer Infiltration and Pyrolysis Mass Analysis

The mass analysis showed successful infiltration into the samples with an increase of percent mass gain throughout the re-infiltration process. Graph in Figure 8 shows typical curves for the mass gain through this process. The graph shows that the mass increase for the sample for the first re-infiltration ranged from 5.02% to 5.85%. The percent mass increased evenly for both samples until the third PIP process. During the pyrolysis treatment of this cycle, sample two in the graph in Figure 8 lost a significant piece from one corner, shown in Figure 9. This loss of materials continued to occur to a lesser degree for the subsequent PIP cycles.

5.2. Microstructure

The laminates that were pyrolyzed, and not subjected to any re-infiltration, had a void content greater than 40%. A typical cross section of this material is shown in Figure 10. The macro voids, voids with cross sectional areas greater than 1960 μm^2, in the inter-laminar matrix of this material, not including voids in the fiber tows were analyzed. The inter-laminar macro void content was found to be 7.2 ± 1.6%. These voids ranged from cracks to irregular shaped pockets and were found randomly throughout the material. The average size of the voids was 8006 ± 6728 μm^2. The largest of these voids were found to have a cross sectional area of 26270 $\pm$336 μm^2.

Figure 11 is a typical cross section of the material after the PIP process and final heat treatment. The inter-laminar macro void content after the final heat treatment was found to be 2.7 ± 0.3%. In this image it can be seen that the some of the macro voids that

developed from the initial fabrication process had been filled partially and some had been completely filled with SiC from the sequential re-infiltration cycles. There was a significant reduction of these voids after the samples had been subjected to the complete manufacturing process; however the average size of these voids did not decrease. Figure 12 shows a matrix with ZrB_2 particles with dense SiC along with a crack that was filled with polymer derived SiC. Figure 13 is a void that was partially filled with SiC. The void had an original cross section, prior to the re-infiltration cycles, of 11290 ± 43 μm^2. In this image it can be seen that the crack leading to the pore was filled, preventing any further re-infiltration of the void. This left a residual void with a cross sectional area of 3151 ± 36 μm^2 in the material.

The typical micro pores, voids under 10 μm across, are shown in Figure 14. These voids were interconnected and found uniformly throughout the matrix of the material. The micro void content prior to the re-infiltration process was found to be 32 ± 2.1%. After re-infiltration, image shown in Figure 15, the micro void content was significantly reduced to 6.6 ± 1.6%.

In Figure 16 an image of the fiber tows prior to any re-infiltration is presented. In this image it can be seen that there was matrix material between the fibers indicating the tows were penetrated during the prepreg manufacturing process. The weak interface between the fibers and the matrix, and the low density due to micro porosity in the matrix allowed for loss of material from between the fiber tows during the mechanical sample preparation process. As the matrix micro void content decreased from the re-infiltration process and the macro voids were filled, the loss of material from around the fibers decreased as well, as shown in Figure 17.

5.3. Flexure Test

The failures from the flexure test were tension failures at the bottom surface between the two lower supports. A typical failure can be seen in Figure 18. This image shows fiber pullout and bridging, as labeled. At the location of the fiber bridging there is a deviation in the crack progression along the fiber direction, indicated by the red arrow. These mechanisms are responsible for the graceful failure and made it possible for the samples to carry load after failure, as shown in the stress-strain curve.

Figure 19 shows a typical flexural stress versus strain curve of the CFCCs manufactured using OOA and PIP processes. The flexural strength and modulus were observed to be 27.5 ± 3.89 MPa and 12.7 ± 3.72 GPa respectively. Test results indicate that the failure of the CFCCs samples is not catastrophic compared to monolithic ceramics. The crack propagation is retarded in the CFCC due to addition of the fiber reinforcements and the less than fully dense matrix.

6. CONCLUSIONS

CFCCs were successfully manufactured using low cost OOA and PIP processes. The mass analysis showed successful infiltration into the samples with an increase of percent mass gain of up to 16% due to the re-infiltration process; however, there was damage to some of the samples during the pyrolysis cycles. The pyrolysis process will need to be investigated to prevent failure during these cycles.

The microstructure analysis shows that the samples were successfully re-infiltrated and the void content was significantly reduced. The inter-laminar macro void content was significantly reduced from 7.2 ± 1.6% to 2.7 ± 0.3%. However, the average

size of voids, 8006 ± 6728 μm^2, and the maximum size, 26270 ±336 μm^2 was not found to be reduced. It was found that cracks leading to the larger void would fill and prevent the complete re-infiltration of these voids.

The micro pores were found to be interconnected and uniformly distributed throughout the matrix of the material. The micro void content was found to be significantly reduced from the re-infiltration process as well, from 32 ± 2.1% to 6.6 ± 1.6%.

The flexural strength and modulus were observed to be 27.5 ± 3.89 MPa and 12.7 ± 3.72 GPa respectively. Flexure tests results indicate that the failure of the CFCCs samples was graceful due to addition of the continuous fiber mats and the less than fully dense matrix allowing for fiber bridging, pullout and crack deviation.

7. REFERENCES

1. Kernel, W., *Ceramic Matrix Composites*, Wiley-VCH Verlag GmbH & Co. KGaA, Weinheim, 2008.

2. Colombo, P., Mera, G., Riedel, R., and Soraru, G. "Polymer Derived Ceramic: 40 Years of Research and Innovation in Advanced Ceramics." *Journal of American Ceramic Society* 93 (2010): 1805 – 1837.

3. Verbeek, W. "Production of Shaped Articles of Homogeneous Mixtures of Silicon Carbide and Nitride." Ger. Offen. 2218960 (Bayer AG), November 8, U.S. Patent No. 3853567, 1973.

4. Yajima, S., Hayashi, J., and Imori, M. "Development of High Tensile Strength Silicon Carbide Fibre Using an Organosilicon Polymer Precursor.'' *Nature* 273 (1978): 525–527.

5. Johnson, S., Gasch, M., Leiser, D., Stewart, D., Stackpoole, M., Thorton, J., and Espinoza, C. "Development of New TPS at NASA Ames Research Center." *15th AIAA International Space Planes and Hypersonic Systems and Technologies Conference*, Dayton, Ohio, April 28 – May 1, 2008. American Institute of Aeronautics and Astronautics. pp. 1-15.

6. Nejhad, M., Chandramouli, M, and Yousefpour, A. “Processing and Performance of Continuous Fiber Continuous Fiber Ceramic Composites by Preceramic Polymer Pyrolysis: I – Filament Winding.” *Journal of Composite Materials* 35 (2001):2207 – 2237.

7. Nejhad, M., Chandramouli, M, and Yousefpour, A. “Processing and Performance of Continuous Fiber Continuous Fiber Ceramic Composites by Preceramic Polymer Pyrolysis: II – Resin Transfer Molding.” *Journal of Composite Materials* 35 (2001):2239 – 2255.

8. Lee, S., Weinmann, M., and Aldinger, F. “Processing and Properties of C/Si-B-C-N Fiber-Reinforced Ceramic Matrix Composites Prepared by Precuros Impregnation and Pyrolysis.” *Acta Materialia* 56 (2008): 1529 – 1538.

9. Yao, L., Feng, Z., and Cheng, Q. “Low Velocity Impact Damage Evaluation of 2D C/SiC Composite Material.” *Advanced Materials Research* 79–82 (2009): 1835 – 1838.

10. Zhu, S., Minzuno, M., Kagawa, Y., and Mutoh, Y. “Monotonic Tension, Fatigue and Creep Behavior of SiC-Fiber-Reinforced SiC-Matrix Composites: A Review.” *Composites Science and Technology* 59 (1999): 833 – 851.

11. Sayir, A. “Carbon Fiber Reinforced Hafnium Carbide Composite.” *Journal of Materials Science* 39 (2004): 5995 – 6003.

12. Al-Dawery, I. and Butler, E. “Fabrication of High-Temperature Resistant Oxide Ceramic Matrix Composites.” *Composites: Part A* 32(2001): 1007 – 1012.

Table 1. Properties of SMP-10 as obtained from Starfire Systems data sheet

Property	**SMP-10 (AHPCS)**
Density	0.998 g/cm^3
Appearance	Amber liquid
Viscosity	40-100 cps @ 25^{o}C
Flash Point	89^{o}C
Moisture Absorption	<0.1% in 24 hours at room temperature
Surface Tension	30 dynes/cm^2
Volatile	H
Hazard Identification	Non Hazardous
Storage	Vacuum container or inert environment; Refrigerated
Green Cure	180-400^{o}C
Amorphous SiC	850-1200^{o}C
Nano-Crystalline SiC	1250-1700^{o}C

Table 2. Properties of ZrB_2 grade B as obtained from H.C. Starck data sheet

Property	**ZrB_2**
Density	6.09 g/cm3
Appearance	Grey-Black
Hafnium	Min. 0.2%
Average Particle Size/Laser Diffraction D50	1.5-3.0 µm(90% < 6.0 µm)

Table 3. Properties of Hi-Nicalon as obtained from COI Ceramics, Inc. data sheet

Property	**Hi-Nicalon**
Fiber Denier	1800
Density	2.74 g/cm^3
Composition	62:37:0.5 wt.% (Si:C:O)
Filament Diameter	14 um
Tensile Strength	2.8 GPa
Tensile Modulus	270 GPa

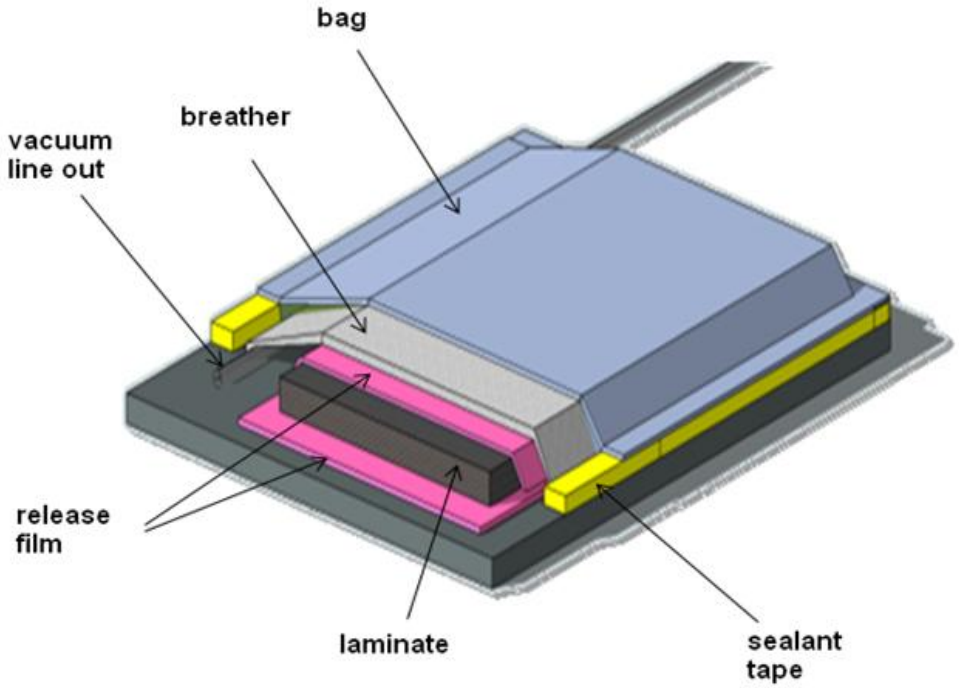

Figure 1. Out-of-autoclave bagging configuration

Figure 2. Image of flat panel out-of-autoclave bag setup

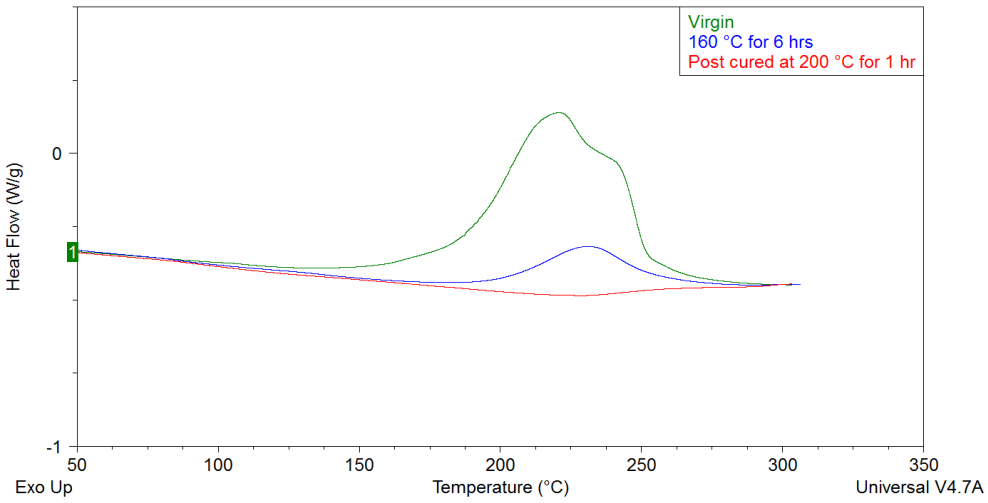

Figure 3. Differential scanning calorimetry thermogram of SMP-10 at three cure levels

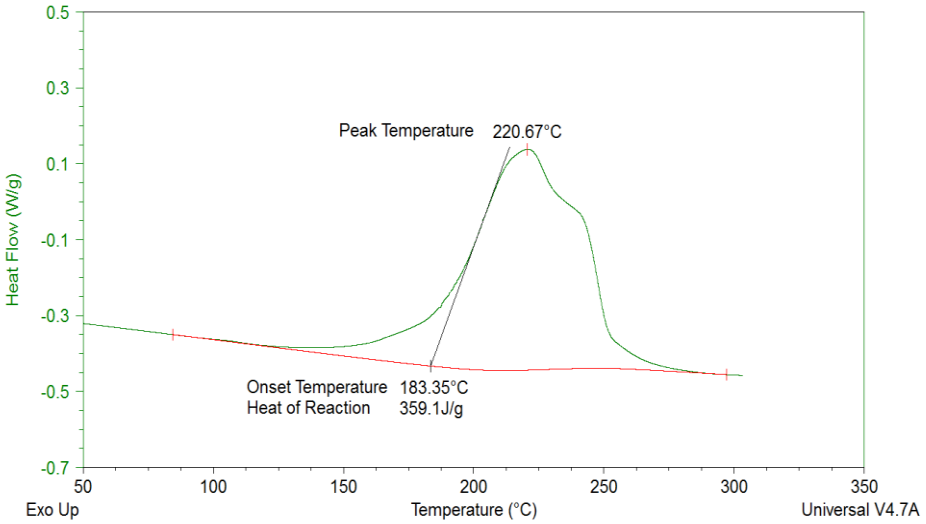

Figure 4. Differential scanning calorimetry thermogram of uncured SMP-10

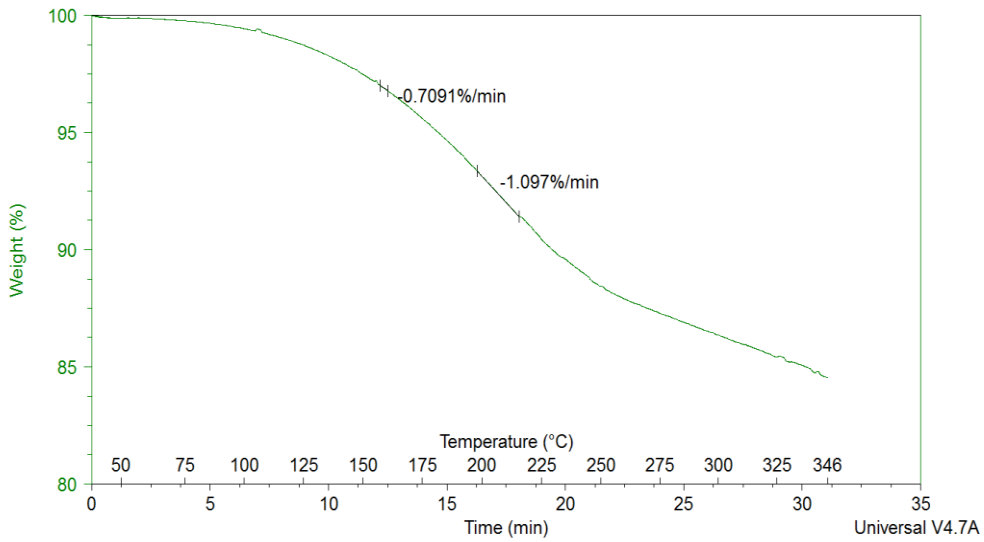

Figure 5. Thermogravimetric analysis thermogram of uncured SMP-10

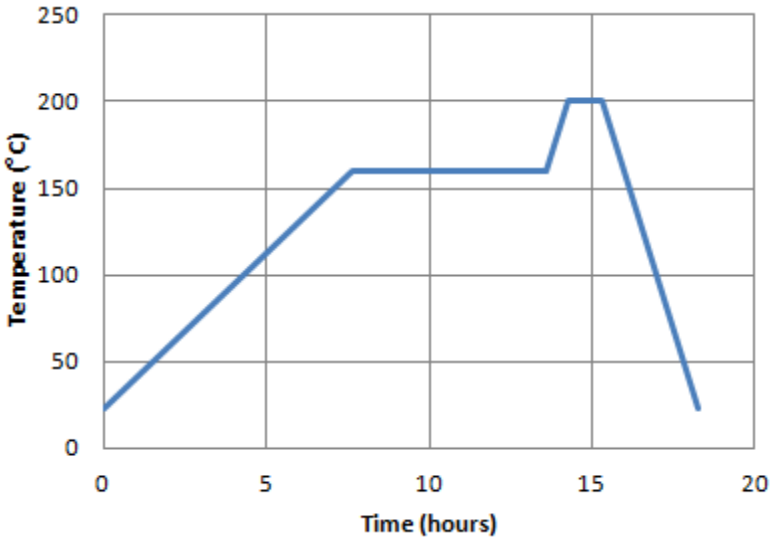

Figure 6. Greenbody cure cycle for SMP-10

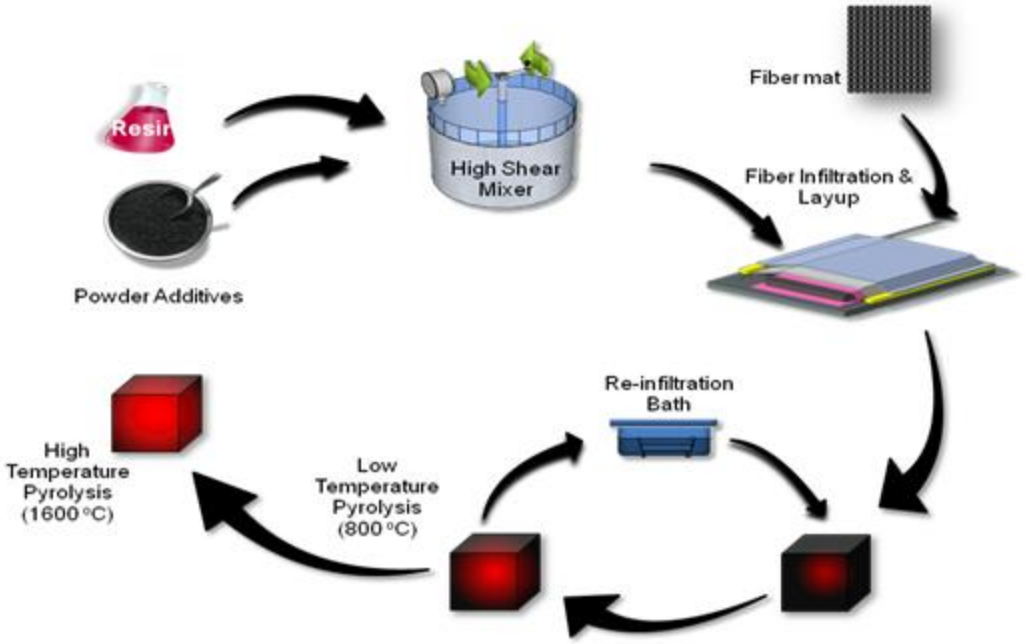

Figure 7. Flow chart of the OOA modified PIP manufacturing process

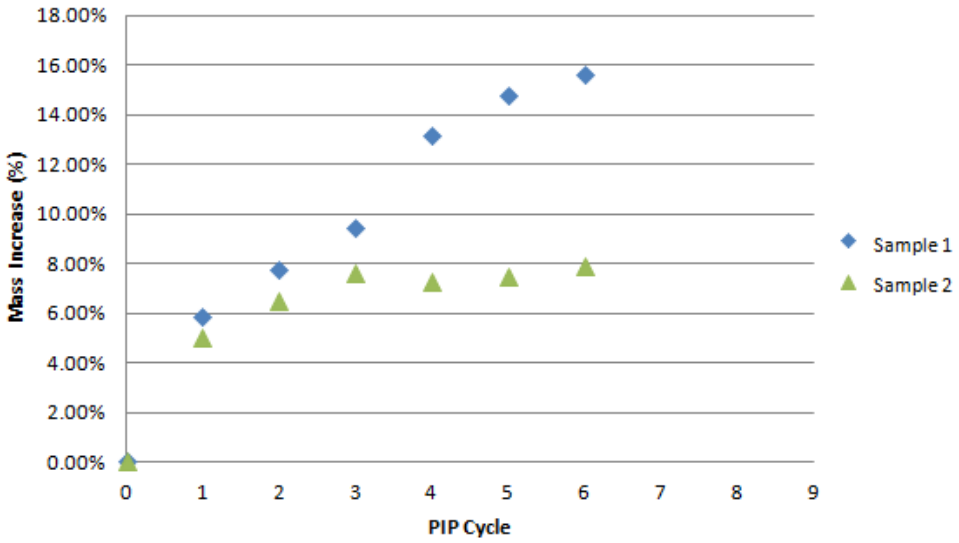

Figure 8. Graph showing the percent mass increase of the ZrB_2-SiC/SiC_f CFCCs per PIP cycle

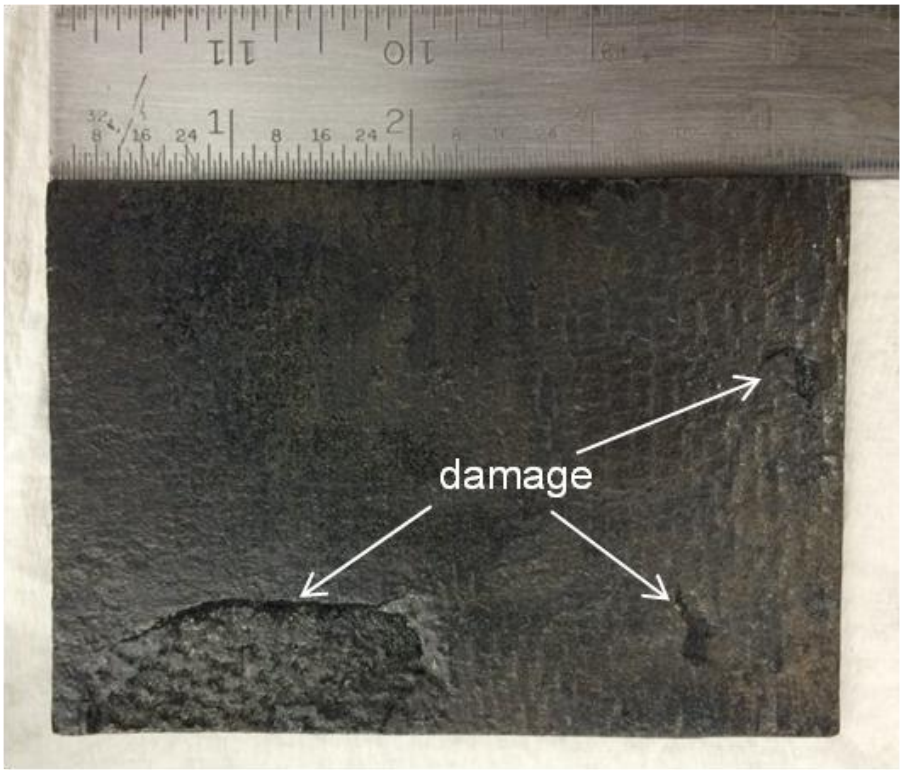

Figure 9. Optical image of ZrB_2-SiC/SiC_f sample after third PIP cycle

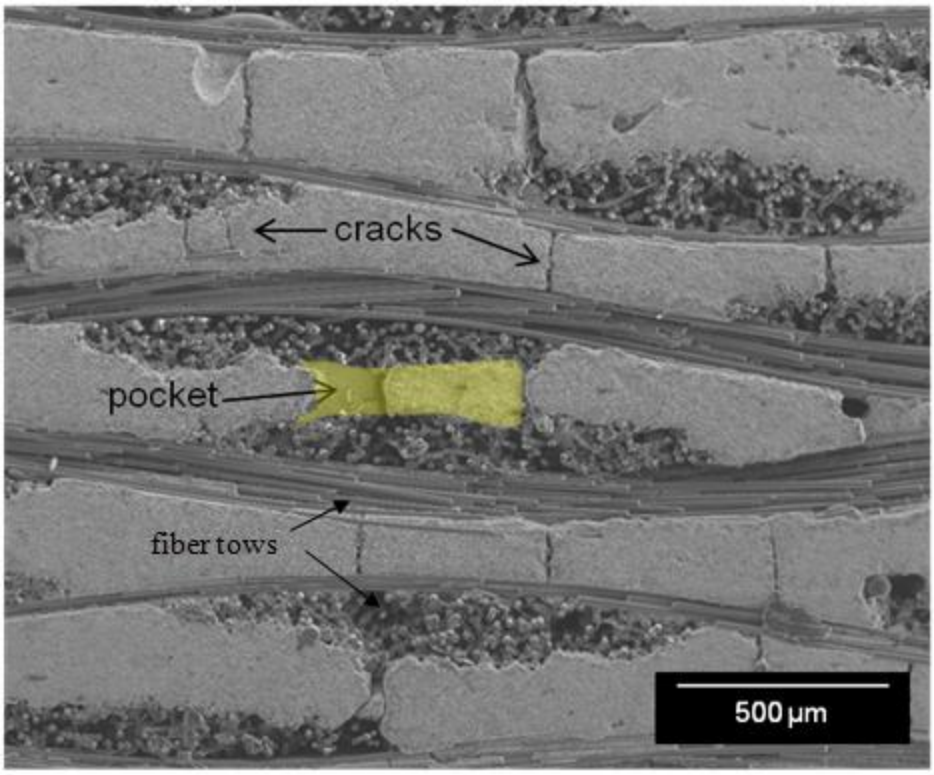

Figure 10. SEM image of ZrB_2-SiC/SiC_f showing macro voids prior to re-infiltration process

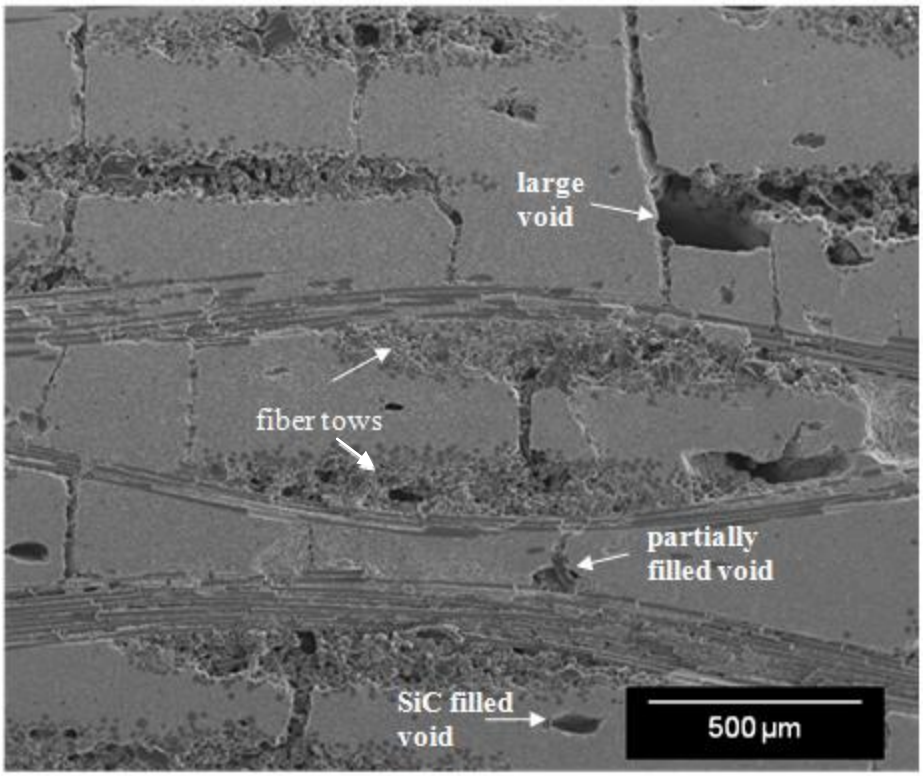

Figure 11. SEM image of ZrB_2-SiC/SiC_f showing macro voids post high temperature heat treatment

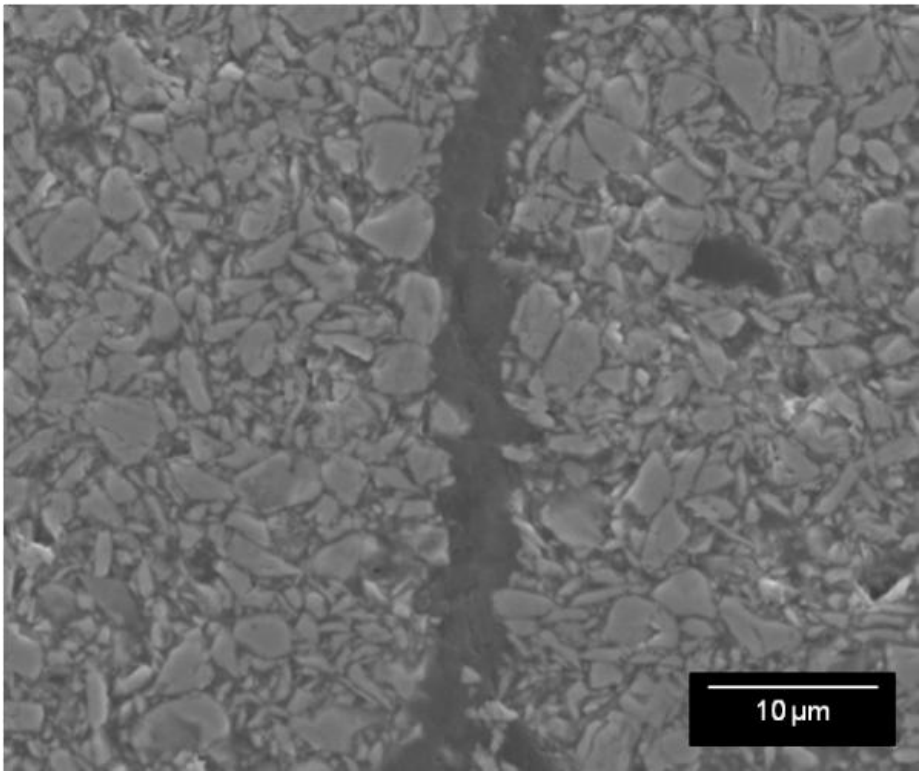

Figure 12. SEM image of ZrB_2-SiC/SiC_f show infiltrated crack post high temperature heat treatment

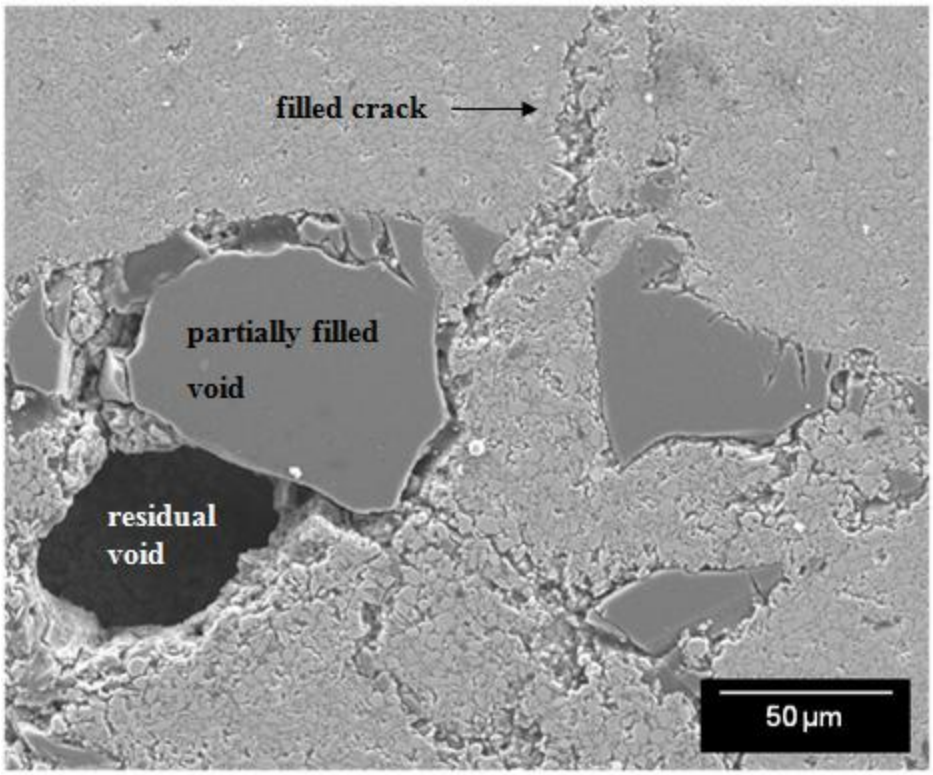

Figure 13. SEM image of ZrB_2-SiC/SiC_f showing fill characteristics of macro void post high temperature heat treatment

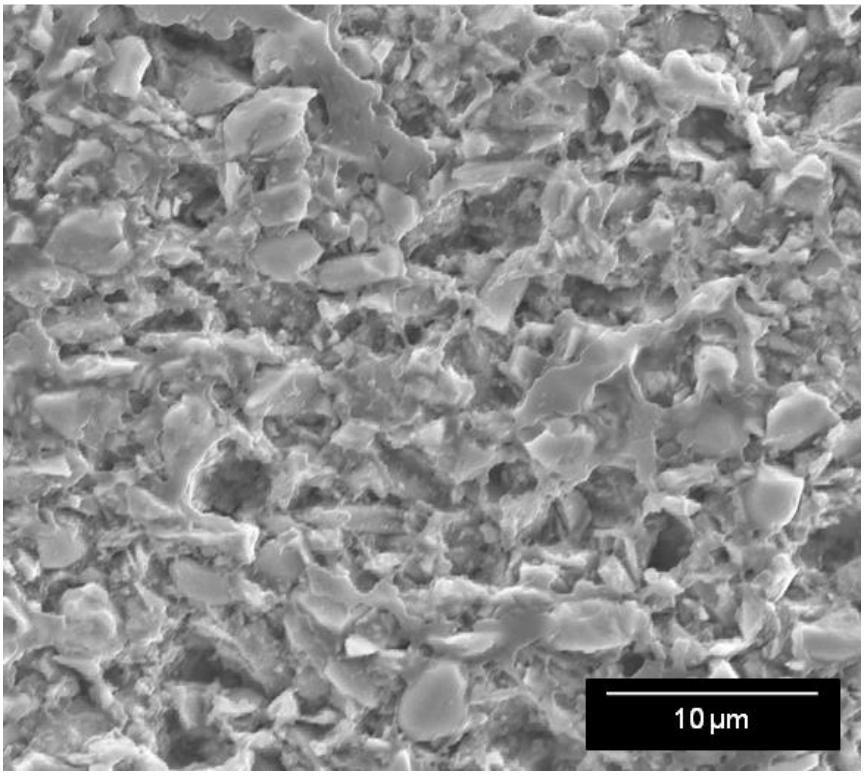

Figure 14. SEM image of ZrB_2-SiC/SiC_f showing micro voids prior to re-infiltration process

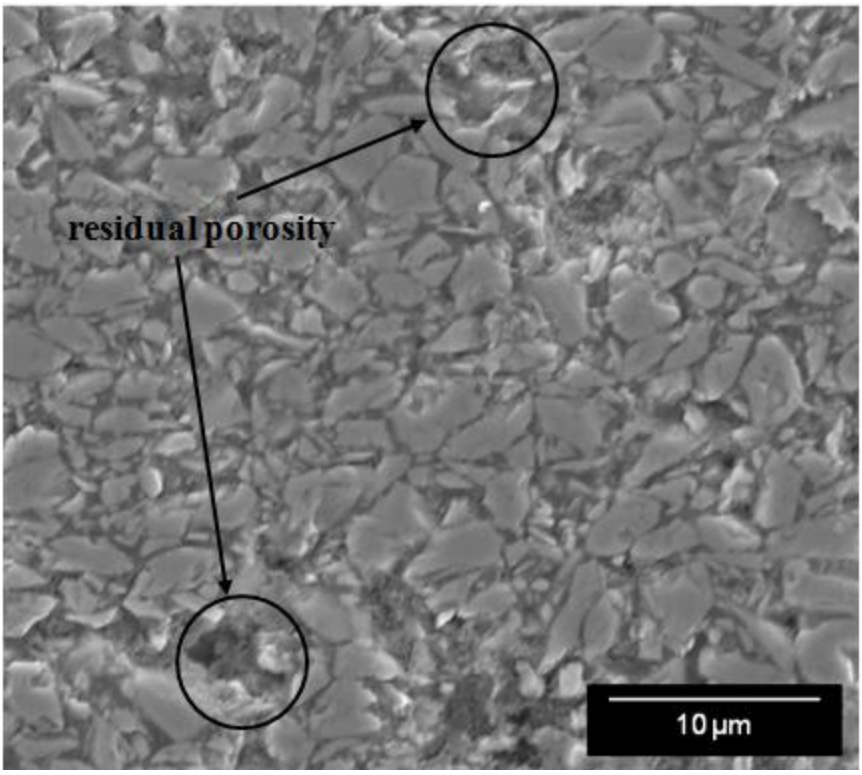

Figure 15. SEM image of ZrB_2-SiC/SiC_f showing micro voids post high temperature heat treatment

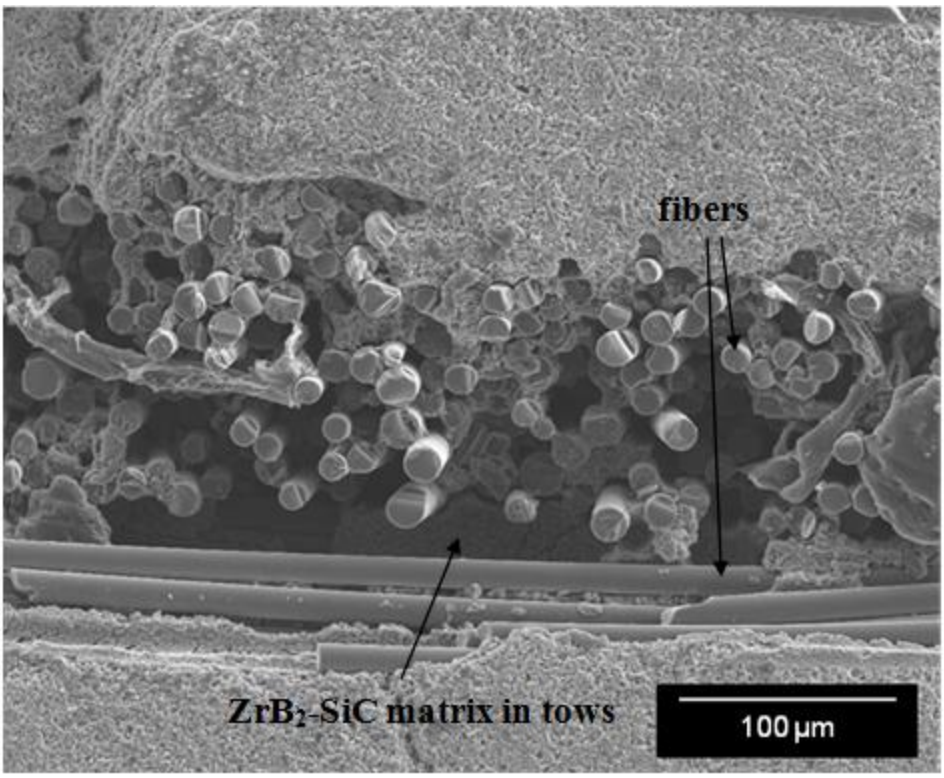

Figure 16. SEM image of ZrB_2-SiC/SiC_f showing tow characteristics prior to re-infiltration process

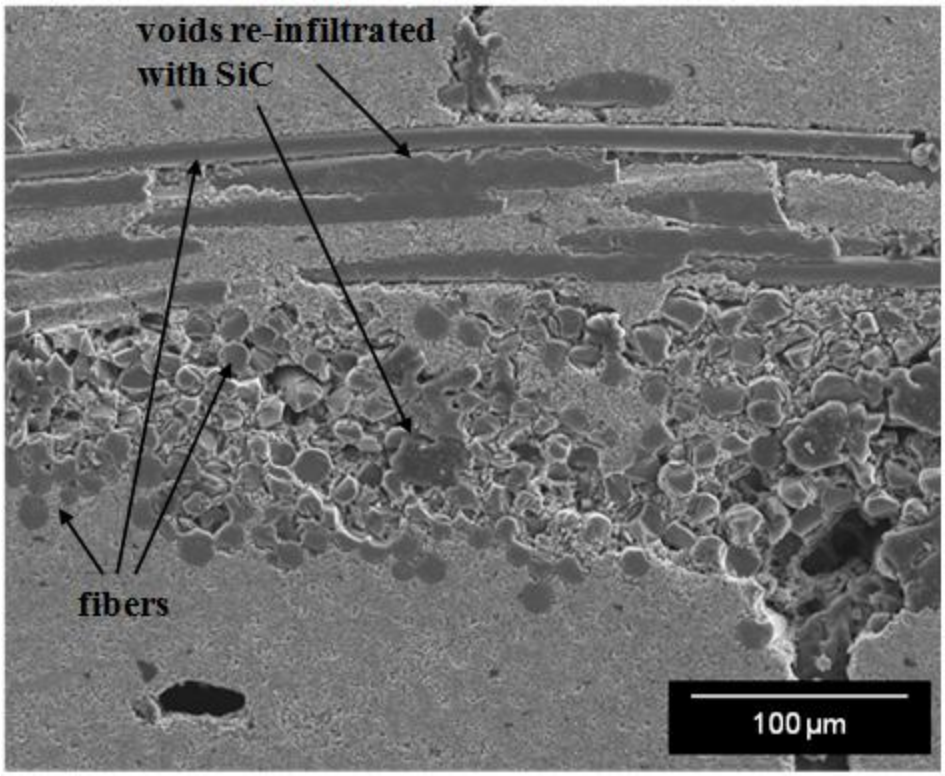

Figure 17. SEM image of ZrB_2-SiC/SiC_f showing tow characteristics after final PIP cycle and heat treatment

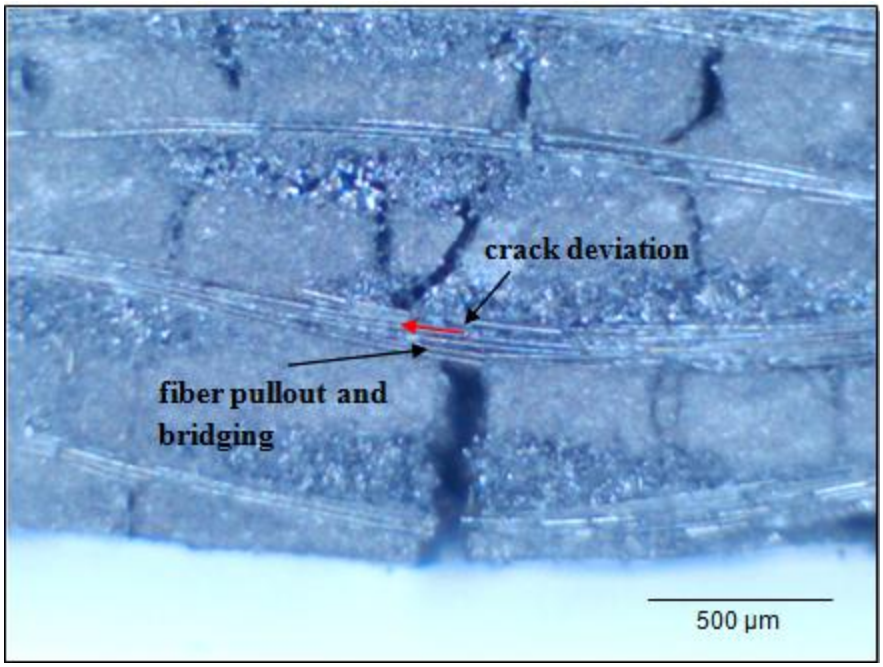

Figure 18. Optical image of ZrB_2-SiC/SiC_f CFCC flexural test specimen after testing

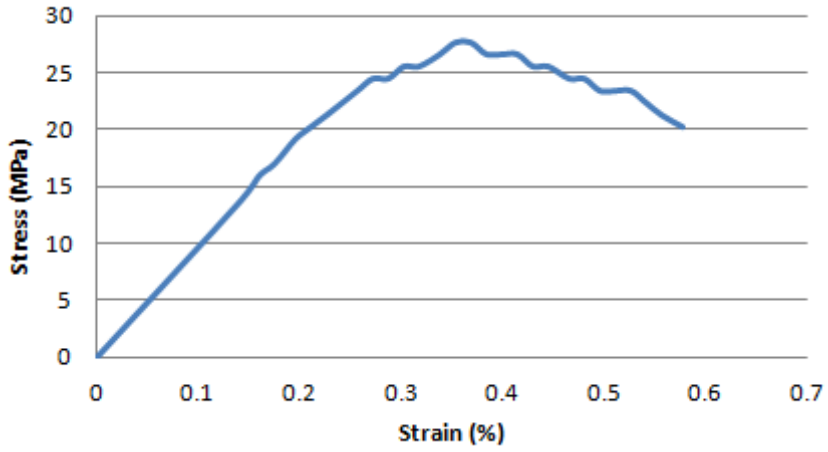

Figure 19. Graph showing typical stress vs. strain behavior of the ZrB_2-SiC/SiC_f CFCCs

II. DRY PRESS PIP FABRICATION PROCESS OF SIC/SIC$_F$ COMPOSITES FOR NUCLEAR APPLICATIONS

J. Nicholas[a], R. Meinders[a], K. Chandrashekhara[a], G. Hilmas[b] and C. Castano[c]

[a]*Department of Mechanical and Aerospace Engineering*

[b]*Department of Materials Science and Engineering*

[c]*Department of Mining and Nuclear Engineering*

Missouri University of Science and Technology, Rolla, MO 65409

ABSTRACT

Continuous fiber reinforced ceramic composites produced from the polymer infiltration and pyrolysis process for use in nuclear applications have been limited due to the problems involved with the older generation of polymers that produced materials with insufficient microstructure to withstand the harsh environment of nuclear reactors. The current study was to determine if nuclear grade materials are achievable from the polymer infiltration and pyrolysis process, with the new generation of polymer precursor producing stoichiometric SiC, and the availability of high purity fibers. Residual porosity in the polymer derived ceramic matrix is a major challenge in the fabrication of nuclear grade SiC/SiC$_f$ composites. The majority of residual pores are developed during greenbody fabrication. In the present work, a uniaxial press mold was developed to minimize the maximum size of the pores in the initial greenbody. Thermogravimetric analysis was performed to develop a pyrolysis temperature profile. SiC/SiC$_f$ samples were produced from slurry infused plain weave SiC mats. The characteristics of the pores were analyzed using SEM techniques to determine size and distribution. ASTM standards

were used to determine apparent porosity (relationship of open pores to the exterior volume), and apparent specific gravity (portion of the specimen which is impervious). The phase composition of the matrix of the SiC/SiC_f composite greatly influences the integrity of the material in the presence of nuclear irradiation induced swelling of the material. To determine the phase present in the material produced from the modified polymer infiltration and pyrolysis process, x-ray diffraction analysis was performed. The mechanical performance of the developed continuous fiber reinforced ceramic composite was evaluated using 4-point flexure test at temperatures range from room temperature to 1500 °C.

1. INTRODUCTION

Continuous silicon carbide fiber-reinforced silicon carbide composites (SiC/SiC_f) are considered excellent candidates for nuclear applications due to high thermal conductivity (120 W/m·K), low thermal expansion (4.0×10^{-6} /°C) and exceptional resistance to thermal shock without the drawbacks of monolithic ceramics. SiC engineering ceramics demonstrates high strength and chemical inertness at high temperature and has demonstrated excellent stability in high radiation environments [1-3]; however, monolithic SiC is a brittle material and is considered unreliable as a structural design component due to unpredictable strength in the presence of flaws [4]. Continuous fiber reinforcement decreases sensitivity to flaws, increases fracture toughness and offers substantial improvements in damage tolerance over monolithic ceramic materials. Complex failure mechanisms of continuous fiber-reinforced ceramic composites such as matrix cracking, delamination, fiber pull-out and fiber breakage increase the toughness of the ceramic materials [5-7].

Several processes have been applied to manufacturing of continuous fiber-reinforced ceramic composites (CFCCs). Currently, chemical vapor infiltration (CVI), and nano-infiltration and transient eutectic (NITE) processes have produced nuclear grade materials commercially, but both processes are cost prohibitive and require additives (e.g. boron, aluminum) that are inappropriate for nuclear applications [8]. The polymer infiltration and pyrolysis (PIP) process is one of the most promising methods to produce low cost CFCCs due to the low-temperature required for processing and the simple processing equipment [9-12]. Previously SiC/SiC_f composite materials produced from the PIP process have not been extensively investigated in the nuclear field due to anticipated poor radiation stability of polymer-derived SiC; however, acceptable irradiation performance through a polymer precursor route is considered achievable [13].

There are three main causes for the instability of CFCCs produced from the PIP process [14]. First, CFCCs fabricated using the PIP process have residual porosities of 10-25%. The high level of porosity not only has a negative impact on the strength but it also decreases thermal conductivity and hermeticity. With poor hermeticity oxygen can easily migrate into the material and degrade the strength of the interphase and fibers compromising the overall strength of the material. Second, non-stoichiometric matrix derived from preceramic polymers have shown poor performance due to excess carbon reacting with oxygen at elevated temperatures lowering the high temperature performance of the material produced. Third, is the phase composition of the SiC produced. The beta phase, or cubic form, of crystalline SiC has shown the best performance for nuclear application due to isotropic swelling minimizing internal stresses. To produce this phase of SiC the material must be subjected to temperature in

excess of 1200 ºC, which exceed degradation temperatures of older generations of SiC fibers [14,15].

Commercialization of high yield polymer precursors and availability of high purity, heat-resistant SiC fibers have brought new possibilities for the PIP process to produce nuclear grade SiC/SiC_f composite materials. Polycarbosilanes have reported near stoichiometric yields as high as 78% after pyrolysis with relatively low volumetric shrinkage. These same polymers have been shown to produce β-SiC at temperatures ranging from 1250 ºC to 1600 ºC. New high purity SiC fibers have made these processing temperatures possible. With these new developments, high powder loaded resin combined with the fiber reinforcement; it is possible to produce material with sufficient microstructure from the PIP process for nuclear applications.

2. MATERIAL

The material for this project was selected with the intent of producing high quality CFCCs for nuclear applications. SMP-10 (Starfire Systems, Inc. Schenectady, NY), was selected as the polymer precursor for its high ceramic yield with near stoichiometric derived SiC, relatively low volumetric shrinkage, and ease of use. Beta phase SiC powder (US Research Nanomaterials, Inc. Houston, TX) was selected as filler to limit the effect of the volumetric shrinkage of the matrix. The main focus of this study was to show that a matrix sufficient for nuclear application can be produced using the PIP process; therefore, the fiber selected was Hi-Nicalon SiC fiber (COI Ceramics, Inc. manufactured by Nippon Carbon Co., Ltd of Japan) without sizing.

2.1. Polymer Precursor

The allylhydridopolycarbosilane designated SMP-10 is a polymer precursor that can be used to produce β-SiC. This is an ultra high purity precursor that yields a near stoichiometric Si:C ratio upon pyrolysis completion. The properties, provided by the manufacturer are listed in Table 1. At room temperature the resin was a amber-colored liquid with a viscosity of 100 cps. The polymer undergoes a low temperature green cure between 180 ºC and 400 ºC. Amorphous SiC is formed at 850-1200 ºC with a high ceramic yield of 72-78% with low volumetric shrinkage. Nano-crystalline β-SiC is then formed at 1250-1700 ºC. The SiC formed is stable up to 1800 ºC in air and has a 1:1 silicon to carbon atomic ratio.

2.2. Micro Particle Filler

From the data sheet, the β-SiC particles were reported as greater than 99% pure. The powder was incorporated into a slurry for the dry press process to decrease the volumetric shrinkage during the pyrolysis stage of the PIP process and to minimize the number of re-infiltration cycles to achieve a fully dense material. Table 2 shows some of the properties provided by US Research Nanomaterials, Inc for the β-SiC micro particles.

2.3. Fiber Reinforcement

The SiC fiber selected for this study was Hi-Nicalon ceramic fiber acquired from COI Ceramics, Inc. The Hi-Nicalon fiber is a multi-filament silicon carbide-type fiber that is reported by the manufacturer to be near oxygen free and homogeneously composed of ultra-fine β-SiC crystallites and carbon. The high purity of these fibers contributes to the high resistance to oxidation and thermal stability. These fibers are

primarily produced for use in high temperature ceramic composites as reinforcement. Hi-Nicalon ceramic fibers are available as multi-filament tows, woven cloth and as chopped fibers. For this investigation a plain weave woven cloth has been used. Table 3 shows the properties provided by COI Ceramics, Inc.

3. MANUFACTURING

For this study the Hi-Nicalon fiber mats were laid into an aluminum compression mold. The resin and the micro particles were mixed into a slurry and applied to fibers in a hand lay-up process. The composite was then heated and compressed. The samples were then removed and heated to amorphous ceramic cure temperatures. The samples were subjected to re-infiltration before they were finally pyrolyzed at high temperatures to produce a higher density crystalline matrix composite.

3.1. Slurry

The slurry production started with an initial vacuum degassing of the resin and drying of the β-SiC powder. The two components were then weighed and mixed manually. The slurry for the initial impregnation of the fiber mat was SMP-10 loaded with β-SiC at 44.5% by volume. The viscosity of the slurry was then lowered to less than 125 Cp by diluting with a solvent, methyl ethyl ketone at 5% by volume. This was done to aid infiltration and to achieve a fiber volume fraction of 40%.

3.2. Laminate Lay-Up and Compression

A uniaxial dry pressing method was used to compress the laminate. This was done to eliminate any large pores. The SMP-10 was the binder for this process. An image of

the die and punch is presented in Figure 1. First the mat was cut to the shape of the die. The slurry was combined with the Hi-Nicalon fiber mat in the die to produce a fiber volume fraction of 40%. The slurry was applied, using a spreader blade, bi-directionally to increase tow penetration. After sufficient impregnation the solvent was evaporated from the fiber mat at ambient conditions. The next layer was then placed into the die and the process was repeated until a 5 layer laminate was formed. The die was then closed and compressed at 1.38 MPa (200 psi) while under a vacuum of -28.9 ± 0.3 in. Hg and held for 1 hour to evacuate any trapped gases.

3.3. Green Body Cure

During the green body cure cycle the liquid SMP-10 resin system polymerized to a rigid, cross-linked polymer. The green cure conditions, according to the manufacturer, have a profound effect on the final sample's properties. For the polymer cure cycle a heating rate of 5 ºC a minute up to 180 ºC while the die was under the pressure and vacuum previously described in the layup process was utilized. The slow heating rate was used to avoid cracking as volatiles were produced. The samples were cured at 180 ºC for 2 hours and post cured at 200 °C for 1 hour.

3.4. Low Temperature Pyrolysis

During the low temperature pyrolysis step the polymer's organic oligomers were pyrolyzed off leaving silicon carbide. Thermogravimetric analysis was performed on cured SMP-10 polymer, results shown in Figure 2, to determine a pyrolysis cycle to prevent failure of the composite due to internal pressures from volatile formed as the organics decomposed. Here it is shown that there is a small loss in weight at 200 ºC. As

the temperature increases above 200 ºC the weight decreases slightly up to just ~500 ºC then there are larger declines in mass and also step decreases in mass. The linear slope declines are due to the organic vaporizing off and the steps are due to solid masses being projected off of the scale from the internal pressure of volatile formation.

As a result, the samples were heated to 800 ºC in a furnace under an argon atmosphere following the developed pyrolysis cycle, shown in Figure 3. The argon was used to prevent the oxidation of the SiC and to produce a near stoichiometric ratio of Si:C. As the oligomers evaporate the polymer under goes a volumetric shrinkage leaving voids in the amorphous ceramic matrix. This leaves the sample brittle and weak. To decrease the voids created in the samples the material was re-infiltrated.

3.5. Re-Infiltration

Re-infiltration was performed in a SMP-10 bath. The samples were submerged and held in vacuum of -28.9 ± 0.3 in. Hg. for 24 hrs before returning to atmospheric pressure and held for 24 hrs. The process was repeated four times to ensure thorough re-infiltration. The samples were then green cured at atmospheric conditions, and subjected to low temperature pyrolysis. This step was repeated twice to decrease the void content in the samples.

3.6. High Temperature Pyrolysis

Once the re-infiltration cycles were complete, the samples were machined using a precision saw (Isomet 2000; Buehler, Lake Bluff, IL) with a diamond blade set to a cutting load of 400 grams and a cutting speed of 800 revolutions per minute. The material was cut to a preliminary sample size of 75 mm x 105 mm and pyrolyzed at high

temperature to form a crystalline ceramic from the amorphous SiC. The samples were heated at 5 ºC per minute to 1400 ºC under an argon atmosphere and held for 20 hours. The samples were then cooled and machined to test size specifications using the precision saw.

4. MICROSTRUCTURE ANALYSIS

4.1. Microscopy

The properties of CFCCs are greatly influenced by defects in the form of voids. Processing of polymer precursors inherently creates these defects; therefore, the quality of CFCCs produced using the PIP process is dependent on effective re-infiltration of the material following the initial amorphous pyrolyzation. Voids in the green body are formed by several sources. Initial voids are formed in the fiber tows due to an inability for the slurry to penetrate into the center. During the lay-up process voids are produced by air entrapment between the lamina, and other voids in the green body are formed as volatiles are trapped during the cure cycle. The void characteristics of the PIP produced material was analyzed using a Hitachi S-4700 Scanning Electron Microscope (SEM). The Hitachi S-4700 Field Emission SEM was equipped with a field emission single crystal tungsten electron gun. Samples were cut from the center of un-tested flexure specimens using the Buehler precision saw. These samples were then mounted using a two part epoxy resin system. The mounted specimens were polished to a finish of 3 μm and images were captured at 100X, 700X and 2500X magnification.

4.2. Archimedes Density (Porosity)

The porosity and density of the composite were evaluated using a test based on ASTM standard C20-00, "Standard Test Methods for Apparent Porosity, Water Absorption, Apparent Specific Gravity, and Bulk Density of Burned Refractory Brick and Shapes by Boiling Water" and C373-14, "Standard Test Method for Water Absorption, Bulk Density, Apparent Porosity, and Apparent Specific Gravity of Fired Whiteware Products, Ceramic Tiles and Glass Tiles." Square specimens with dimensions of 12.7 mm x 12.7 mm x 2 mm were dried by heating to 120 °C for 2 hours and then weighed to find the dry weight. The specimen was next submerged in water, boiled for 2 hours, then returned to room temperature and allowed to soak for 12 hours. The saturated specimen's suspended weight and the saturated weight was measured. From these measurements the bulk density, apparent porosity (relationship of open pores to the exterior volume), and apparent specific gravity (portion of the specimen which is impervious) were determined as per the aforementioned ASTM standards.

4.3. X-Ray Diffraction

The phase composition of the matrix of the SiC/SiC_f composite greatly influences the integrity of the material in the presence of nuclear irradiation induced swelling of the material. To determine the phase present in the material produced from the PIP process x-ray diffraction (XRD) analysis was performed. A PANalytical X-Pert Multi-purpose Diffractometer equipped with a PiXcel detector and a 15 sample changer was used allowing for rapid data collection with excellent signal to noise ratio.

5. FLEXURE TEST

The specifics of the 4-point flexure tests performed for this investigation were based on ASTM standard C1341-06, “Standard Test Method for Flexural Properties of Continuous Fiber-Reinforced Advanced Ceramic Composites” and C1211-13, “Standard Test Method of Flexural Strength of Advanced Ceramics at Elevated Temperatures.” The flexure tests were performed to provide information on the strength, toughness and to analyze the stress-strain behavior of the CFCCs. Specimens were tested in an Instron SFL advanced high temperature environmental system on an Instron 5881 frame using a graphite 4-point flexure test fixture. The support span of the fixture was 40 mm with a load span of 20 mm. The width of the samples was 3 mm to fit the flexure fixture. The length of the specimens was set to allow for at least 5% overhang past the outer supports to minimize shear failures and prevent the specimens from slipping through the supports. The final test specimen dimensions were set as 3 mm x 2 mm x 45 mm. The tests were performed at room temperature and up to 1500 °C.

6. RESULTS

6.1. Microstructure

The microstructure was analyzed for pore characteristics and density using the aforementioned SEM and Archimedes density and porosity measurements. The crystalline structure was analyzed using the XRD technique previously discussed.

6.1.1. Microscopy

Figure 4 shows that there was a presence of large macro voids with cross sectional areas of up to 0.27 mm^2. From Figure 5 it can be seen that the tows have been infiltrated

by polymer derived SiC matrix material. Figure 6 shows the typical micro pores, voids under 10 μm across. These voids were interconnected and found uniformly throughout the matrix of the material.

6.1.2. X-Ray Diffraction

Figure 7 is the 2-theta peak pattern produced from the XRD analysis. The top lines on the graph represent the JCPDS file for SiC as labeled. From this figure it can be seen that there was a presence of crystalline phase of SiC according to the peaks labeled; however, further investigation is needed to identify what polytypes were presence.

6.1.3. Porosity and Density Analysis

Table 4 shows the density and porosity as determined from the aforementioned process. The bulk density of the composite was found to be 2.16 g/cm^3. The apparent porosity, percentage of open pores, was found to be 22%. The percentage of closed pores was calculated to be 11%. This gives a total percentage of porosity to be 33%.

6.2. Flexure Test Results

Figure 8, shows the flexural modulus vs. temperature of the CFCCs manufactured using the DPIP processes. The modulus was found to be ~25 GPa from room temperature up to 800 °C then drop to ~22.5 GPa at 1300 °C to 1400 °C with a significant drop at 1500 °C. The flexural strength, seen in Figure 9, shows that the strength at room temperature was ~40 MPa, then increased to over ~65 MPa at 800 °C, followed by a drop back down to ~40 MPa at 1300 °C and 1400 °C with a significant loss of strength at 1500 °C.

The stress-strain curve, seen in Figure 10, shows the flexural characteristics of SiC/SiC$_f$ material produced from the PIP process. Here it can be seen that there was

graceful failure for the room temperature test with a maximum strength at just under 45 MPa; however, for the test at 1400 °C the failure became brittle in nature without any toughening from the fibers.

Figure 11a shows the graceful failure of the CFCCs at room temperature with the top of the image being the bottom surface during the flexure test. From this image the fiber pullout can be seen at the top of the image. The crack deviation can also be seen as the crack progressed through the thickness of the specimen. Figure 11b shows the brittle failure of the test specimen with no evidence of fiber pull-out and minimal crack deviation through the thickness of the specimen.

7. CONCLUSIONS

From the microscopy it was seen that there was SiC material infiltrated into the fibers tows; however, there were still macro voids that have a negative impact on the mechanical properties and will require additional re-infiltrations. The matrix was uniform with interconnected micro voids. These voids indicate that multiple re-infiltrations, beyond the two performed, were required to produce a fully dense SiC/SiC_f material. The micro voids found suggest that the matrix can be re-infiltrated to increase the density.

The finding from the porometry analysis supports the microscopy analysis. From the porometry it was concluded that there was residual porosity that was open. This indicates that additional re-infiltrations were necessary beyond the infiltrations performed on these samples. The apparent porosity was found to be 22% indicating the material could be re-infiltrated to a more dense material. The calculated 11% closed pores would imply that the highest possible achievable density would still be less than 90%.

The XRD indicates SiC crystalline polytypes were present and further investigation is required to determine the specific types present.

The flexure tests show that the material has graceful failure below 800 °C which indicates the fiber re-enforcement has a toughening effect. To increase the temperature of effective toughening, a coating on the fibers will need to be applied to ensure a weak interface at elevated temperature. The stress-strain curve indicates that this material has low strength due to the void content. Additional re-infiltrations were required to increase the material's overall performance.

8. REFERENCES

1. R. J. Price, "Effects of Fast-Neutron Irradiation on Pyrolytic Silicon Carbide," *Journal of Nuclear Materials* 33 (1969): 17-22.

2. L. L. Snead, T. Nozawa, Y. Katoh, T.-S. Byun, S. Kondo & D. A. Petti, "Handbook of SiC Properties for Fuel Perfomance Modeling," *Journal of Nuclear Materials* 371 (2007): 329-377.

3. G. Newsome, L. L. Snead, T. Hinoki, Y. Katoh & D. Peters, "Evaluation of Neutron Irradiated Silicon Carbide and Silicon Carbide Composites," *Journal of Nuclear Materials* 371 (2007): 76-89.

4. R. J. Price & G. R. Hopkins, "Flexural Strength of Proof-Tested and Neutron-Irradiated Silicon Carbide," *Journal of Nuclear Materials* 108 (1982): 732-738.

5. X. Zhang, L. Xu, S. Du, J. Han, P. Hu & W. Han, "Fabrication and Mechanical Properties of ZrB_2-SiCw Ceramic Matrix Composite," *Materials Letters* 62 (2008): 1058-1060.

6. P. Liaw, "Continous Fiber Reinforced Ceramic Composites," *Journal of the Chinese Institute of Engineers* 21 (2011): 701-718.

7. J. Nicholas, V.G.K. Menta, K. Chandrahekhara, J. Watts, B. Lai, G. Hilmas & W. Fahrenholtz, "Processsing of Continuous Fiber Reinforced Ceramic Composites for Ultra High Temperature Applications using Polymer Precursors," Proceedings of SAMPE Conference, pp. 1-12, Baltimore, MD, May 21-24, 2012.

8. A. Ivekovic, S. Novak, G. Drazic, D. Blagoeva & S. Gonzalez de Vicente, "Current Status and Prospects of SiCf/SiC for Fusion Structural Applications," *Journal of the European Ceramic Society* 33 (2013): 1577-1589.

9. J. He, M. Scarlete & J. Harrod, "Silicon-Nitride and Silicon Carbonitride by the Pyrolysis of Poly(methylsiladiazan)," *Journal of the American Ceramic Society* 78 (1995): 3009-3017.

10. L. V. Interrante, C. W. Whitmarsh, W. Shewood, H.-J. Wu, R. Lewis & G. Maciel, "High Yield Polycarbosilane Precursors to Stoichiometric SiC. Synthesis, Pyrolysis and Application," *Materials Research Society Proceedings,* San Fransico, 1994 doi:10.1557/PROC-346-595.

11. R. Laine & F. Bobonneau, "Preceramic Polymer Routes to Silicon-Carbide," *Chemisty of Materials* 5 (1993): 260-279.

12. K. Sato, A. Tezuka, O. Funayama, T. Isoda, Y. Terada, S. Kato & M. Iwata, "Fabrication and Pressure Testing of a Gas-Turbine Component Manufactured by a Preceramic-Polymer-Impregnation Method," *Composite Science and Technology* 59 (1999): 853-859.

13. Y. Katoh, K. Ozawa, C. Shih, T. Nozawa, R. J. Shinavski, H. Akira & L. L. Snead, "Continuous SiC Fiber, CVI SiC Matrix Composites for Nuclear Applications: Properties and Irradiation Effects," *Journal of Nuclear Materials,* doi.org/10.1016/j.jnucmat.2013.06.040, 2013.

14. R. Naslain, "Design, Preparation and Properties of Non-Oxide CMCs for Applications in Engines and Nuclear Reactors: An Overview," *Composite Science and Technology 64* (2004)*:* 155-170.

15. S. Goujard & L. Vandenbulcke, "Deposition of Si-B-C Materials from the Vapor Phase for Applications in Ceramic Matrix Composites," *Ceramic Transactions* 46 (1994): 925-35.

Table 1. Properties of SMP-10 as obtained from Starfire Systems data sheet

Property	SMP-10
Density (g/cm^3)	0.998
Appearance	Clear, Amber Liquid
Viscosity (cps at 25 ºC)	40 to 100
Compatible Solvents	Hexanes, Tetrahydorfuran, Ketones
Flash Point (ºC)	89
Surface Tension (N/m^2)	3

Table 2. Properties of β-SiC particles as obtained from US Research Nanomaterials, Inc.

Property	β-SiC particles
Density (g/cm^3)	3.216
Size (μm)	1-40
Decomposition Temperature (ºC)	2700
Compressibility Coefficient	$0.21x10^{-6}$

Table 3. Properties of Hi-Nicalon as obtained from COI Ceramics, Inc. data sheet

Property	Hi-Nicalon
Fiber (denier)	1800
Density (g/cm^3)	2.74
Composition (wt.% (Si:C:O))	62:37:0.5
Filament Diameter (μm)	14
Tensile Strength (GPa)	2.8
Tensile Modulus (GPa)	270

Table 4. Density and porosity of DPIP derived SiC/SiC_f material

Property	DPIP SiC/SiC_f
Bulk Density (g/cm^3)	2.16
Apparent Porosity (%)	22
Closed Porosity (%)	11
Total Porosity (%)	33

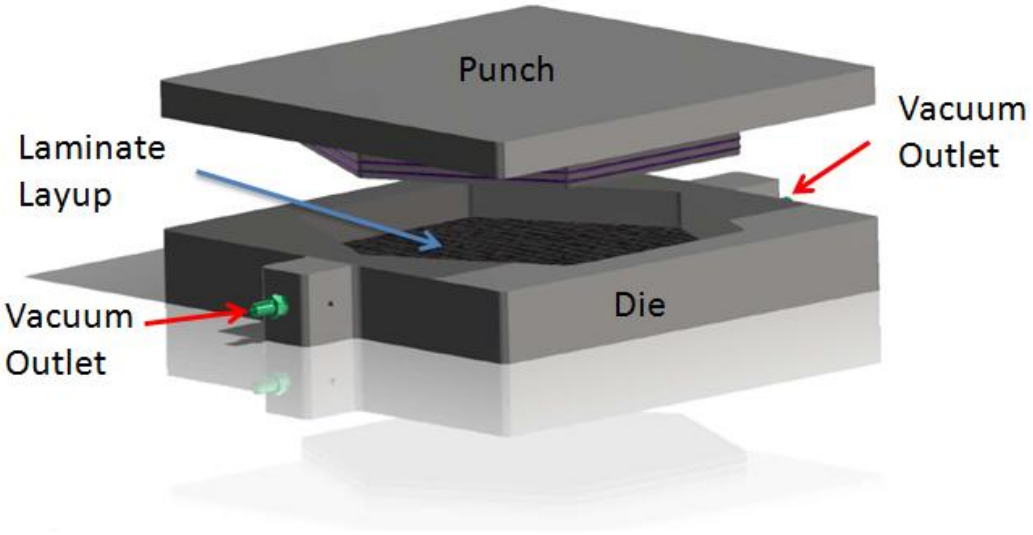

Figure 1. Die and punch developed at MS&T

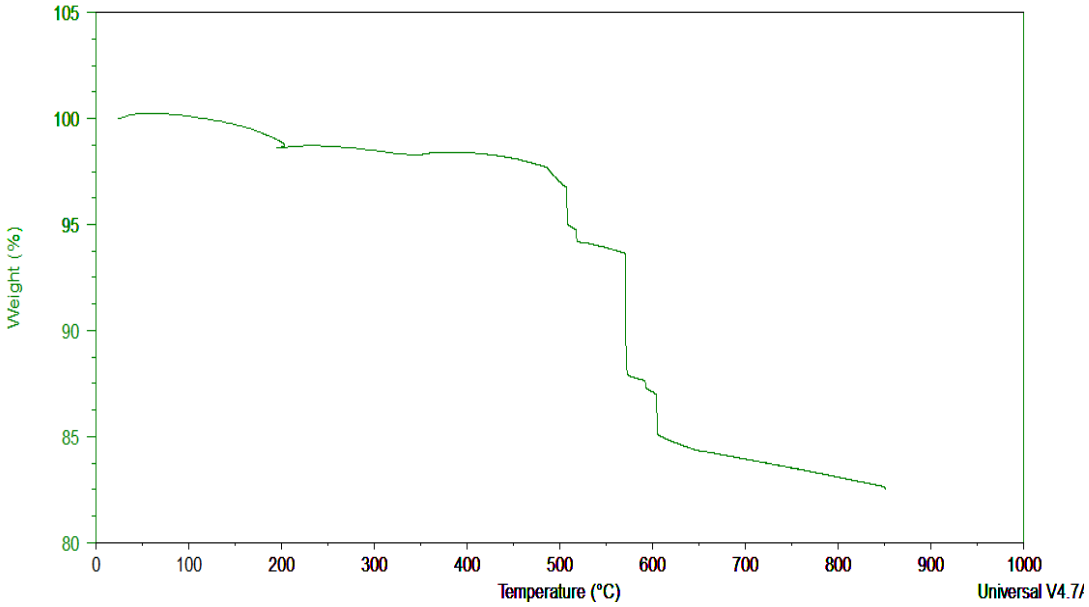

Figure 2. Thermogravimetric analysis of cured SMP-10 resin

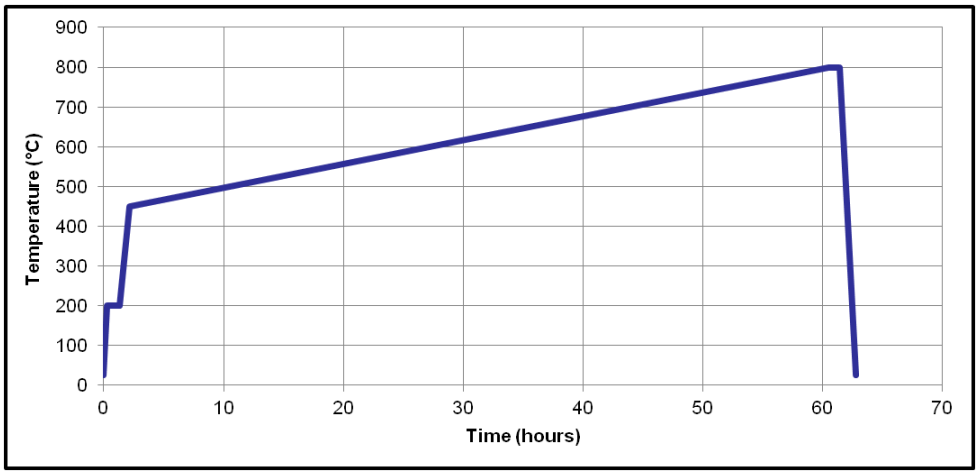

Figure 3. Developed pyrolysis temperature profile

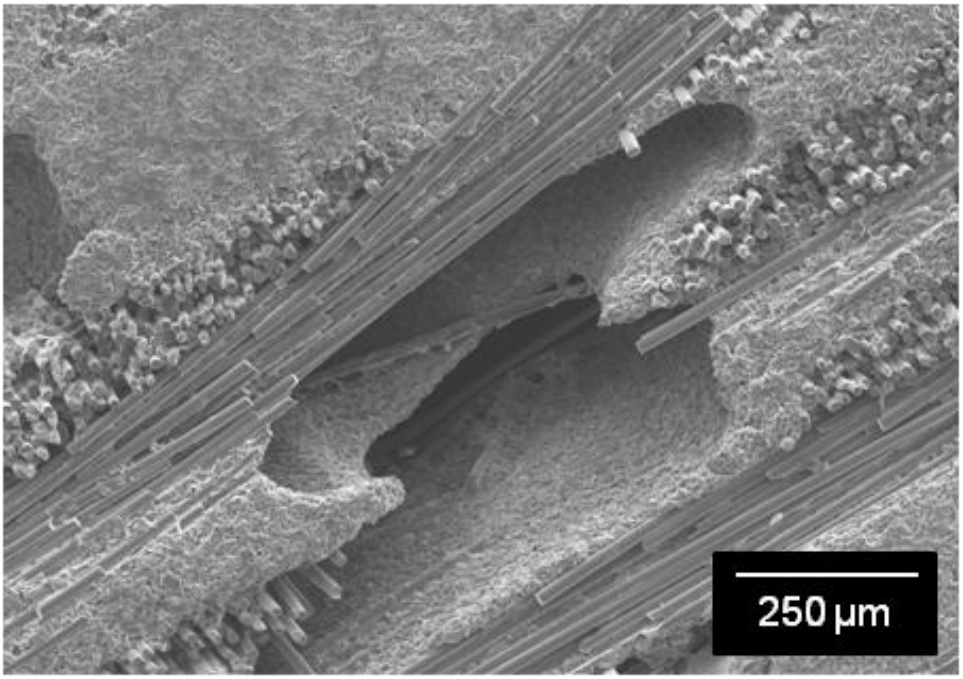

Figure 4. Scanning electron microscopic image of a large void

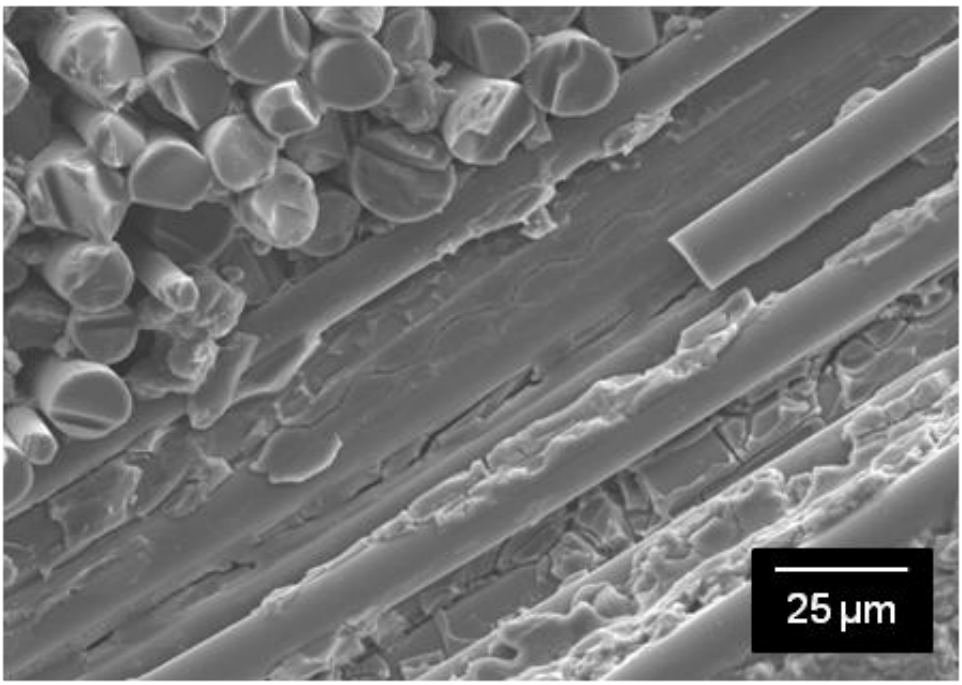

Figure 5. Scanning electron microscopic image of polymer derived SiC infiltrated into fiber tows

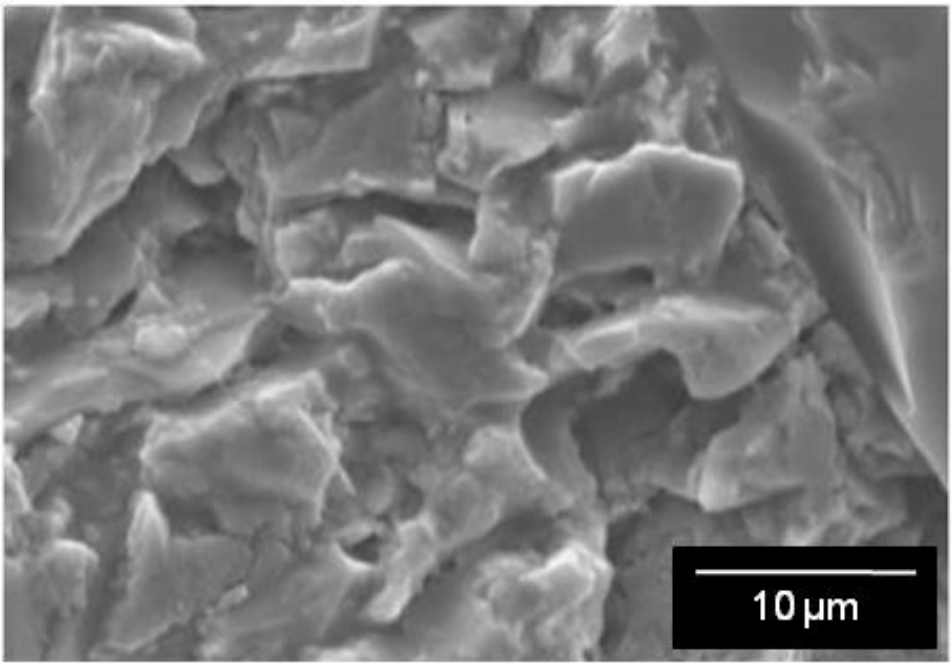

Figure 6. Scanning electron microscopic image showing micro porosity in matrix material

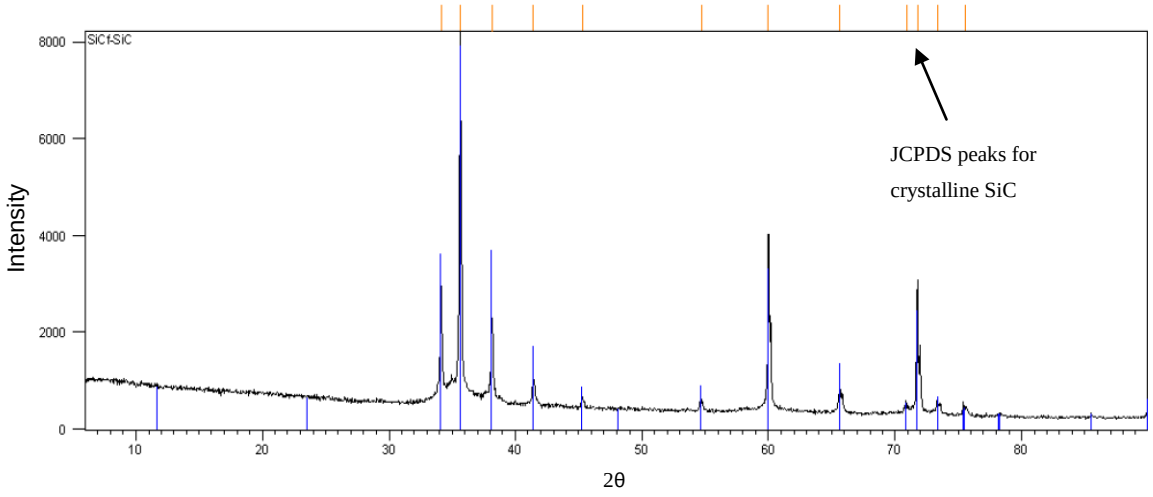

Figure 7. 2Theta peak pattern produced from XRD analysis

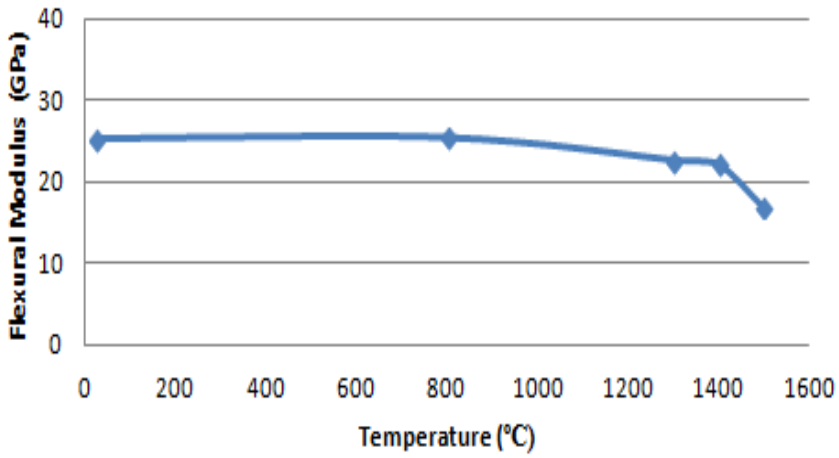

Figure 8. Flexural modulus versus temperature of the SiC/SiC_f composite

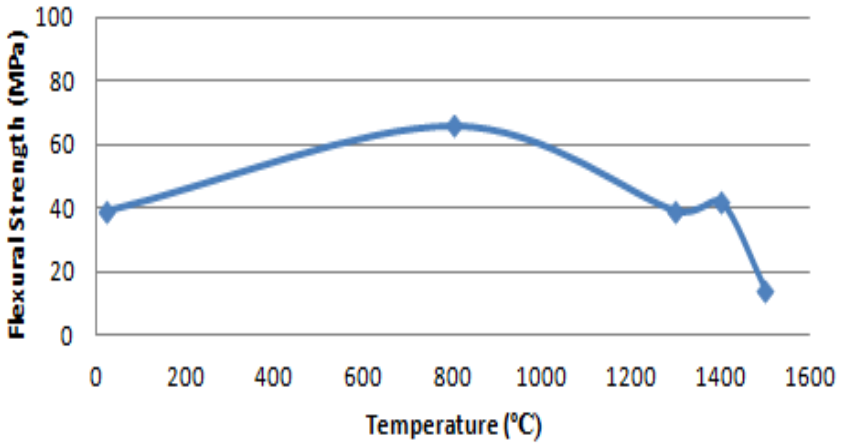

Figure 9. Flexural strength versus temperature of the SiC/SiC$_f$ composite

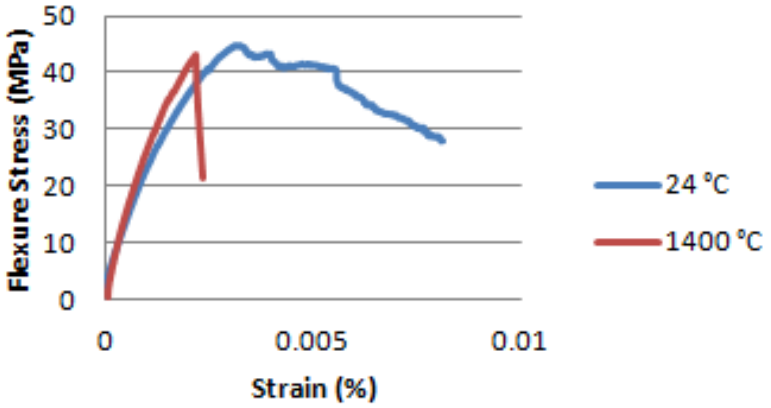

Figure 10. Stress-strain curves at 24 °C and 1400 °C

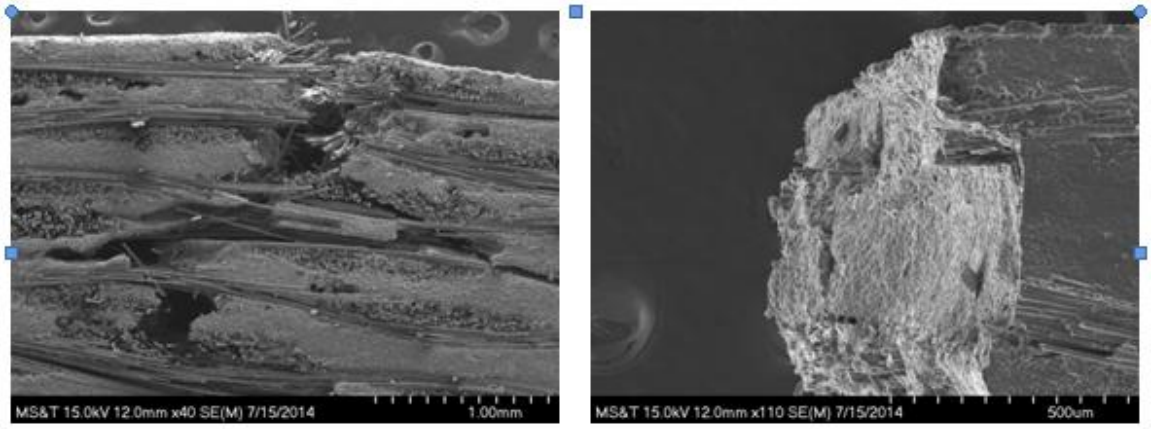

Figure 11. SEM images captured with the Hitachi S4700 (a) graceful failure (b) brittle failure

III. EFFECTS OF ACCELERATED ENVIRONMENTAL AGING ON GLASS FIBER REINFORCED THERMOSET POLYURETHANE COMPOSITES

J. Nicholas, M. Mohamed, G. S. Dhaliwal, S. Anandan and K. Chandrashekhara*

Department of Mechanical and Aerospace Engineering

Missouri University of Science and Technology, Rolla, MO 65409

ABSTRACT

In the present study, the effects on the microstructure and the impact behavior of thermoset polyurethane composite material, exposed to an accelerated aging environment, were assessed. A combined hygrothermal and ultraviolet (UV) chamber is used in an accelerated aging procedure to simulate temperate climate conditions. The samples were manufactured using a vacuum assisted resin transfer molding (VARTM) technique using a novel two-part polyurethane resin (Methylene diphenyl diisocyanate/ Polyol) infused into plane weave E-glass fiber mats. Samples were exposed to the UV/moisture rich environment for 250, 500, 750 and 1000 h. Effect of UV exposure on color change of composite specimens was evaluated using colorimetry. The rate of color change and the total change in color for the fiber reinforced composite was shown to be much less than that of pure polyurethane. Optical microscopy observations revealed that the color change was limited to surface discoloration due to the fiber reinforcement limiting degradation to the surface polymer matrix microstructure even after extended UVexposure. The accelerated aging effect on the glass fiber reinforced polyurethane was examined using low velocity impact tests to evaluate impact properties of the material throughout the aging process. The test showed that the bulk composite material was

resistant to the UV aging by demonstrating no significant change in impact properties due to the accelerated aging process.

1. INTRODUCTION

Polyurethane (PU) composites have become an accepted alternative in the infrastructure industry, especially for applications requiring high strength and durability. Polyurethanes have several factors the make them desirable polymers for composites. PU systems are a low cost, high performance polymer. Polyurethane durability contributes significantly to the long lifetime of many products. This longevity of PU products life cycle leads to a resource conservation, an important environmental considerations that often favor the selection of polyurethanes. Another significant factor in the success of polyurethane is the ability to produce PU in various forms, from flexible, easily deformed to rigid load bearing materials. Polyurethanes made from petroleum-based polyols and isocyanates have achieved widespread applications in foams, coatings, structural materials and in composites due to their excellent abrasion resistance, toughness, strength, cost benefits and potential environmental reliability [1,2]. By use of various polyols and polyisocyanates, polyurethanes can be created to be both thermoplastic or thermoset polymers, and their mechanical, thermal, and chemical properties can be designed for the intended purpose [2-4]. There is a wide range of isocyanates and polyols commercially available thus leading to almost unlimited possibilities for polyurethane material formulations. Because of the inherent versatility in polyurethane synthesis, the properties of this class of polymer can be easily engineered to their intended application's environments and make an excellent component for a fiber reinforced composite material

[5-7]. Two serious threats to the potential durability of composite laminates are their susceptibility to environmental exposure and to impact damage [8].

One potential use of polyurethane composites is in structural applications. Many structural applications will involve exposure to environmental effects such as moisture and ultraviolet (UV) exposure cycles, which lead to a reduction of the physical and mechanical properties of the polymer [9]. Many efforts have been made to investigate the effects of UV on polyurethane and improve the UV stability PU [9-18]. UV exposure has been shown to change the color of the PU material caused by the photo-oxidation of Methylene diisocyanate (MDI) in the central methylene group leading to the formation of hydroperoxides that then lead to the formation of quinine-imide structures, known as strong chromophores, resulting in the discoloration of the PU [14]. Jana and Bhunia [18] have studied the effects of UV aging on physicomechanical properties of two part thermoplastic polyurethane. The results showed after 720 h of UV aging that there was an increase in surface roughness of samples and some ridges were observed to form on the surface. As the UV aging increased to 2160 h the surface roughness increased further and large holes formed that significantly reduced the mechanical properties. It has also been found that photo-oxidation of PU surface leads to an increase in surface free energy and its polar component; simultaneously, water adhesion to polymer increases significantly during UV-irradiation. These phenomena increase the potential for degradation during the aging process [2]. Studies have shown that the degree that the environment affects the polymer depends on the specific chemical properties of the polymer and that there is a direct link between physico-chemical and mechanical change with extended environmental exposure [8,10,18-21]. Connolly et al. [19] studied the changes in physical

properties due to UV, environmental exposure and chemical exposure for polyurethane (PU) and unsaturated polyestereurethane hybrid (UPE-PU) resin-based profiles with identical glass fiber reinforcement. The study showed varying results depending on the chemical characteristics of the polymer. With new formulations of PU being used to make polymer composite there is a need to study how the environment affects these new materials.

Residual impact damage from tool falling during manufacturing or installation, hail damage or other low velocity impact event greatly affects the mechanical properties of composite materials. Many studies have been performed to investigate both numerically and experimentally the low velocity impact damage modes of composites such as surface indentation, matrix cracking, fiber breakage, delamination and fiber shear-out [22-25]. These damage modes can be difficult to visually detect and are known to be detrimental to the mechanical properties of the composite with the greatest effect on the compressive strength after impact as found by Challenger [26] and Ghelli et al. [27]. Several studies have been concentrated on the understanding of the low velocity impact behavior of laminate composites subjected to environmental conditioning [8,28-31]. These studies have shown a degradation of impact resistance due to exposure to aging environment. Pang et al. [31] report that after UV radiation the glass reinforced epoxy impact specimens were more vulnerable to impact induced damages. In their study, extensive delamination, interfacial debonding and matrix cracking occurred in the UV attacked specimens. Kim et al. [8] investigated the internal damage and compressive residual strength variation of accelerated-aged woven Glass/Phenolic composite laminate by impact loading. The results show that, as aging time increases, initial failure energy

and residual compressive strength decrease. As aging cycles increase, failure initiation energy is decreased due to surface degradation caused by ultraviolet light. These studies have found that exposure to the aging environment has enhanced the damage effects of the polymer composites tested. Although studies have been conducted to evaluate the affect of aging on the impact properties of a number of composite systems, there is currently a lack of understanding of the affect of UV radiation on the impact properties for glass fiber reinforced thermoset PU.

The present work is aimed to examine the aging behavior of new generation thermoset PU composite exposed to accelerated weathering conditions. Glass fiber reinforced flat plates specimens are fabricated, conditioned, impacted and examined using microscopy. The effect of accelerated aging on the microstructure and impact resistance properties of composite laminates are studied by comparing samples with varying exposure times to a control sample that was not subjected to the aging environment.

1.1. Materials and Manufacturing

In this work, woven fiber based composites were chosen because they offer improved performance over unidirectional type composites. The woven fiber structure increases resistance to matrix splitting and delamination growth from impact damage [32]. The plain weave E-glass fiber mats, coated with a sizing to ensure compatibility with the PU resin system, were obtained from Owens Corning Inc. OH.

Low viscosity thermoset polyurethane resin system compatible with VARTM was obtained from Bayer MaterialScience, PA. The two-part PU resin system consists of two components. Component A is an Isocyanate (NB#840859 ISO) namely, Methylene

diphenyl diisocyanate (MDI-Aromatic). Component B is a Polyol (RTM NB#840871). The mix ratio by weight for the A and B components is 92:100 (manufacturer recommended). The major challenge in using this PU resin system for vacuum infusion processes is moisture sensitivity. The isocyanate portion of the reacting components tends to react with water to produce carbon dioxide, which results in foaming. To address this issue, the mold is heated to 200 °C and cooled in a dry environment to room temperature ensuring removal of all moisture from the mold. Also to remove adsorbed moisture, and prevent void formation, E-glass fibers and all bagging materials used are dried at 110 °C for several hrs prior to manufacturing. Six panels, measuring 12 in. x 12 in., with six layers of E-glass fiber are manufactured utilizing a double bag VARTM process. Figure 1 shows the VARTM process setup.

Fiber reinforcement layup is prepared on a rigid aluminum mold with a layer of removable plastic flow-enhancement medium to reduce fill time. A layer of peel ply is used to facilitate easy removal of manufactured part. The layup was sealed using a vacuum bag under a 28 in. Hg vacuum. The layup was infused at room temperature and cured at room temperature (24 °C) for 8 h, followed with the post curing cycle of 70 °C for 1 h and 80 °C for 4 h, the final thickness of the composite plate was measured to be 3 mm (0.118 in.). Specimens were cut to the required sizes from the panels manufactured.

1.2. Accelerated Aging

To study the effect of in use environmental aging on the polyurethane composite samples a simulated accelerated aging environment was created using a QUV Accelerated Weathering Tester. The tests were performed in accordance with ASTM G154. The test chamber is equipped with UVA-340 fluorescent bulbs to produce an

accurate simulation of sunlight in the critical short wavelength region of the spectrum; wavelengths from the solar cut-off of 295-365 nm at an irradiation of 0.89 W/m^2. The chamber was operated under a repeated aging cycle conditions of 8 hrs UV exposure at 60 ºC in a dry environment, followed by a 4 hrs condensation cycle at 50 ºC without UV radiation. Sixty samples with size 76.2 mm x 76.2 mm x 3 mm (3 in. x 3 in. x 0.118 in.) were placed in the chamber for aging. A portion of the specimens were removed from the QUV chamber test at regular time intervals of 250 hours. The samples were held at ambient conditions for 24 h prior to testing. A representation of the aging cycle can be seen in Figure 2.

1.3. Colorimetry

The PU composites were analyzed for color change based on ASTM D2244. The observed color change was measured using images captured with an 18 megapixel digital camera with RGB primary color filters and fixed low pass filter in front of a complementary metal oxide semiconductor image sensor. Samples, of size 10 mm by 4 mm, were cut from the aged panels. The images were illuminated/captured with a 45°/0° configuration to reduce glare effects. The images were then analyzed using Photo Shop software to determine the average RGB levels of each sample. The RGB information was then converted to tristimulus values X, Y, Z then into color coordinates for CIEL*a*b* with a reference white of D65/0°. The total color difference ΔE was calculated with the virgin composite as the reference.

1.4. Microstructure Analysis

To determine microstructure changes due to exposure to accelerated aging environment, the samples were analyzed using microscopic techniques. Cross-sections of the virgin and aged samples were analyzed and compared using optical microscopy. Sample cross-sections were cut from the panels to the size of 10 mm by 4 mm then mounted in an epoxy mounting system for polishing and microscopic observation. The mounted samples were initially rough ground to a flat surface and then incrementally polished down to 0.05 microns using an automatic polisher. The samples were then viewed using a HiROX optical microscope model KH-8700 at 500x magnification and digital images were captured. Using ImageJ post processing software the depth of the top weave fibers from the surface of the samples were measured at 10 locations for the environmental exposure times of 0, 250, 500, 750 and 1000 hrs and then analyzed.

1.5. Impact test

Low velocity impact characteristics of six layers woven E-glass/PU laminates were conducted based on ASTM D7136/D7136M-15 in order to compare the results for virgin and aged laminates. A Dynatup Instron Model 9250 impact testing machine with both impulse control and a data system was used to conduct the low-velocity impact tests. The machine uses a free-fall hemispherical impactor comprised of a hardened steel tup with a diameter of 12.7 mm (0.5 in.) and mass of 6.48 kg. The required energy was controlled by the set drop height. The low-velocity impact test fixture is made of steel, with a 44.45 mm × 44.45 mm (1.75 in. × 1.75 in.) opening with the 3 mm thick test specimens at 76.2 mm 76.2 mm (3 in. x 3 in.) were clamped along all four edges. In this

study, the effects of three different impact energies (10, 20, 30 J) were investigated on the samples with the environmental exposure times of 0, 250, 500, 750 and 1000 hrs. Each test was replicated three times. The contact force, deflection, contact times were recorded and the absorbed energy was calculated. Digital image processing of transmission and reflective light photography was used for external damage and internal damage evaluations respectively.

2. RESULTS AND DISCUSSION

2.1. Colorimetry

Figure 3 shows color variation of PU composite sample tested at Missouri S&T composite lab. From left to right the color change can be seen from virgin material to 1000 hrs at 250 hr increments. The CIEL*a*b* values for the total color change can be found in the graph of Figure 4. The PU profiles appear to have a more rapid color change up to 750 hrs exposure with a significant decrease in change between 750 hrs and 1000 hrs. This color change trend is similar to the previous findings; however, the rate of change for the current study is much slower and the total change slightly less, compared to the results reported previously. Rosu et al [13] studying pure PU, found that when using a UVA-351 to simulate the UV spectral portion of sunlight filtered through a window there was 70% of the total color change in the first 40 hrs with max ΔE of above 30 after 200 h exposure. The findings from the current work show that it took greater than 500 h for ΔE to reach 70% of the total color change with max ΔE below 25 at 1000 h exposure.

The polyurethane resin contains nearly 50% by volume isocyanate, which is very susceptible to discoloration [13]; therefore, the matrix of the composite becomes darker. This color shifting can be ascribed to oxidation reactions which lead to the formation of an oxidized layer on the polymer surface. This layer can be seen in Figure 5. In this image, it can be seen that the discoloration occurs only on the surface directly exposed to the UV radiation where as the opposite surface has no discoloration. It can also be seen that the matrix rich areas of the surface have greater depth of color change (left and right peripherals of the image) and that the glass fibers tend to retard the penetration of the UV oxidative damage. These observations are in good agreement with those found in a study by Rek and Bravar [12] which have shown the formation of an oxidized structure for aged polyurethane following UV irradiation. Woo et al. [33] have also shown that UV-exposure darkens the color of polymer composites.

2.2. Microstructure Analysis Results

The microscopic images of a virgin sample, image (a), and one that has been exposed for 1000 hrs, image (b), to the aging environment can be found in Figure 6. It can been seen in image 6(a) that the PU matrix component covers the fibers completely; however, in image 6(b) there are fibers that have been exposed at the surface. This is due to the surface being modified by the aging process. During aging of the PU the urethane linkage (C-NH) is the most sensitive to UV degradation. The breakage of the urethane bond combined with the elevated temperature in the UV chamber (50-60°C) facilitates the movement of the soft and hard segment to form aggregates inside the polymer structure. These soft and hard segment phase separation usually exists in polyurethane materials, however, it only exists on a small scale within the polymer chain [18]. The

polymer under goes a phase separation allowing the soft segment to have more freedom to move after the breaking of the urethane linkage in the polyurethane chain and the hard segments then undergo enthalpy relaxation resulting from the physical aging of these amorphous segments [9]. These combined phenomena result in the surface retracting and allowing the fibers at the surface to be exposed.

The evolution of fiber exposure is represented by the box plot in Figure 7. On this plot the average depth is represented by the data point and the maximum and minimum depth measurement is represented by the error bars for each exposure time. Here it is shown that the average depth is 20 μm before environmental exposure and drops to -10 μm at 1000 hrs of exposure to the accelerated aging environment. With the average depth at -10 μm at 1000 hrs many of the fibers in the top weave are exposed. The maximum depth is still in the positive regime implying that there were still some fibers covered by the matrix. On the opposite end of the extreme, the minimum shows that the depth of the fibers can reach -25 μm. With the average diameter of the fibers being 20 μm this minimum means that there is complete fiber exposure. This can be seen in the image 6(b). The exposure of fibers can prevent the transfer of load from fiber to matrix in the surface of the composite and reduce the mechanical properties of the bulk composite.

2.3. Impact Test Results

The results of the impact test of the glass fiber reinforced polyurethane after aging shows that the composite has better resistance to UV damage than pure polyurethane and alternative polymer reinforced composites. As previously stated other composites systems have shown degradation in impact resistance due to exposure to aging

environments. The current study shows no evidence degradation of bulk impact properties.

The impact damage of a virgin specimen is shown in Figure 8. Figure 8 (a-1) and (a-2) is a sample that was subjected to impact energy 10 J. In this image moderate through thickness cracking of the matrix in the impacted surface can be seen with slight fiber shear-out on the reverse side. It was observed that an impression of the tup was left on the impacted surface. Internal delamination due to mismatched binding stiffness propagating along the woven fibers can also be seen in this image. With impact energy events increased to 20 J and 30 J, Figure 8 (b-1)/(b-2) and Figure 8 (c-1)/(c-2) respectively, the impacted surface showed an increase in through thickness matrix cracking with a more significant tup impression as the energy of the impact event increased. It was observed that the internal delamination area became more extensive along with an increase in fiber shear-out. Delamination in the outermost layer on the opposing side propagated along the woven tow for the higher energy events. For the impact energy of 20 J the opposing surface showed an increase in fiber shear-out along with slight fiber breakage. For the impact energy of 30 J fiber breakage on the impacted surface and significant fiber breakage and shear-out on the opposing surface were observed.

The age accelerated samples showed similar damage characteristics as the unexposed samples. There was no increased through thickness matrix cracking, fiber shear-out or breakage. There was however a measurable difference in the total area of delamination. Figure 9 compares the average measured delamination area, including the standard deviation, to the hours the samples were exposed to the UV aging environment

at the impact energies of 10 J, 20 J and 30 J. From this data it was determined that the average impact damage area decreased as the samples were exposed to the aging environment for 1000 hours by an average of 28%, 24% and 26% for 10 J, 20 J and 30 J impact energies respectively. The decrease in damage area is attributed to the surface erosion of the matrix and to embrittlement of the matrix. The greater variance of the area of damage at higher impact energy level is thought to be due to the presence and location of residual voids from the manufacturing process that have a greater affect on the impact properties at higher impact energies.

Figure 10 shows the typical impact load-time history curves of the impacted laminate samples under impact energy levels of 10J, 20J and 30J. The Hertzian failure (F_1), or the occurrence of initial damage in the composite, corresponds to the first load drop in the load-time history curve. There was no significant difference in the F_1 of the composite due to aging in any of the sample at all impact energies tested. F_1 was determined to occur at 700 ± 170 N. As previously determined, only the exposed surface is affected by the environmental aging due to the fibers retarding the oxidation of the matrix below the outer tows. This prevents the matrix bulk hardness from being affected greatly from the environmental ageing process for these impact energies.

From Figure 10 damage propagation can be seen, as the impact loading of the samples increase to maximum load. As expected, the maximum contact force increases with impact energy. Maximum contact forces are similar for aged as well as virgin samples. This can be due to the fact that the effect of aging is seen on a thin layer on the surface of the samples only.

The results of impact testing show that there is little variation in statistical force, energy and displacement for all tests (Table 1). This table shows there is no apparent change in maximum load (F_{max}) correlating to the exposure time, at all impact energy levels. The average F_{max} at 10 J, 20 J and 30 J was calculated to be 5759.90 ± 185.69 N, 7408.60 ± 264.77 N and 7746.10 ± 488.43 N respectively. All aged samples had F_{max} varying less than ± 10% of the virgin sample's F_{max} at the tested impact energy level, without an increasing or decreasing trend as the exposure time increased.

In addition, there is no measurable change in the absorbed energy or energy at maximum load (E_{max}) as the environmental exposure time was increased to 1000 h. The average E_{max} at 10 J, 20 J and 30 J was found to be 9.750 ± 0.209 J, 16.935 ± 0.752 J and 18.436 ± 1.7513 J respectively. The average total absorbed energy at 10 J, 20 J and 30 J was determined to be 4.153 ± 0.102 J, 13.183 ± 0.676 J and 24.686 ± 0.731 J respectively. All aged samples had absorbed energy levels and E_{max} varying less than ± 10% of the virgin sample's varying without an increasing or decreasing trend as the environmental aging time increased to 1000 hrs, at all impact energy levels.

The variation of deflection at the maximum force of exposed samples compared to the virgin samples is less than ± 10%. This shows that there is no significant change in dynamic stiffness due to the environmental aging. These results indicates that bulk composites impact properties were not significantly affected by the aging process due to the fiber limiting the oxidation effect to the surface and preventing degradation of the materials bulk properties.

3. CONCLUSIONS

Color change and chemical structure degradation of the thermoset polyurethane was observed to increase with aging time. The PU profiles appear to have a rapid color change up to 750 hrs exposure with a significant decrease in rate of degradation between 750 hrs and 1000 hrs. The findings from the current work shows that it took greater than 500 hrs for 70% of the total color change.

The polymer undergoes a phase separation allowing the soft segment to have more freedom to move. After the breaking of the urethane linkage in the polyurethane chain, the hard segments then undergo enthalpy relaxation. These combined phenomena cause the polymer matrix to retract and expose the surface fibers. It is shown that the average retraction of the surface polymer is 30 μm at 1000 hrs of exposure to the accelerated aging environment. This retraction exposes many of the fibers in the top weave of the composite causing an increased roughness in the surface of the composite on the surface directly exposed to the UV radiation.

This degradation is limited to the surface of the PU/Glass fiber composite due to the fiber tows acting as a barrier to prevent oxidation in the polymer matrix below the outer most fibers exposed to the UV radiation. This phenomenon prevented the degradation of the bulk impact properties of the composites. The Hertzian failure at all impact energies tested was determined to occur at 700 ± 170 N. All aged samples had F_{max}, E_{max}, total absorbed energy and deflection at F_{max} varying less than ± 10% of the virgin sample at the tested impact energy level, without an increasing or decreasing trend as the exposure time increased. Though the impact properties did not measurably vary as the exposure time increased, a decrease in the damage area was observed.

4. REFERENCES

1. Loos MR, Yang L, Feke DL, Manas-Zloczower I, Unal S, Younes U. Enhancement of fatigue life of polyurethane composites containing carbon nanotubes. Compos Part B Eng 2013;44:740-4.

2. Zia KM, Bhatti HN, Bhatti IA. Methods of polyurethane and polyurethane composites, recycling and recovery: a review. React Funct Polym 2007;67: 675-92.

3. Younes U. Development of PU-based RTM and VARTM technology. In: Composites, Las Vegas, NV, Feb. 9-11; 2010.

4. Bareis D, Heberer D, Connolly M. Advances in urethane composites resins with tunable reaction times. In: American Composites Manufacturers Association, Ft. Lauderdale, Florida, Feb. 2-4; 2011.

5. Chunjing H, Guodong L, Haoxiong N, Jianxiang N. Synthesis and characterization of polyurethane. J Wuhan Univ Technol Mater Sci Ed 2010;25:984-6.

6. Nayani M, Gunashekar S, Abu-Zahra N. Synthesis and characterization of polyurethane-nanoclay composites. Int J Polym Sci 2013;2013:1-6.

7. Buzzi O, Fityus S, Sasaki Y, Sloan S. Structure and properties of expanding polyurethane foam in the foundation remediation in expansive soil. Mech Mater 2008;40:1012-21.

8. Kim JH, Kim DH, Kim HS, Park BJ. A study on low velocity impact of woven glass/phenolic composite laminates considering environmental effects. Key Eng Mater 2005;297e300:1303-8.

9. Boubakri A, Guermazi N, Elleuch K, Ayedi HF. Study of UV-aging of thermoplastic polyurethane materials. Mater Sci Eng A 2010;1649-1654:527.

10. Ludwick A, Aglan H, Abdalla MO, Calhoun M. Degradation behavior of an ultraviolet and hygrothermally aged polyurethane elastomer: fourier transform infrared and differential scanning calorimetry studies. J Appl Polym Sci 2008;110(2):712-8.

11. Chen TK, Shieh TS, Chui JY. Studies on the first DSC endotherm of polyurethane hard segment based on 4,40 -diphenylmethane diisocyanate and 1,4- butanediol. Macromolecules 1998;31:1312-20.

12. Rev V, Bravar M. Ultraviolet degradation of polyester-based polyurethane. J Elastomer Plastics 1983;15(1):33-42.

13. Rosu D, Rosu L, Cascaval CN. IR-change and yellowing of polyurethane as a result of UV irradiation. Polym Degrad Stab 2009;94(4):591-6.

14. Wilhelm C, Rivaton A, Gardette JL. Infrared analysis of the photochemical behaviour of segmented polyurethanes 3. Aromatic diisocyanate based polymers. Polymer 1998;39(5):1223-32.

15. Wang H, Liu Y, Sun B, Huang S, Tian J. Aging behavior of the polyether polyurethane films irradiated by UV. Adv Mater Res 2013;748:16-21.

16. Liu Y, Liu Y, Liu S, Tan H. Effect of accelerated xenon lamp aging on the mechanical properties and structure of thermoplastic polyurethane for stratospheric airship envelopment. J Wuhan Univ Technol-Mater Sci Ed 2014;29(6): 1270-6.

17. Barb R-A, Magnus B, Innerbichler S, Greunz T, Wiesbauer M, Marksteiner R, et al. VUV treatment combined with mechanical strain of stretchable polymer foils resulting in cell alignment. Appl Surf Sci 2015;325:105-11.

18. Jana RN, Bhunia H. Accelerated hygrothermal and UV aging of thermoplastic polyurethanes. High Perform Polym 2010;22:3-15.

19. Connolly J, King J, Shidaker T, Duncan A. Characterization of pultruded polyurethane composites: environmental exposure and component assembly testing. In: American Composite Manufacturers Association, St. Louis, MO, Oct. 18-20; 2006.

20. Sakulsaknimitr W, Wirasate S, Pipatpanyanugoon K, Atorngitjawat P. Structure and thermal properties of polyurethanes synthesized with cardanoldiol. J Polym Environ 2015;23:216-26.

21. Boubakri A, Haddar N, Elleuch K, Bienvenu Y. Impact of aging conditions on mechanical properties of thermoplastic polyurethane. Mater Des 2010;31: 4194-201.

22. Boumbimba RM, Froustey C, Viot P, Gerard P. Low velocity impact response and damage of laminate composite glass fibre/epoxy based tri-block copolymer. Compos Part B Eng 2015;76:332-42.

23. Caputo F, De Luca A, Lamanna G, Borrelli R, Mercurio U. Numerical study for the structural analysis of composite laminates subjected to low velocity impact. Compos Part B Eng 2014;67:296-302.

24. Singh H, Namala KK, Mahajan P. A damage evolution study of E-glass/epoxy composite under low velocity impact. Compos Part B Eng 2015;76:235-48.

25. Zouggar K, Boukhoulda FB, Haddag B, Nouari M. Numerical and experimental investigations of S-glass/polyester composite laminate plate under low energy impact. Compos Part B Eng 2016;89:169-86.

26. Challenger KD. The damage tolerance of carbon fiber reinforced composites a workshop summary. Compos Struct 1986;6:295-318.

27. Ghelli D, Minak G. Low velocity impact and compression after impact tests on thin carbon/epoxy laminate. Compos Part B Eng 2011;42:2067-79.

28. Atas C, Dogan A. An experimental investigation on the repeated impact response of glass/epoxy composites subjected to thermal ageing. Compos Part B Eng 2015;75:127-34.

29. Mokhtar H, Sicot O, Rousseau J, Aminanda Y, Aivazzadeh S. The influence of ageing on the impact damage of carbon epoxy composites. Procedia Eng 2011;10:2615-20.

30. Boukhoulda FB, Guillaumat L, Lataillade JL, Adda-Bedia E, Lousdad A. Aging-impact coupling based analysis upon glass/polyester composite material in hygrothermal environment. Mater Des 2011;32:4080-7.

31. Pang S-S, Li G, Helms JE, Ibekwe SI. Influence of ultraviolet radiation on the low velocity impact response of laminated beams. Compos Part B Eng 2001;32(6):521-8.

32. Karakuzua E, Erbila E, Aktas M. Impact characterization of glass/epoxy composite plates: an experimental and numerical study. Compos Part B 2010;41: 388-95.

33. Woo RSC, Chen Y, Zhu H, Li J, Leung CKY, Kim JK. Environmental degradation of epoxy-organoclay nanocomposites due to UV exposure. Part 1: photo- degradation. Compos Sci Technol 2007;67:3448-56.

Table 1. Calculated statistical data of force, energy and deflection for 10 J, 20 J and 30 J impact energy levels with exposure times of 0, 250, 500, 750 and 1000 hrs.

Impact energy (J)	Exposure time (h)	Statistical data	Maximum load (N)	Absorbed energy (J)	E_{max} (J)	Displacement at F_{max} (mm)
10	0	Average	5504.55	4.145	9.502	3.434
		Std. dev.	184.34	0.584	0.623	0.219
		COV	3.35%	14.10%	6.56%	6.38%
	250	Average	5794.30	4.110	9.602	3.274
		Std. dev.	248.64	0.095	0.247	0.262
		COV	4.29%	2.32%	2.57%	8.01%
	500	Average	5724.35	4.308	9.726	3.585
		Std. dev.	138.95	0.004	0.347	0.257
		COV	2.43%	0.10%	3.57%	7.16%
	750	Average	6024.93	4.031	9.919	3.213
		Std. dev.	125.65	0.238	0.189	0.199
		COV	2.09%	5.91%	1.90%	6.19%
	1000	Average	5751.27	4.172	10.000	3.577
		Std. dev.	88.21	0.246	0.041	0.139
		COV	1.53%	5.89%	0.41%	3.89%
20	0	Average	7432.47	13.001	17.483	4.677
		Std. dev.	415.72	1.072	2.249	0.505
		COV	5.59%	8.24%	12.87%	10.81%
	250	Average	7501.57	12.260	15.737	4.209
		Std. dev.	452.51	0.232	3.080	0.286
		COV	6.03%	1.89%	19.57%	6.79%
	500	Average	7780.53	13.107	16.809	4.330
		Std. dev.	511.84	1.255	2.538	0.289
		COV	6.58%	9.57%	15.10%	6.68%

Table 1. Calculated statistical data of force, energy and deflection for 10 J, 20 J and 30 J impact energy levels with exposure times of 0, 250, 500, 750 and 1000 hrs. (cont.)

Impact energy (J)	Exposure time (h)	Statistical data	Maximum load (N)	Absorbed energy (J)	E_{max} (J)	Displacement at F_{max} (mm)
	750	Average	7245.90	13.425	16.996	4.222
		Std. dev.	726.36	1.482	3.480	0.468
		COV	10.02%	11.04%	20.48%	11.08%
	1000	Average	7082.37	14.122	17.649	4.706
		Std. dev.	383.14	0.271	1.526	0.164
		COV	5.41%	1.92%	8.65%	3.49%
30	0	Average	7955.75	24.812	17.953	4.561
		Std. dev.	758.51	0.502	1.990	0.227
		COV	9.53%	2.02%	11.08%	4.99%
	250	Average	8494.73	23.790	21.387	4.924
		Std. dev.	594.58	0.899	3.184	0.654
		COV	7.00%	3.78%	14.89%	13.29%
	500	Average	7389.10	25.537	18.393	4.712
		Std. dev.	1106.48	0.644	2.562	0.093
		COV	14.97%	2.52%	13.93%	1.97%
	750	Average	7301.17	25.189	16.782	4.598
		Std. dev.	255.92	0.402	0.720	0.113
		COV	3.51%	1.59%	4.29%	2.46%
	1000	Average	7589.63	24.100	17.667	4.333
		Std. dev.	437.49	0.323	2.127	0.238
		COV	5.76%	1.34%	12.04%	5.49%

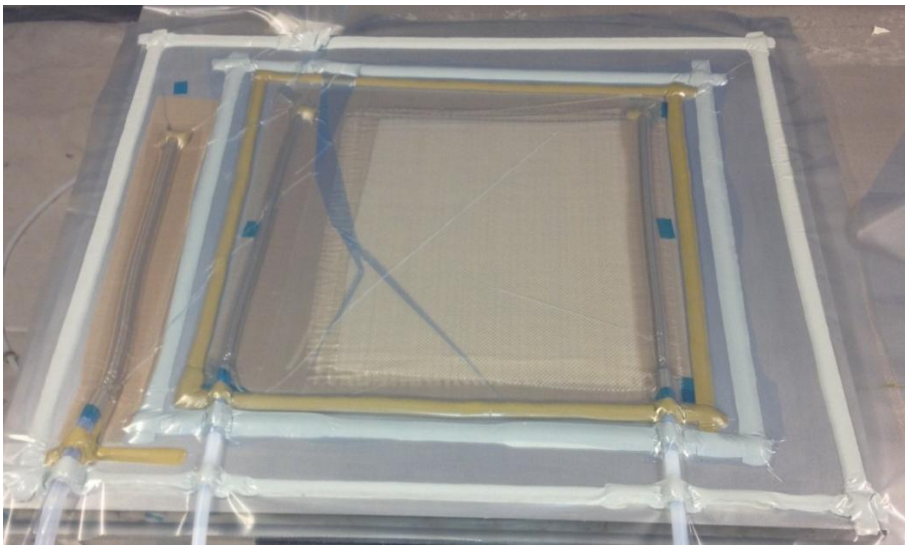

Figure 1. VARTM double bag setup with full vacuum applied before resin infiltration

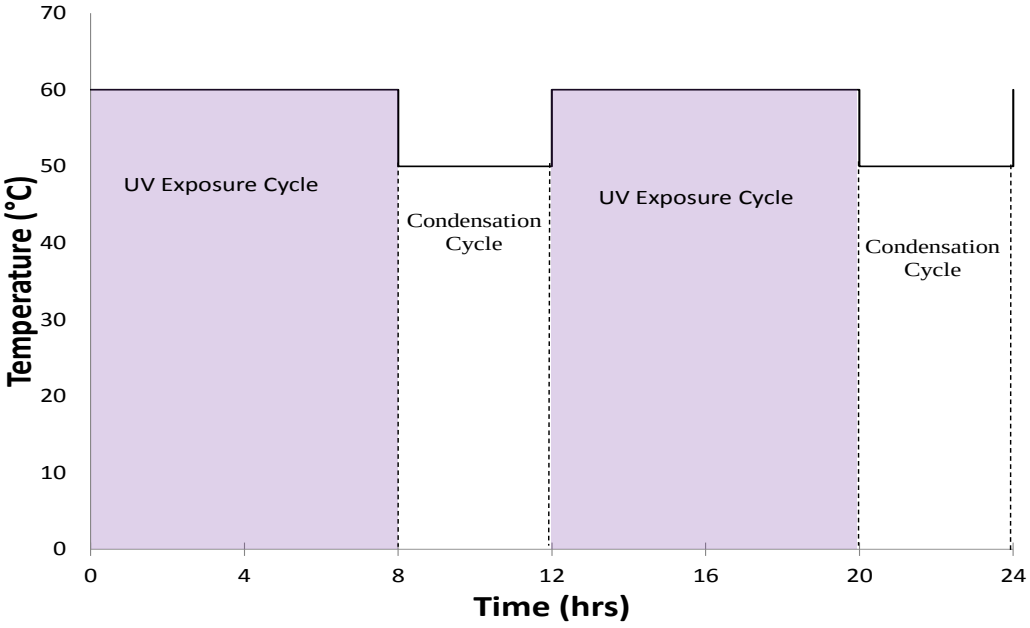

Figure 2. 24 hour representation of the PU composite aging cycle

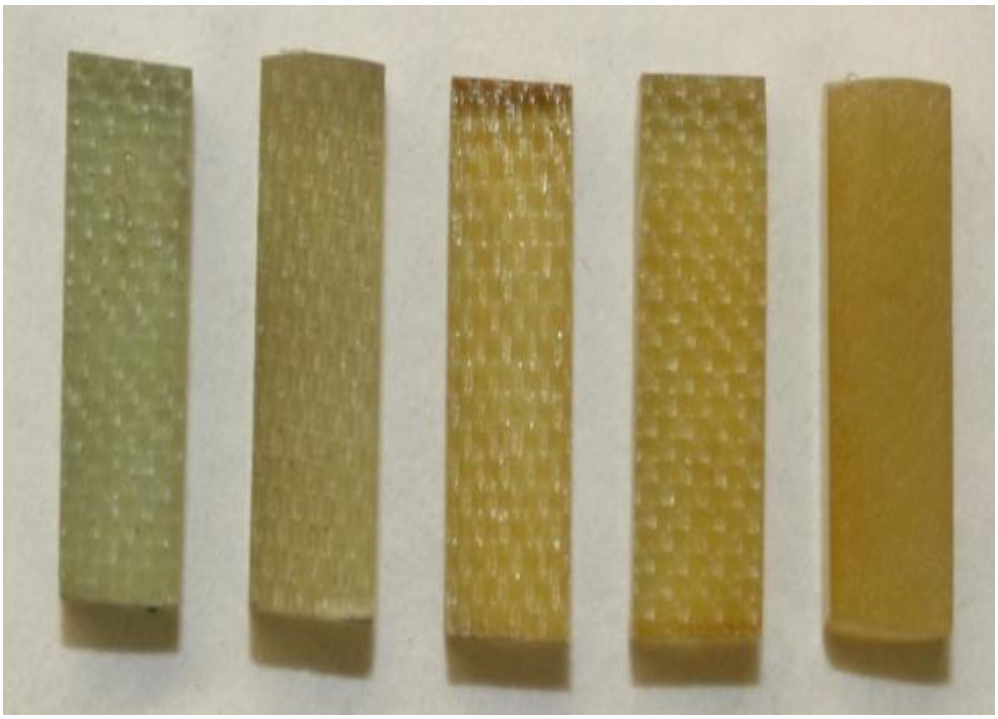

Figure 3. Fiberglass reinforced PU composite samples with accelerated exposure times left to right 0 hrs, 250 hrs, 500 hrs, 750 hrs and 1000 hrs

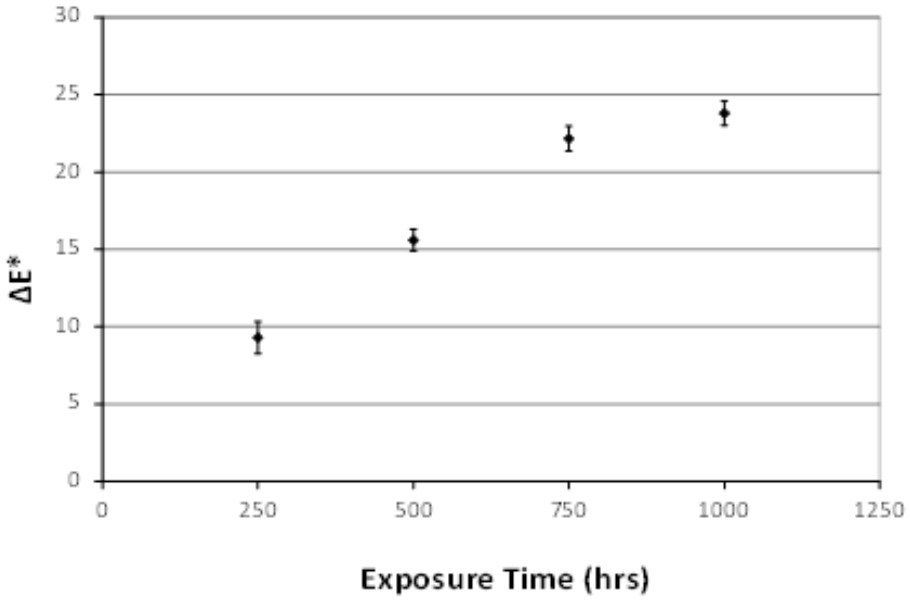

Figure 4. Total color change denoted in CIEL*a*b* values

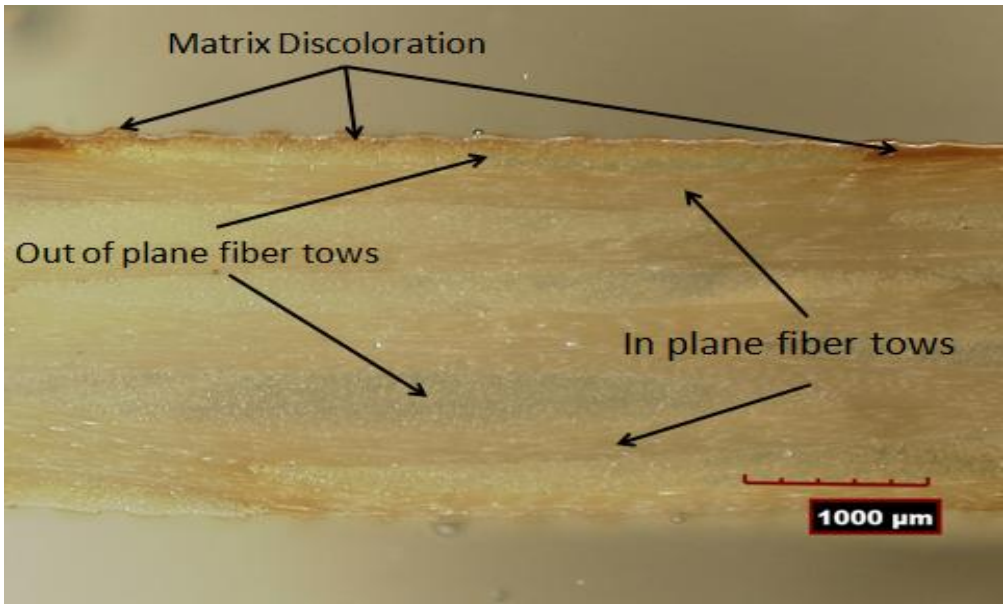

Figure 5. Cross section of fiberglass reinforced PU composite samples exposed for 1000 hrs to accelerated aging environment

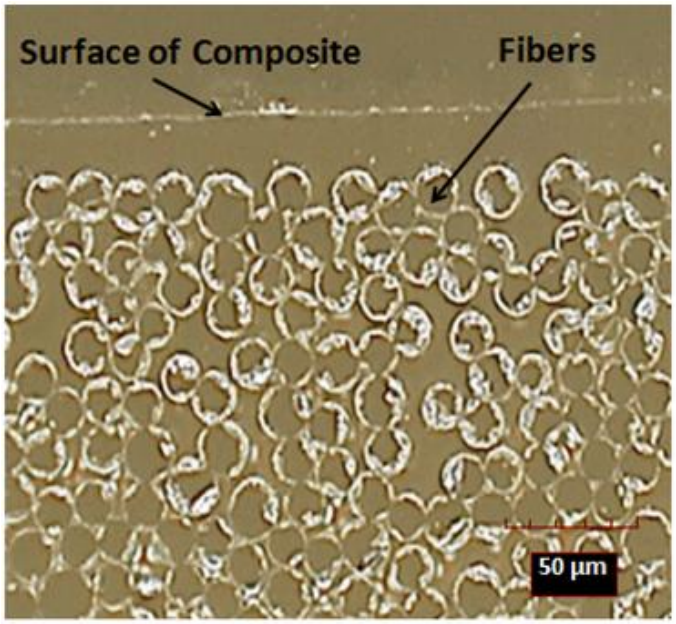

(a)

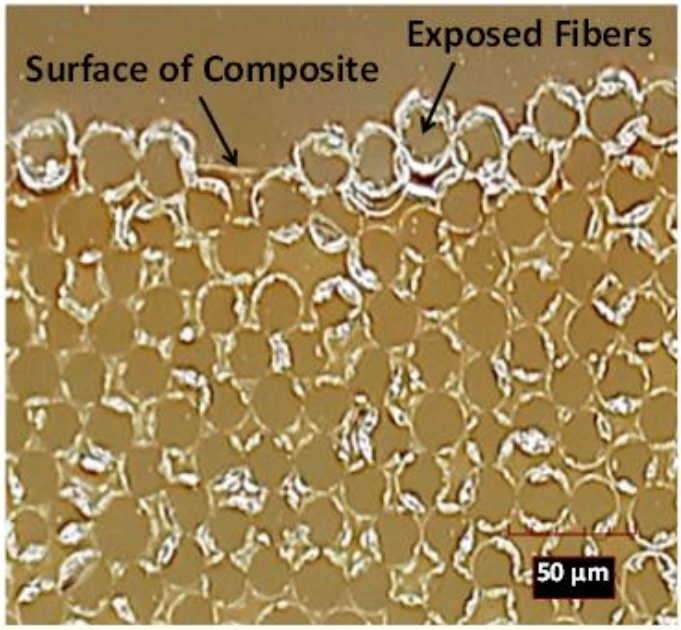

(b)

Figure 6. Microscopic image of fiberglass reinforced PU composite samples captured with a HiROX KH-8700 at 500x magnification (a) 0 hrs of environment exposure (b) 1000 hrs of environmental exposure

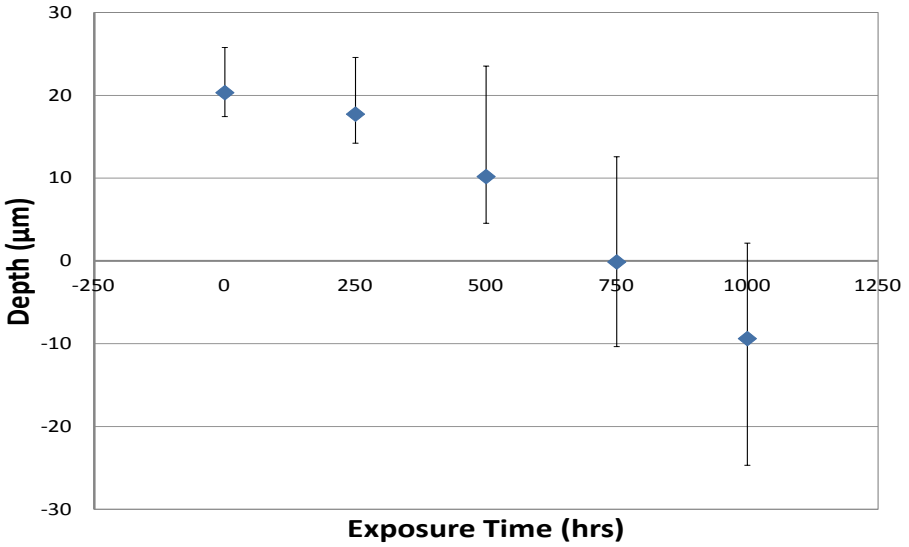

Figure 7. Box plot of average measured fiber depth from exposed surface of composite at 0, 250, 750 and 1000 hrs

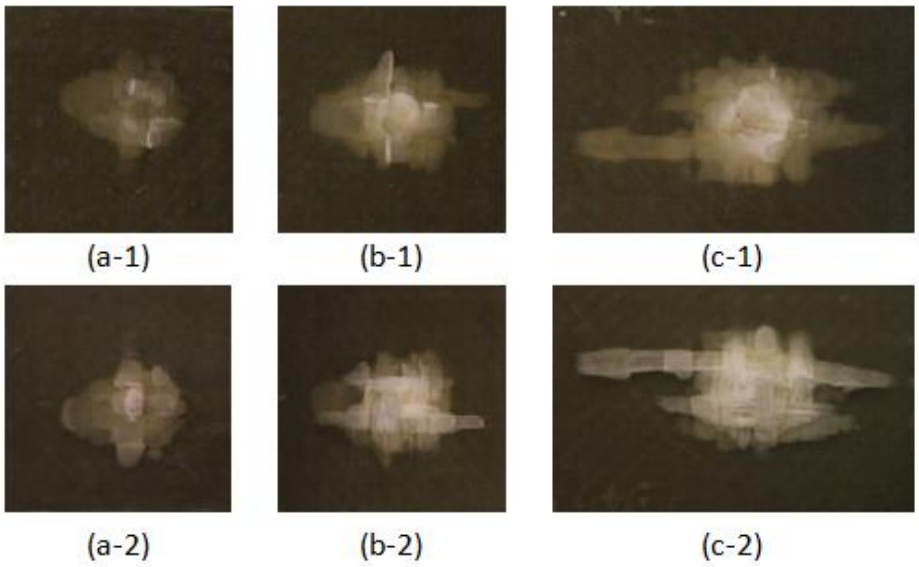

Figure 8. Fiberglass reinforced PU composite samples without aging (a-1) 10 J top impacted surface (a-2) 10 J bottom surface (b-1) 20 J top impacted surface (b-2) 20 J bottom surface (c-1) 30 J top impacted surface (c-2) 30 J bottom surface

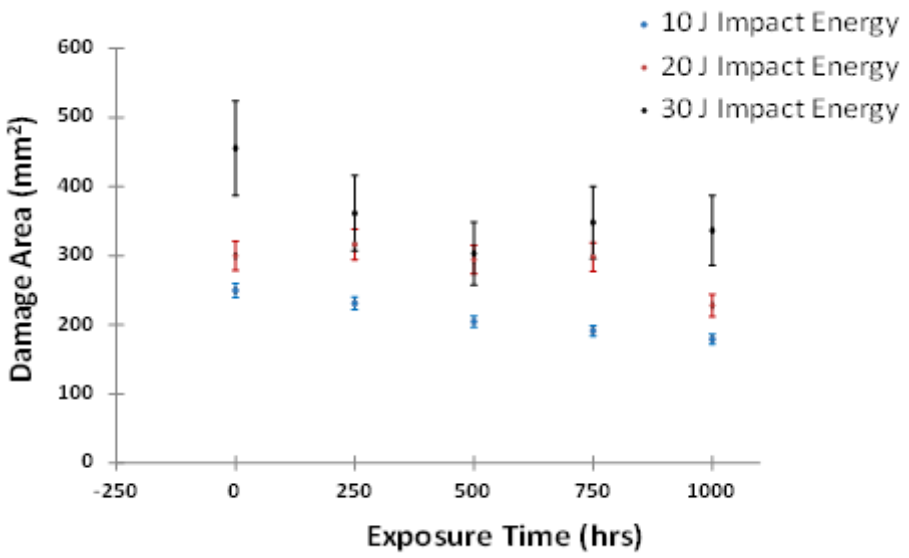

Figure 9. Average impact damage area with standard deviation of impacted samples

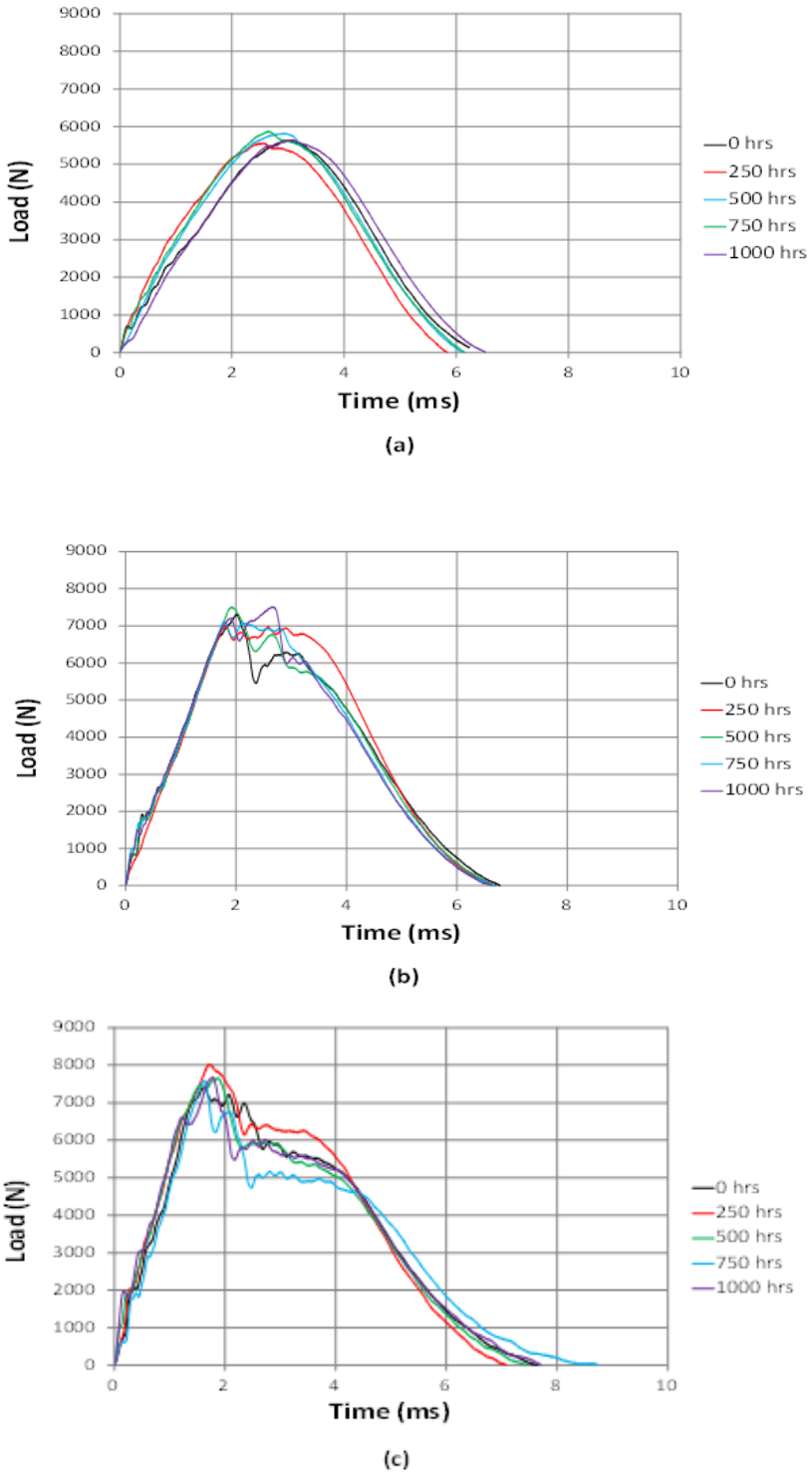

Figure 10. Impact load versus time of UV aged samples at impact energy of (a) 10 J, (b) 20 J, and (c) 30 J

SECTION

4. CONCLUSIONS

The first paper in this work offers a methodology to produce continuous fiber reinforced ZrB_2-SiC/SiC_f composite materials for ultra high temperature applications. A modified out-of-autoclave polymer infiltration and pyrolysis fabrication process was developed and implemented using an allylhydridopolycarbosilane preceramic polymer. A low cost vacuum bagging process was adapted to manufacture the material. The polymer infiltration and pyrolysis process effectively produced a toughened material.

The microstructure analysis shows that the samples were successfully re-infiltrated and the void content was significantly reduced. The inter-laminar macro void content was significantly reduced from 7.2 ± 1.6% to 2.7 ± 0.3%. However, the average size of voids, 8006 ± 6728 μm^2, and the maximum size, 26270 ± 336 μm^2 was not found to be reduced. It was found that cracks leading to the larger void would fill and prevent the complete re-infiltration of these voids. The micro pores were found to be interconnected and uniform throughout the matrix of the material. The micro void content was found to be significantly reduced from the re-infiltration process as well, from 32 ± 2.1% to 6.6 ± 1.6%.

The flexural strength and modulus were observed to be 27.5 ± 3.89 MPa and 12.7 ± 3.72 GPa respectively. Flexure tests results indicate that the failure of the CFCCs samples was not catastrophic due to addition of the continuous fiber mats and the less than fully dense matrix allowing for fiber bridging, pullout and crack deviation.

The material developed here can be used in ultra high temperature applications that do not require a material to have high strength but do require the material to be tough. Further re-infiltrations and fiber coating will have to be investigated to further improve the mechanical properties.

The second paper developed a process to produce continuous fiber reinforced SiC/SiC_f for possible use in nuclear applications. A dry press process was adapted to produce a greenbody of β-SiC continuous fiber reinforced β-SiC particles using an allylhydridopolycarbosilane preceramic polymer as the binder. The polymer infiltration and pyrolysis process was then implemented to produce a pure SiC/SiC_f continuous fiber reinforced ceramic composite. A pyrolyzation temperature profile was optimized using thermogravimetric analysis and prevented any measured damage for occurring during repeated cycles.

From the microscopy it was seen that there was SiC material infiltrated into the fibers tows; however, there were still macro voids with cross sectional areas of up to 0.27 mm^2. The matrix was uniform with interconnected micro voids with width less than 10 μm. These voids indicate that multiple re-infiltrations, beyond the two performed, were required to produce a fully dense SiC/SiC_f material. The interconnected nature of the micro voids found suggests that the matrix can be re-infiltrated to increase the density.

The finding from the porometry analysis supports the microscopy analysis. From the porometry it was concluded that there was residual porosity that was open. This indicates that additional re-infiltrations were necessary beyond the infiltrations performed on these samples. The apparent porosity was found to be 22% indicating the material

could be re-infiltrated to a more dense material. The calculated 11% closed pores would imply that the highest possible achievable density would still be less than 90%.

A final heat treatment was shown to produce a crystalline matrix material. The XRD indicates SiC crystalline polytypes were present and further investigation is required to determine the specific types present.

The thermo-mechanical properties were investigated from room to high temperature using an advanced high temperature environmental system 4-point flexure test. The flexure tests show that the material has graceful failure below 800 °C which indicates the fiber re-enforcement has a toughening effect. To increase the temperature of effective toughening, a coating on the fibers will need to be applied to ensure a weak interface at elevated temperature. The stress-strain curve indicates that this material has low strength due to the void content. Additional re-infiltrations were required to increase the material's overall performance.

The process developed here has produced continuous fiber reinforced ceramic SiC/SiC_f materials that could be used, as is, in multilayer hybrid design for use nuclear applications. To use this material as a single material for nuclear application further research in to densification and crystallinity will need to be conducted to produce hermetic pure β-SiC composite materials.

The third paper produced a glass fiber reinforced polyurethane composites manufactured from a novel two-part resin system using a low cost vacuum assisted resin transfer method. The material was aged using a hygrothermal and ultraviolet chamber to simulate temperate climate conditions.

Effect of UV exposure on color change of composite specimens was evaluated using image processing and colorimetry. Color change and chemical structure degradation of the thermoset polyurethane was observed to increase with aging time. The PU profiles appear to have a rapid color change up to 750 hrs exposure with a significant decrease in rate of degradation between 750 hrs and 1000 hrs. The findings from the current work shows that it took greater than 500 hrs for 70% of the total color change.

The effects of the aging on the microstructure were assessed using optical microscopy. The polymer undergoes a phase separation allowing the soft segment to have more freedom to move. After the breaking of the urethane linkage in the polyurethane chain, the hard segments then undergo enthalpy relaxation. These combined phenomena cause the polymer matrix to retract and expose the surface fibers. It is shown that the average retraction of the surface polymer is 30 μm at 1000 hrs of exposure to the accelerated aging environment. This retraction exposes many of the fibers in the top weave of the composite causing an increased roughness in the surface of the composite on the surface directly exposed to the UV radiation.

The accelerated aging effect on the impact resistant behavior was examined using low velocity impact. This degradation is limited to the surface of the PU/Glass fiber composite due to the fiber tows acting as a barrier to prevent oxidation in the polymer matrix below the outer most fibers exposed to UV radiation. This phenomenon prevented the degradation of the bulk impact properties of the composites. The Hertzian failure at all impact energies tested was determined to occur at 700 ± 170 N. All aged samples had F_{max}, E_{max}, total absorbed energy and deflection at F_{max} varying less than ± 10% of the virgin sample at the tested impact energy level, without an increasing or decreasing trend

as the exposure time increased. Though the impact properties did not measurably vary as the exposure time increased, a decrease in the damage area was observed. The material and process used for this paper produce a new generation composite material that was less susceptible than previous studies.

BIBLIOGRAPHY

1. Y. Matsuda, N. Akikawa and T. Satoh, "Manufacturing of 3-D SiC/SiC Composite Combustor Liner," *Ceramic Engineering and Science Proceedings,* vol. 22, no. 3, pp. 463-470, 2001.

2. K.-I. Watanabe, N. Suzumura, T. Nakamura, H. Murata, T. Araki and T. Natsumura, "Development of CMC Vane for Gas Turbine Engine," in *27th Annual Cocoa Beach Conference on Advanced Ceramics and Composites: B: Ceramic Engineering And Science Proceedings, Volume 24, Issue 4*, Hoboken, NJ, John Wiley & Sons, Inc., 2008, pp. 599-604.

3. M. Dietchman, "Next Generation Technologies for Today's Warfighter," in *ONR Naval S&T Partnership Conference*, Arlington, 2010.

4. W. E. Windes, P. A. Lessing, Y. Katoh, L. L. Snead, E. Lara-Curzio, J. Klett, J. C. Henager and R. J. Shinazsk, "Structural Ceramic Composites for Nuclear Applictation," Idaho National Laboratory, Idaho Falls, 2005.

5. F. Abdi, S. Kiefer, A. Bhattacharya and J. Price, "Evaluation Of Structural Performance of a Continous Fiber-Reinforced Ceramic Composite Gas Trubine Combustor Liner," in *49th Ineternational SAMPE Symposium and Exhibition: Materials and Processing Technology*, Long Beach, 3005.

6. J. Li, L. Zhang, L. Cheng, Y. Xu, S. Qiao, G. Jiao, J. Zhang and X. Luan, "Materials Characterization in Continuous Fiber-Reinforced Ceramic Composites Served in Simulating Environment," *Key Engineering Materials,* vol. 351, pp. 31-36, 2007.

7. J. Nicholas, V. Menta, K. Chandrahekhara, J. Watts, B. Lai, G. Hilmas and W. Fahrenholtz, "Processsing of Continuous Fiber Reinforced Ceramic Composites for Ultra High Temperature Applications using Polymer Precursors," in *International SAMPE Technical Conference*, Baltimore, 2012.

8. P. Yonathan, J.-H. Lee, D.-H. Yoon, W.-J. Kim and J.-Y. Park, "Improvement Of SiC_f/SiC Density by Slurry Infiltration and Tape Stacking," *Materials Research Bulletin*, vol. 44, no. 11, pp. 2116-2122, 2009.

9. O. Buzzi, S. Fityus, Y. Sasaki and S. Sloan, "Structure and Properties of Expanding Polyurethane Foam in the Foundation Remediation in Expansive Soil," *Mechanics of Materials,* vol. 40, pp. 1012-1021, 2008.

10. H. Chunjing, L. Guodong, N. Haoxiong and N. Jianxiang, "Synthesis and Characterization of Polyurethane," *Journal of Wuhan University of Technology. Materials Science edition,* vol. 25, pp. 984-986, 2010.

11. D. Bareis, D. Heberer and M. Connolly, "Advances in Urethane Composites Resins with Tunable Reaction Times," in *American Composites Manufacturers Association* , Ft. Lauderdale, Florida, Feb. 2-4, 2011.

12. C. T. Sims, N. S. Stoloff and W. C. Hagel, *Superalloys II*, New York: Wiley & Sons, 1987.

13. Y. Yamambe-Mitarai, Y. Ro, H. Harada and T. Maruko, "Ir-base Refractory Supperalloys for Ultra-High Temperartures," *Metallurigical and Materials Transactions A,* vol. 29, no. 2, pp. 537-549, 1998.

14. Y. Yamabe-Mitari, Y. Ro and H. Harada, "Microstructure Dependence of Strength of Ir-Based Refractory Superalloys," *Intermetallics,* vol. 7, no. 1, pp. 49-58, 1999.

15. X. H. Yu, Y. Yamabe-Mitarai, Y. Ro and H. Harada, "Design of Quaternary Ir-Nb-Ni-Al Refractory Superalloys," *Meallurgical and Materials Transactions A,* vol. 31, no. 1, pp. 173-178, 2000.

16. E. W. Neuman, G. E. Hilmas and W. G. Fahrenholtz, "Strength of Zirconium Diboride to 2300 °C," *Journal of the American Ceramic Society,* vol. 96, no. 1, pp. 47-50, 2013.

17. S. R. Levine, E. J. Opila, M. C. Halbig, J. D. Kiser and M. Singh, "Evaluation Of Ultra-High Temperature Ceramics for Aeropropulsion use," *Journal of European Ceramic Society,* vol. 22, no. 14-15, pp. 2757-2767, 2002.

18. M. S. Asl, F. Golmohammadi, M. G. Kakroudi and M. Shokouhimehr, "Synergetic effects of SiC and Csf in ZrB_2-based ceramic composites. Part 1: Densification behavior," *Ceramics International,* vol. 42, no. 3, pp. 4498-4506, 2016.

19. S. Kim, J.-M. Chae, S.-M. Lee, Y.-S. Oh, H.-T. Kim and B.-K. Jang, "Change In Microstructures and Physical Properties of ZrB_2-SiC Ceramics Hot-Pressed With Variety Of SiC Sources," *Ceramic Internatiional,* vol. 40, pp. 3477-3483, 2014.

20. X. Zhang, L. Xu, S. Du, J. Han, P. Hu and W. Han, "Fabrication and Mechanical Properties of ZrB_2-SiCw Ceramic Matrix Composite," *Materials Letters,* vol. 62, no. 6-7, pp. 1058-1060, 2008.

21. P. Liaw, "Continous Fiber Reinforced Ceramic Composites," *Journal of the Chinese Institute of Engineers,* vol. 21, no. 6, pp. 701-718, 2011.

22. C.-P. Yang, G.-Q. Jiaso and B. Wang, "Modeling Oxidation Damage of Continuous Fiber Reinforced Ceramic Matrix Composites," *Acta Mechanica Sinica,* vol. 27, no. 3, pp. 382-388, 2011.

23. *The Composite Materials Handbook MIL 17,* Volume 5 Ceramic Matrix Composite, ASTM International, West Conshohocken, PA, 2002.

24. P. Colombo, G. Mera, R. Riedel and G. Soraru, "Polymer Derived Ceramic: 40 Years of Research and Innovation in Advanced Ceramics," *Journal of American Ceramic Society,* vol. 93, no. 7, pp. 1805-1837, 2010.

25. P. Greil, "Polymer Derived Engineering Cermics," *Advanced Engineeing Materials,* vol. 2, no. 6, pp. 339-348, 2000.

26. P. Colombo, R. Riedel, G. D. Soraru and H.-J. Kleebe, Polymer Derived Ceramics, Lancaster: DEStech Publications, Inc, 2010.

27. R. Brook, Processing of Ceramics, Part II. Materials Science and Technology: A Comprehensive Treatment, New York: John Wiley & Son, 1995.

28. S. Shah and R. Raj, "Mechanical Properties of a Fully Dense Polymer Derived Ceramic Made by a Novel Pressure Casting Process," *Acta Materialia,* vol. 50, no. 16, pp. 4093-4103, 2002.

29. W. Verbeek, "Production of Shaped Articles of Homogeneous Mixtures of Silicon Carbide and Nitride," Ger. Offen. 2218960 (Bayer AG) Patent 3853567, 8 November 1973.

30. S. Yajima, J. Hayashi and M. Imori, "Development of High Tensile Strength Silicon Carbide Fibre Using an Organosilicon Polymer," *Nature,* vol. 273, no. June, pp. 525-527, 1978.

31. S. Johnson, M. Gasch, D. Leiser, D. Stewart, M. Stackpoole, J. Thorton and C. Espinoza, "Development of New TPS at NASA Ames Research Center," in *15th AIAA INternational Space Planes and Hypersonic Systems and Technologies Conference,* Dayton, 2008.

32. M. Nejhad, M. Chandramouli and A. Yousefpour, "Processing And Performance of Continuous Fiber Ceramic Composites by Preceramic Polymer Pyrolysis: I - Filament Winding," *Journal of Composite Materials,* vol. 35, pp. 2207-2237, 2001.

33. M. Nejhad, M. Chandramouli and A. Yousefpour, "Processing And Preformance of Continuous Fiber Ceramic Composites by Preceramic Polymer Pyrolysis: II - Resin Transfer Molding," *Journal of Composite Materials,* vol. 35, pp. 2239-2255, 2001.

34. S. Lee, M. Weinmann and F. Aldinger, "Processing and Properties of C/Si-B-C-N Fiber-Reinforced Ceramic Matrix Composites Prepared By Precursor Impregnation and Pyrolysis," *Acta Materialia 56,* pp. 1529-1539, 2008.

35. L. Yao, Z. Feng and Q. Cheng, "Low Velocity Impact Damage Evaluation of 2D C/SiC Composite Material," in *Advanced Materials Research*, Qingdao, 2009.

36. S. Zhu, M. Minzuno, Y. Kagawa and Y. Mutoh, "Monotonic Tension, Fatigue and Creep Behavior of SiC-Fiber-Reinforced SiC-Matrix Composites: A Review," *Composite Science and Technology,* vol. 59, no. 6, pp. 833-851, 1999.

37. A. Sayir, "Carbon Fiber Reinforced Hafnium Carbide Composite," *Journal of materials science,* vol. 39, no. 19, pp. 5995-6003, 2004.

38. I. Al-Dawery and E. G. Butler, "Fabrication of High-Temperature Resistant Oxide Ceramic Matrix Composites," *Composites-Part A: Applied Science and Manufacturing,* vol. 32, no. 8, pp. 1007-1012, 2001.

39. R. Munro, "Material Properties of a Sintered Alpha-SiC," *Journal of physical and chemical reference data,* vol. 26, no. 5, pp. 1195-1203, 1997.

40. Avco Corporation, Research and Advanced Development Division, Air Force Materials Laboratory (U.S.). Materials Physics Division, Thermodynamics of Certain Refractory Compounds, H. L. Schick, Ed., Acedemic Press, 1966.

41. R. Sreeja, B. Swaminathan, A. Painuly, T. V. Sebastian and S. Packirisamy, "Allylhydridopolycarbosilane (AHPCS) as Matrix Resin for C/SiC Ceramic Matrix Composite," *Materials Science and Engineering B: Solid-State Materials for Advanced Technology,* vol. 168, no. 1, pp. 204-207, 2010.

42. Y. W. Lee, S. Lee, H. Kim, C. Joung and C. Degueldre, "Study On The Mechanical Properties and Thermal Conductivity of Silicaon Carbide-, Zirconia- and Magnesia Aluminate-Based Simulated Inert Matrix Nuclear Fuel Materials After Cyclic Thermal Shock," *Journal of Nuclear Materials,* vol. 319, pp. 15-23, 2003.

43. L. V. Interrante, C. W. Whitmarsh, W. Shewood, H.-J. Wu, R. Lewis and G. Maciel, "High Yield Polycarbosilane Precursors to Stoichiometric SiC. Synthesis, Pyrolysis and Application," in *MRS Proceedings* , Sanfransico, 1994.

44. S. Dong, Y. Katoh, A. Kohyama, S. Schwab and L. Snead, "Microstrutural Evaluation and Mecahnical Performances of SiC/SiC Composites by Polymer Impregnation/Microwave Pyrolysis (PIMP) Process"," *Ceramics International,* vol. 28, no. 8, pp. 899-905, 2002.

45. K. V. Moraes and L. V. Interrante, "Processing, Fracture Toughness, and Vickers Hardness of Allylhdidopolycarbosilane-Derived Silicon Carbide," *Journal of the American Ceramc Society,* vol. 86, no. 2, pp. 342-346, 2003.

46. K. Shiina and M. Kumada, "Thermal Rearangement of Hexamethyldisilane to Trimethyl(Dimethylsilylmethyl)Silane," *Journal of Organic Chemistry,* vol. 23, p. 139, 1958.

47. C. Whitmarch and L. Interrante, "Synthesis and Structure of a Highly Branched Polycarbosilane Derived From (Chloromethyl)Tricholorosilane," *Organometaillics,* vol. 10, no. 5, pp. 1336-1344, 1991.

48. M. Z. Berbon, D. R. Dietrich, D. B. Marshall and D. P. H. Hasselman, "Transverse Thermal Conductivity of Thin C/SiC Composites Fabricated by Slurry Infiltration," *Journal of the American Ceramic Society,* vol. 84, no. 10, pp. 2229-2234, 2001.

49. W. Kernel, Ceramic Matrix Composites, Weinheim: Wiley_VCH GmbH & Co. KGaA, 2008.

50. K. Nakano, A. Kamiya, H. Ogawa and Y. Nishino, "Fabrication And Mechanical Properties Of Carbon Fiber Reinforced Silicon Carbide Composites," *Journal of Ceramic Society Japan,* vol. 100, no. 4, pp. 472-75, 1992.

51. K. Park and T. Vasilos, "Processing, Microstructure and Mechanical Properites of Hot Pressed SiC Continuous Fiber/SiC Composites," *Journal of Material Science,* vol. 32, pp. 295-300, 1997.

52. R. Bodet, N. Jia and R. E. Tressler, "Microstructural Instability and the Resultant Strength of Si-C-O (Nicalon) and Si-N-C-O(HPZ) Fibers," *Journal of Europe Ceramic Society,* vol. 16, no. 6, pp. 653-664, 1996.

53. S. Dong, Y. Katoh and A. Kohyama, "Preparation of SiC/SiC Composites by Hot Pressing, using Tyranno-sa Fibers as Reinforcement," *Journal of the American Ceramic Society,* vol. 86, no. 1, pp. 26-32, 2003.

54. J. G. Binner, Advanced Ceramic Processing and Technology, vol. 1, Park Ridge, New Jersey: Noyes Publications, 1990.

55. R. Funk, H. Schachner, C. Triquet, M. Kornmann and B. Lux, "Coating of Cemented Carbide Cutting Tools with Alumina by Vapor Deposition," *Journal of the Electrochemical Society,* vol. 123, no. 2, pp. 285-289, 1976.

56. J. Lidstrom and R. Johannesson, "Nucleation of AL-20-3 Layers on Cemented Carbide Tools," *Journal of the Electrochemical Society,* vol. 123, no. 4, pp. 555-559, 1976.

57. J. Goela and R. Taylor, "Monolithic Material Fabrication by Chemical Vapour Deposition," *Journal of Materials Science,* vol. 23, no. 12, pp. 4331-4339, 1988.

58. X. Fan, X. Yin, Y. Cheng, L. Zhang and L. Cheng, "Microstructure And Tribological Behaviors of C/C-Bn Composites Fabricated by Chemical Vapor Inifiltration," *Ceramics International,* vol. 38, no. 8, pp. 6137-6144, 2012.

59. J. He, M. Scarlete and J. Harrod, "Silicon-Nitride and Silicon Carbonitride by the Pyrolysis of Poly(methylsiladiazan)," *Journal of the American Ceramic Society,* vol. 78, no. 11, pp. 3009-3017, 1995.

60. R. Laine and F. Bobonneau, "Preceramic Polymer Routes to Silicon-Carbide," *Chemisty of Materials,* vol. 5, no. 3, pp. 260-279, 1993.

61. K. Sato, A. Tezuka, O. Funayama, T. Isoda, Y. Terada, S. Kato and M. Iwata, "Fabrication and Pressure Testing of a Gas-Turbine Component Manufactured by a Preceramic-Polymer-Impregnation Method," *Composite Science and Technology,* vol. 59, no. 6, pp. 853-859, 1999.

62. M. Mohamed, S. Hawkins and S. Chandrashekhara, "Manufacturing and Performance Elaluation of Polyurethane Composites Using One-part and Two-part Resin Systems," *Polymer and Polymer Composites,* pp. 333-344, 2015.

63. A. Boubakri, N. Guermazi, K. Elleuch and H. F. Ayedi, "Study of UV-aging of Thermoplastic Polyurethane Materials," *Materials Science and Engineering A,* Vols. 1649-1654, p. 527, 2010.

64. T. K. Chen, T. S. Shieh and J. Y. Chui, "Studies on the First DSC Endotherm of Polyurethane Hard Segment Based on 4,4'-Dimphenymethane Diisocyanate and 1,4-Butanediol," *Macromolecules,* vol. 31, pp. 1312-1320, 1998.

65. V. Rev and M. Bravar, "Ultraviolet Degradation of Polyester-based Polyurethane," *Journal of Elastomer and Plastics,* vol. 15, no. 1, pp. 33-42, 1983.

66. D. Rosu, L. Rosu and C. N. Cascaval, "IR-change and Yellowing of Polyurethane as a result of UV Irradiation," *Polymer Degradation and Stability*, vol. 94, no. 4, pp. 591-596, 2009.

67. C. Wilhelm, A. Rivaton and J. L. Gardette, "Infrared Analysis of the Photochemical behaviour of Segmented Polyurethanes 3. Aromatic Diisocyanate based polymers," *Polymer*, vol. 39, no. 5, pp. 1223-1232, 1998.

68. H. Wang, Y. Liu, B. Sun, S. Huang and J. Tian, "Aging Behavior of the Polyether Polyurethane Films Irradiated by UV," *Advanced Materials Research*, vol. 748, pp. 16-21, 2013.

VITA

James Robert Nicholas was born in Marshall, MO to Thomas E. Nicholas and Becky S. Nicholas. He received his Bachelors of Science degree in Mechanical Engineering in May of 2008 from the Missouri University of Science and Technology (formerly University of Missouri-Rolla), Rolla, Missouri. He then worked as a systems engineer for Shick Solutions in Kansas City, MO. He returned to the Missouri University of Science and Technology to complete his Masters of Science degree in Mechanical Engineering in May of 2013.

Directly after completion of his Masters of Science degree, Mr. James R. Nicholas has been enrolled in the Ph.D. Program in Mechanical Engineering at Missouri University of Science and Technology, Rolla, Missouri, USA. He has served both as Graduate Research Assistant and Graduate Teaching Assistant throughout his graduate career in the Department of Mechanical and Aerospace Engineering. In May 2017, he received his Ph.D. degree in Mechanical Engineering from Missouri University of Science and Technology, Rolla, Missouri.